Examining the Effect of Poly(Ethylene Glycol) and Non-Specific Insulin Binding on the Phase Behaviour of PEGylated Phosphocholine Membrane Models

KANWAL TANWIR

A DISSERTATION SUBMITTED TO
THE FACULTY OF GRADUATE STUDIES
IN PARTIAL FULFILLMENT OF THE REQUIREMENTS
FOR THE DEGREE OF
DOCTOR OF PHILOSOPHY

Graduate Program in Chemistry
York University
Toronto, Ontario

April 2016

Abstract

Inclusion of synthetic poly-(ethylene glycol) (PEG)-grafted phospholipids into self-assembled phospholipid matrices is an exceptional method to engineering optimized bio-non-fouling membrane mimetic surfaces. The success of many PEGylated membranes applications, however, depends on the ability to develop a bio-mimetic surface with highly optimized and controllable properties. This study, hence, focused on assessing different aspects of PEGylated phosphocholine membrane models, DPPC/DPPE-PEG2000 (C_{16}/C_{16}) and DSPC/DSPE-PEG2000 (C_{18}/C_{18}). The membrane models include unilamellar vesicles and monolayers. Monolayer as a membrane model was used to examine the phase behavior, morphology, composition, and aliphatic chain length in aqueous media of physiological relevance (PBS). The effect of lateral PEG distribution and its conformations on the phase behavior of monolayers was also studied. The results obtained for both binary mixtures have been summarized in terms of phase diagrams. The effect of non-specific interactions of insulin on the stability and biophysical properties of monolayers for both binary mixtures was studied using monolayer area expansion approach. The data obtained has been analyzed to calculate the insulin penetration area, A_{ins}, and binding degree, χ_{ins}. Unilamellar vesicles were used as a membrane model to examine the morphology and phase behavior of binary mixtures. A comparative analysis has been performed to understand the correlation between PEGylated phosphocholine vesicle membranes and monolayers. Moreover, the changes in insulin conformation upon interactions with unilamellar vesicles with varying PEG content have also been examined. These findings thus imply that the phase behavior of PEGylated phosphocholine membranes may significantly change in response to slight changes in composition which can be used for rational design of PEGylated membranes for various biomedical applications.

Dedicated to my Beloved Parents,
Husband, Siblings and My Life, Ezzah

Acknowledgements

First and foremost, I would like to express my deepest gratitude to my supervisor, Dr. Valeria Tsoukanova for believing in me and giving me exceptional opportunity to work in her research group. She has been very cooperative throughout my PhD work and helped me fulfill my dream which otherwise would not have been possible. I am thankful to all my colleagues for their encouragements and moral support.

I would like to heartily thank my committee members Dr. Slyvie Morin, Dr. Gerald Audette, and Dr. Derek Wilson for their continuing support and cooperation throughout my PhD work. I am also sincerely thankful to Dr. Heinz-Bernhard Kraatz and Dr. Patricia Lakin-Thomas for their valuable time, cooperation and positive feedback.

I am also thankful to Dr. Howard Hunter, Dr. Derek Wilson, and Dr. Logan Donaldson for their cooperation in conducting the NMR and ESI-MS, and CD experiments, as well as Peter Liuni and Tamanna Rob for their assistance in ESI-MS data analysis.

This acknowledgment would not complete without thanking my family. Words cannot express how thankful I am to my parents, grandparents and siblings for all their faith, prayers, love, encouragements, and support, which sustained me this far.

A special thanks to my husband, Dr. Muhammad Naeem Shahid, who supported, motivated and guided me tirelessly in every step throughout my PhD work. Also thanks to my daughter, Ezzah, for being so patient throughout completing my dissertation and cheering me up all the time.

Most of all, I thank ALLAH (SWT) for giving me strength in fulfilling my dreams and guiding me day by day in all my pursuit.

Table of Contents

List of Tables

List of Figures

Symbols and Abbreviations

π – Surface Pressure
$\pi_{t,high}$ – High Pressure Transition
χ_{ins} – Binding degree of insulin
ΔA – Change in monolayer area
ΔA_{ss} – Change in monolayer area
A – Molecular Area
A_{ins} – Penetration area of insulin
A_{pl} – Effective area of phospholipid in a closely packed conformation
Å – Angstrom
C – Compressibility
C_{16} – aliphatic chains containing 16 carbons
C_{16} – aliphatic chains containing 18 carbons
C_{16}/C_{16}-PEG2000 – DPPC/DPPE-PEG2000
C_{18}/C_{18}-PEG2000 – DSPC/DSPE-PEG2000
CD – Circular Dichroism Spectroscopy
DOPE-RH – Rhodamine-dioleoyl-phosphatidylethanolamine labeled (1,2-dioleoyl-sn-glycero-3- phosphatidylethanolamine-*N*-(lissamine Rhodamine B sulfonyl)) probe
DPPC – 1,2-Dipalmitoyl-sn-glycero-3-phosphocholine
DPPE-PEG2000 – 1,2-Dipalmithoyl-s*n*-glycero-3-Phosphoethanolamine-*N*-[poly(ethylene glycol)2000]
DSPC –1,2-Disteroyl-sn-glycero-3-phosphocholine
DSPE-PEG2000 – 1,2-Disteroyl-s*n*-glycero-3-Phosphoethanolamine-*N*-[poly(ethylene glycol)2000]
EFM – Epifluorescence Microscopy
FITC – Fluorescein isothiocyanate fluorophore
G – Gaseous phase
GUV – Giant unilamellar vesicles
k – Botzmann constant
$L_{\beta'}$, L_{β} – Gel Phase
L_d – Liquid Disordered phase
LC – Liquid Condensed phase
LC_{mix} – Rich in both phosphocholine and PEG-phospholipid molecules
LC_{PC} – contain only phosphocholine LC phase
LE – Liquid Expanded phase
LE/LC – Liquid expanded/ Liquid condensed phase coexistence
Min – Minutes
mN/m – Milli newton per meter
MS – Mass Spectrometry
nm^2 – Nano-meter square
NMR – Nuclear Magnetic Resonance Spectroscopy
PBS – Phosphate-buffered saline
PEG – Poly (Ethylene- Glycol)
PEG2000 – Poly (Ethylene- Glycol) with MW of 2000 g/mol

SUV – Small unilamellar vesicles
t – Time
T - Temperature
T_m - chain-melting transition temperature
TRITC –Rhodamine isothiocyanate fluorophore

Peer-Reviewed Articles, Conference Proceedings and Awards

The research conducted over the course of this PhD program has been reported in:

- Tanwir, K. and Tsoukanvoa, V. *Langmuir* **2008**, *24*, 14078 – 14087.
- Tanwir, K.; Shahid, M. N.; Thomas, A; and Tsoukanova, V. *Langmuir* **2012**, *28*, 14000 – 14009.

The research conducted over the course of this PhD program has been presented in:

- **Tanwir, K.**; Shahid, M. N.; Nosrati, N.; Bhayani, T.; Thomas, A.; and Tsoukanova, V. Presentation at Canadian Society for Chemistry Conference, Montreal, Canada **2011.**
- Shahid, M. N.; **Tanwir, K.**; and Tsoukanova, V. Presentation MC10 Conference Manchester, UK **2011**.
- Tsoukanova, V. and **Tanwir, K**. Presentation PacificChem Conference, Hawaii, USA **2010**.
- **Tanwir, K.**; Nosrati, N.; Peechatt, T.; and Tsoukanova V. Presentation at Canadian Society for Chemistry, Toronto, Canada **2010**.
- **Tanwir, K.** and Tsoukanova, V. Presentation at Surface Canada Conference, Hamilton, Canada **2009**.
- **Tanwir, K.** and Tsoukanova, V. Presentation at Canadian Society for Chemistry Conference, Hamilton, Canada **2009**.

Awards and Scholarships:

- Ontario Graduate Scholarship in Science & Technology from 2010 – 2011 at York University.

Chapter 1: Introduction.

Phospholipid membrane-mimetic surfaces have gained tremendous interest over the past few decades for use as exclusion filters for microfluidic devices, biosensors, carriers for RNA in the form of lipoplexes, nanosensor templates as well as vesicles, nanoparticles and microbubbles for the delivery of therapeutics and diagnostic agents [Chen 2013; Chordeiro 2015; Immordino 2006; Karatekin 2012; Liu 2014; Lozano 2009a; Lozano 2009b; Peterca 2011; Popovska 2013; Reulen 2009; Seth 2013; Shi 2010; Silpe 2013; Suga 2013; Sung 2011; Wisniewski 2000; Zhai 2014]. Phospholipid membrane-mimetic surfaces are proven to be physiologically compatible and biologically inert with low intrinsic toxicity [Immordino 2006; Karatekin 2012; Mfuh 2011; Savva 1998;Wade 2001]. However, a major hurdle these surfaces encounter *in vivo* is the undesirable recognition and resistance from various serum components including reticuloendothelial cells, macrophages, serum proteins, and platelets. The former description is referred as a biofouling phenomenon [Immordino 2006; Liu 2014; Savva 1998; Vermette 2003; Wisniewski 2000]. Biofouling has the potential to significantly impair and reduce the *in vivo* efficiency of the biomedical devices coated with membrane-mimetic surfaces [Chordeiro 2015; Savva 1998; Vermette 2003; Wisniewski 2000; Yen 2010]. Several innovative approaches are being explored to enhance the efficiency of biomedical devices by suppressing the non-specific interactions of biomolecules and bypassing the mononuclear phagocyte system (MPS). This also includes the incorporation of grafted PEG chains in the host phospholipid matrix to

engineer bio-non-fouling membrane-mimetic surfaces [Chen 2010; Chen 2013; Gref 2000; Immordino 2006; Karatekin 2012; Liu 2014; Vermette 2003].

1.1. PEGylation of Membrane-Mimetic Surfaces.

Incorporation of a poly (ethylene glycol) (PEG) graft has been considered to be a milestone in the field of novel biomedical applications [Allen 1997; Luna 2011; Popovska 2013; Takemoto 2011; Vermette 2003; Vukovic 2011; Wattendorf 2008]. Figure 1.1 illustrates the chemical structure of PEG monomer with repeating units of ethylene oxide units (EO) connected via oxygen atoms. Inclusion of PEG in numerous biomedical formulations has shown a tremendous success in applied research to develop bio-non-fouling surfaces with controlled properties [Allen 1997; Luna 2011; Popovska 2013; Takemoto 2011; Vukovic 2011; Wattendorf 2008]. PEGylated drug carriers such as Doxil, Lipodox and etc. have been widely used as a favorable choice for the delivery of various therapeutic agents [Bozzuto 2015; Vukovic 2011]. Highly hydrated PEG chains are commonly used in numerous biomedical applications due to their distinctive properties including chemical inertness, lack of toxicity, low antigenicity, biocompatibility, and good solubility [Antonietti 2003; Bianco-Peled 2001; Luna 2011; Naumann 2001; Savva 1998; Shahid 2011; Vukovic 2011; Wattendorf 2008]. PEG chains are believed to repel protein adhesion and improve the efficiency/performance of these membrane-mimetic surfaces. Two mechanisms are usually associated with PEG chains protecting the surface against protein or other biomolecule adhesion. These are (i) steric repulsion and/or (ii) formation of a hydration shell (solvent-mediated structuring) [Gref

2012; Immordino 2006; Kenworthy 1995; Keratekin 2012; Liu 2014; Luna 2011; Hristova 1995; Stepniewski 2011; Vermette 2003; Wattendorf 2008]. PEG steric repulsion is believed to occur when a protein or other biomolecule makes contact with the polymer layer and the PEG chains resist this compression by increasing their local concentration as well as the free energy [Taylor 2012; Vermette 2003]. Formation of hydration shell refers to the structuring of water molecules around PEG chain through hydrogen bonding [Buzzuto 2015; Naumann 1999; Vermette 2003; Wattendorf 2008]. It is believed that each EO (ether oxygen) unit in the PEG chain is bound to two or three water molecules [Buzzuto 2015; Naumann 1999]. This creates a hydration shell around PEG chains in a gauche conformation as can be seen in Figure 1.2 [Buzzuto 2015; Castro 2014; Gref 2012; Savva 1998; Vermette 2003; Wattendorf 2008]. This *gauche* conformation (as opposed to a *trans* conformation) further aids in resistance against proteins and other serum components and subsequently provide escape from the MPS [Buzzuto 2015; Castro 2014; Gref 2012; Savva 1998; Vermette 2003; Wattendorf 2008]. Recently, polymer chain flexibility along with hydrophilicity has been proposed as another major contributing factor to protect the surfaces against biomolecules adsorption [Gref 2012; Wattendorf 2008]. Reports suggested that polymers (e.g. maltopentaose and dextran) more hydrophilic in nature than PEG molecules had a shorter circulation time and were not sufficient enough to protect the surfaces against opsonization [Blume 1993; Gref 2012]. It is believed that the flexible, mobile, and rapidly changing conformations of PEG chains form a dense “conformational cloud” making it challenging for the immune system to generate an antibody for it [Gref 2012; Torchilin 1995]. Hence, PEG possesses

both features, hydrophilicity and flexibility, to make it an excellent candidate for protecting surfaces against non-specific protein binding [Gref 2012].

Surfaces modifications with PEG are applied in several ways including (i) covalent grafting, (ii) physical adsorption and (iii) incorporation of PEG-phospholipid conjugates [Damodaran 2010; Das Santos 2007; Immordino 2006; Moghimi 2001; Pallua 2011; Wattendorf 2008]. The latter method will be used in our study due to its promising results in suppressing the protein adsorption onto membrane-mimetic surfaces [Baekmark 1995; Immordino 2006; Stepniewski 2011; Takemoto 2011]. Most importantly, the non-fouling property of PEG molecules essentially relies on the surface chain density and the molecular weight (MW) or chain length being incorporated in the membranes [Castro 2014; Damodaran 2010; Efremova 2001; Gref 2000; Hristova 1995; Karatekin 2012; Liu 2014; Luna 2011; Taylor 2012; Vermette 2003; Wattendorf 2008]. Hence, a development of dense and thick layers of PEG chains with appropriate molecular weight is of great potential interest in the biomedical field to efficiently protect the membrane-mimetic surfaces against dissolved biomolecules adsorption.

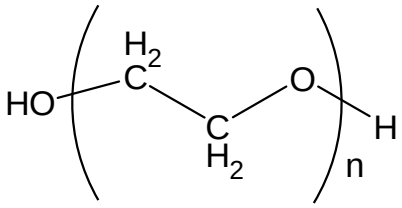

Figure 1.1. Illustration of poly(ethylene glycol) PEG monomer chemical structure with "n" representing the repeating unit.

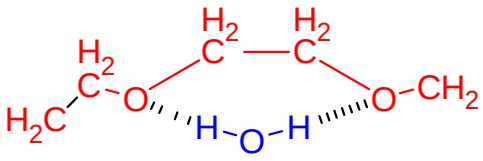

Figure 1.2. Chemical drawing demonstrating the *gauche* conformation of poly(ethylene glycol) PEG and its hydrogen bonding with water molecule. Structure is drawn based on Bjorling 1991, Naumann 1999 and Wattendorf et al. 2008.

1.2. Types of PEG Chain Length Grafted onto Membrane-Mimetic Surfaces.

There is a wide range of PEG molecules available commercially in terms of molecular weight or chain length to be incorporated into membrane-mimetic surfaces. However, the success of these PEGylated membranes is highly dependent on the type of application and type of PEG chain being employed [Efremova 2001; Gref 2000; Hristova 1995; Liu 2014; Luna 2011; Vermette 2003; Wattendorf 2008; Xu 2000]. For example, PEGylation of membrane-mimetic surfaces with low molecular weight PEG (less than 1000 Da) have been reported to reduce the biomolecule interaction only at a very high PEG surface density (in a range of 20 – 50 mol%) [Needham 2000; Pappalardo 2005]. PEG molecules with short chain length tend to form mushroom conformations, which is not always effective against dissolved biomolecules adsorption [Hasan 2015; Luna 2011]. Intermediate PEG chain length ranging from 1000 – 5000 Da is more frequently used in order to achieve optimum dissolved biomolecule repellence [Gref 2000; Hasan 2015; Hashizaki 2003; Hristova 1995; Liu 2014; Moghimi 2001; Morille 2008; Vermette 2003; Wattendorf 2008]. This range has also been identified as suitable for its use as a copolymer to suppress opsonization and subsequently low phagocytic uptake [Gref 2000; Moghimi 2001; Wattendorf 2008]. Long PEG chain lengths over 5000 Da have been used in membrane models but these studies do not show further reduction in protein adsorption as that from intermediate PEG chain length [Gref 2000; Vermette 2003]. Furthermore, it has also been suggested that incorporation of long PEG chain length results in a phase separation in membrane models [Bedu-Addo 1996; Pappalardo 2005], which might be a disadvantage for biomedical applications including nanosensor templates, microfluidic

devices and therapeutic/diagnostic agents carriers. Overall, a PEG chain length of 2000 Da has shown tremendous success for optimum repellency against non-specific protein interactions and avoidance from mononuclear phagocytic system (MPS) and hence, has been used in our studies [Gref 2000; Liu 2014; Luna 2011; Moghimi 2001].

1.3. PEG Grafting Density on the Membrane-Mimetic Surfaces.

PEG surface grafting density refers to the amount of PEG-phospholipid conjugates being incorporated in the membrane-mimetic surfaces with the optimum bio-non-fouling properties. Numerous reports have associated the performance of PEGylated membrane models with the optimum grafting density of PEG-phospholipid conjugates [Bedu-Addo 1996; Belsito 2000; Edwards 1997; Gref 2000; Lasic 1991; Montesano 2001; Pappalardo 2005; Szleifer 1998; Taylor 2012]. Based on several reported data, liposomes and vesicles usually have a PEG grafting density between 4 – 10 mol% with MW of 2000 – 5000 g/mol for optimum performance [Baekmark 1995; Bedu-Addo 1996; Dos Santos 2007; Gref 2000; Hashizaki 2003; Lasic 1991; Lasic 1995; Liu 2014; Papplardo 2005]. Liposomes are known to become unstable with higher PEG grafting density due to increased lateral pressure among PEG chains [Lasic 1995]. Bilayers can normally incorporate up to 10 mol% of PEG, with MW of 2000 g/mol, without compromising the structural stability [Barenholz 2001; Belsito 2000; Hristova 1995; Ickenstein 2003; Stepniewski 2011]. Based on these studies, it can be surmised that grafting density along with the polymeric chain length (Molecular weight) are critical for

selecting the mixture composition in order to develop PEGylated membrane-mimetic surfaces with highly controllable properties.

As discussed above, it is really important to select an appropriate mixture composition in terms of PEG grafting density to optimize the performance of PEGylated membrane-mimetic surfaces. Many reports have suggested the optimal PEG grafting density in the phospholipid mixtures to be somewhere in the range of 1 – 9 mol% [Allen 2002; Barenholz 2001; Bedu-Addo 1996; Belsito 2000; Dos Santos 2007; Lasic 1991; Lasic 1995; Luna 2011; Stepniewski 2011; Vermette 2003]. However, the specific PEG content in terms of mol% PEG has not been identified yet. Previous studies suggest that optimum performance of PEGylated membrane-mimetic surface can be achieved with a minimum PEG concentration of 2 mol% to a maximum concentration of 20 mol% [Lasic 1995; Luna 2011; Dos Santos 2007]. Hence, this study was also motivated to determine the most efficient PEG content in terms of mol% that can be incorporated in the membrane for optimum performance, an aspect which has not gained much attention yet, to the best of our knowledge.

In addition, the type of PEG chain and its grafting density may not be the only factors contributing towards the effectiveness of membrane-mimetic surfaces. Analysis of the data available in the literature suggests that lateral distribution of PEG can also influence the efficiency of PEGylated membrane-mimetic surfaces. In this study, we have attempted, for the first time, to assess the effect of PEG lateral distribution on the bio-non-fouling properties of membrane-mimetic surfaces. Detailed analyses of lateral

distribution of PEG as well as its effect on the membrane-mimetic surfaces can also help elucidating the mechanistic nature of proteins and membrane-mimetic surfaces interactions.

1.4. Non-Specific Interactions of Proteins with Membrane-Mimetic Surfaces.

Membrane-mimetic surfaces *in vivo* are prone to non-specific interactions with numerous types of dissolved molecules (e.g. proteins), which subsequently leads to disintegration, reduced efficiency, and rapid clearance by MPS [Allen 1991; Dhruv 2009; Kim 1999; Moghimi 2001; Popovska 2013; Savva 1998; Vermette 2003]. Non-specific interaction refers to a non-covalent interaction between membrane-mimetic surfaces and proteins. Non-specific interactions of proteins usually occur as accumulation, penetration and/or adsorption mechanism onto the surfaces [Dhruv 2009; Moghimi 2001; Popovska 2013; Shahid 2013]. Various types of protein/membrane interactions can be associated to non-specific interactions. Among these electrostatic interactions, hydrophobic interactions, and hydrogen bonding are considered as the key players for non-specific interactions between protein and membrane-mimetic surfaces [Dhruv 2009; Grudzielanek 2007; Moghimi 2001; Vermette 2003]. Types of non-specific interactions are in fact based on two important factors: (i) physicochemical properties of membrane and (ii) physicochemical properties of protein that binds to it [Immordino 2006]. Physiochemical characteristics of membrane-mimetic surfaces include phase state, hydrophobicity, net surface charge, morphology, headgroup size, acyl chain length, packing and fluidity of the membrane [Immordino 2006; Moghimi 2001; Shahid 2013; Vermette 2003]. On the

other hand, physiochemical properties of dissolved biomolecules include size, net charge, hydrophobicity/hydrophilicity, and flexibility of structural domains [Dhruv 2009; Immordino 2006; Moghimi 2001; Torchilin 1995; Vermette 2003]. It is of great interest to understand the mechanistic nature of non-specific protein/membrane interactions for the rational design of bio-non-fouling membrane-mimetic surfaces with controlled and predictable characteristics.

1.5. Effect of Phase State on the Interactions of Dissolved Biomolecules and Membrane-Mimetic Surfaces.

Phase state, among other factors, plays a key role in the localization of dissolved biomolecules onto the membrane-mimetic surfaces. For instance, some proteins have a greater tendency towards the liquid disordered (L_d) phase than the gel phase ($L_{\beta'}$) of the membrane. In monolayer models, L_d and $L_{\beta'}$ phases are referred to as liquid expanded (LE) and liquid condensed (LC) phase, respectively. A few proteins have been reported to partition into the liquid condensed phase of the membrane models. Hence, investigating the nature of these preferential interactions can yield significant insights to reduce non-specific protein binding onto membrane-mimetic surfaces.

1.6. Phase Behavior of PEGylated Membrane-Mimetic Surfaces.

Incorporation of PEG-phospholipid may have a great impact on the phase behavior of membrane-mimetic surfaces. Several studies have reported the coexistence of

LC and LE phase in PEGylated phospholipid membranes [Hashizaki 2003; Lozano 2009a; Shahid 2011]. A few studies have suggested that high concentrations of PEG may induce the LE phase, phase separation or formation of open bilayer discs phase in a typical condensed type membrane model [Baekmark 19995; Ickenstein 2003; Kneidl 2014], which can subsequently lead to increased dissolved biomolecule interactions with the membrane. Hence, understanding the effect of PEG-phospholipid on the membrane phase behavior could allow for better tuning the PEGylated membrane-mimetic surfaces for numerous biomedical applications.

1.7. Role of Proteins' Physicochemical Properties on the Non-Specific Interactions with PEGylated Membrane-Mimetic Surfaces.

As described above, physicochemical properties of dissolved biomolecules, for example hydrophobicity, size, shape, charge, and flexibility of structural domains, are considered key parameters in the non-specific interactions with PEGylated membrane-mimetic surfaces [Dhruv 2009; Immordino 2006; Moghimi 2001; Torchilin 1995; Vermette 2003]. When it comes to non-specific interactions, hydrophobic interactions play a prominent role in the protein/ PEGylated membrane interactions [Mollmann 2006; Sezgin 2012; Vermette 2003; Yang 2011]. It is believed that hydrophobic residues of proteins insert into the hydrophobic aliphatic chains of phospholipid molecules in order to minimize their unfavorable energetic exposure to the aqueous environment [Birdi 1976; Mollmann 2006; Sezgin 2012; Vermette 2003]. It has also been suggested that lipids in the membrane adapt to match various lengths of peptide domains in order to ease the access with the phenomenon described as hydrophobic matching [Sezgin 2012].

Hence, it can be deduced that non-specific interactions of proteins with PEG-grafted membrane-mimetic surfaces can be primarily driven by hydrophobic interactions.

The net charge of a protein can also be of great importance in the non-specific interactions with PEGylated membrane-mimetic surfaces. Several studies have suggested that proteins with an overall positive charge at the physiological pH may be more attracted to PEG surfaces bearing a negative charge [Vermette 2003]. On the other hand, the negative charge on the proteins may introduce a negative electrostatic barrier between the protein and PEG-grafted surfaces [Farias 1989; Vermette 2003]. However, it should also be noted that proteins with an overall negative charge may expose their positively charged amino acid residues at a certain conformation, which might result in attractive electrostatic interactions with the PEG-grated membrane-mimetic surfaces as opposed to repulsive interactions. [Nylander 1994; Vermette 2003]. Previous studies have suggested that PEG chains in the membrane-mimetic surfaces might attract some dissolved biomolecules rather than repel them [Efremova 2001; Taylor 2012; Xu 2000]. Moreover, PEG chains on the membrane models have shown significant steric repulsion towards large proteins such as human serum albumin (HSA) [Lee 2016; Rahamati 2008; Vermette 2003]. However, PEG chains might not experience the compression and do not efficiently reduce the penetration of small proteins. Therefore, understanding the intricate interactions of PEG-grafted membranes with small proteins is crucial to designing controlled membrane-mimetic surfaces for various biomedical applications.

1.8. Objectives.

The objectives of this study include:

- to investigate the phase behavior of different types of PEG-grafted phosphocholine membrane under physiological conditions
- to study the effect of aliphatic chain length and PEG content on the phase behavior of PEGylated phosphocholine membrane models
- to elucidate the effect of non-specific interactions of small protein, insulin, on the phase behavior of PEGylated membrane models
- to investigate the effect of insulin/membrane interactions on the conformational changes and folding/unfolding states of insulin
- and, most importantly, to determine the optimal mixture composition, in terms of aliphatic chain length and PEG content, that can stabilize the LC/gel phase in the membrane, enhance the homogeneous distribution of PEG chains as well as reduce the non-specific adsorption of small proteins e.g. insulin on the membrane models.

The outcome of this study can be used to further fill the gap to improve the efficiency of bio-non-fouling membrane-mimetic surfaces in many biomedical applications including nanosensors templates, microbubbles, nanoscale size exclusion filters for microfluidic devices as well as therapeutic carriers.

1.8.1. The Membrane Models for Membrane-Mimetic Surfaces.

Monolayers and unilamellar vesicles have been selected as models for PEG-grafted membrane-mimetic surfaces. Both types of models offer distinct information and are prepared by incorporating PEG-phospholipid conjugates in the host matrix phospholipids, as will be elaborated below in detail.

1.8.1.1. Langmuir Monolayer as a Membrane Model.

Langmuir phospholipid monolayers have been extensively used as two dimensional controlled experimental models for biological membranes as well as precursors of membrane-mimetic surfaces [Collier 2001; Li 2014; Lozano 2009a; Luna 2011; Stefaniu 2014a; Stefaniu 2014b; Stepniewski 2011; Ziblat 2011]. A Langmuir monolayer represents half of a biological membrane (c.f. Figure 1.3 A and B). Monolayers are usually constructed on a Langmuir trough by spreading amphiphilic molecules onto the aqueous phase (Figure 1.3). The Langmuir trough is made of Teflon with two moveable Teflon coated barriers that are used to control the area available to amphiphilic molecules Figure 1.3 C [Gaines 1966]. Upon spreading, the hydrophobic aliphatic chains of phospholipids orient towards the air whereas the hydrophilic region submerge in the aqueous phase [Gaines 1966; Dhruv 2009; Li 2014]. At this point, molecules are disordered, which means that they are spread over a large area and do not experience much interactions from each other [Shahid 2013; Dhruv 2009]. When the barriers begin to compress, amphiphilic molecules come in contact with each other and

form a tightly packed monolayer. This facilitates investigating different aspects including packing and phase state of a monolayer at the air/aqueous interface [Dhruv 2009; Li 2014]. This system can be represented using a surface pressure plot with respect to molecular area available to each molecule. This plot is known as the surface pressure – area, π – A, isotherm [Dhruv 2009; Gaines 1966] and will be described in more detail below. The technical specifications of Langmuir trough as well as equations used to calculate area per phospholipid molecule and molecular area have been explained in detail elsewhere and hence, will not be discussed herein [Shahid 2013; Jebrail 2007; Nosrati 2010

Being a model system prepared on a smooth aqueous surface, monolayers can offer direct control over a wide range of parameters to examine the intermolecular interactions, membrane dynamics as well as generic phase behaviour [Collier 2001; Gaines 1966; Li 2014]. These parameters include surface (lateral) pressure, area per amphiphilic molecule, temperature, surface potential, pH, phospholipid compositions, PEG content, aliphatic chain length, packing conditions, viscosity, molecules mobility, subphase components as well as monolayer/protein interactions [Li 2014; Dhruv 2009; Mohwald 1990; Nunes 2011; Shahid 2011; Shahid 2013; Stefaniu 2014a; Stepniewski 2011; Tanwir 2012; Ziblat 2011]. A major advantage of Langmuir monolayer technique lies in the possibility of interfacing it with various other techniques to acquire extensive knowledge about the physical dimensions of monolayers. Some of the advanced techniques include epifluorescence microscopy (EFM), Brewster angle microscopy (BAM), infrared reflection – absorption spectroscopy (IRRAS), grazing incidence X-ray

diffraction (GIXD), UV-vis absorption, and surface potential [DeWolf 1999; Jebrail 2008; Li 2014; Shahid 2013; Stefaniu 2014a, Stefaniu 2014b; Tsoukanova 2008]. Phospholipid monolayers have been used as one of the key membrane models in this study.

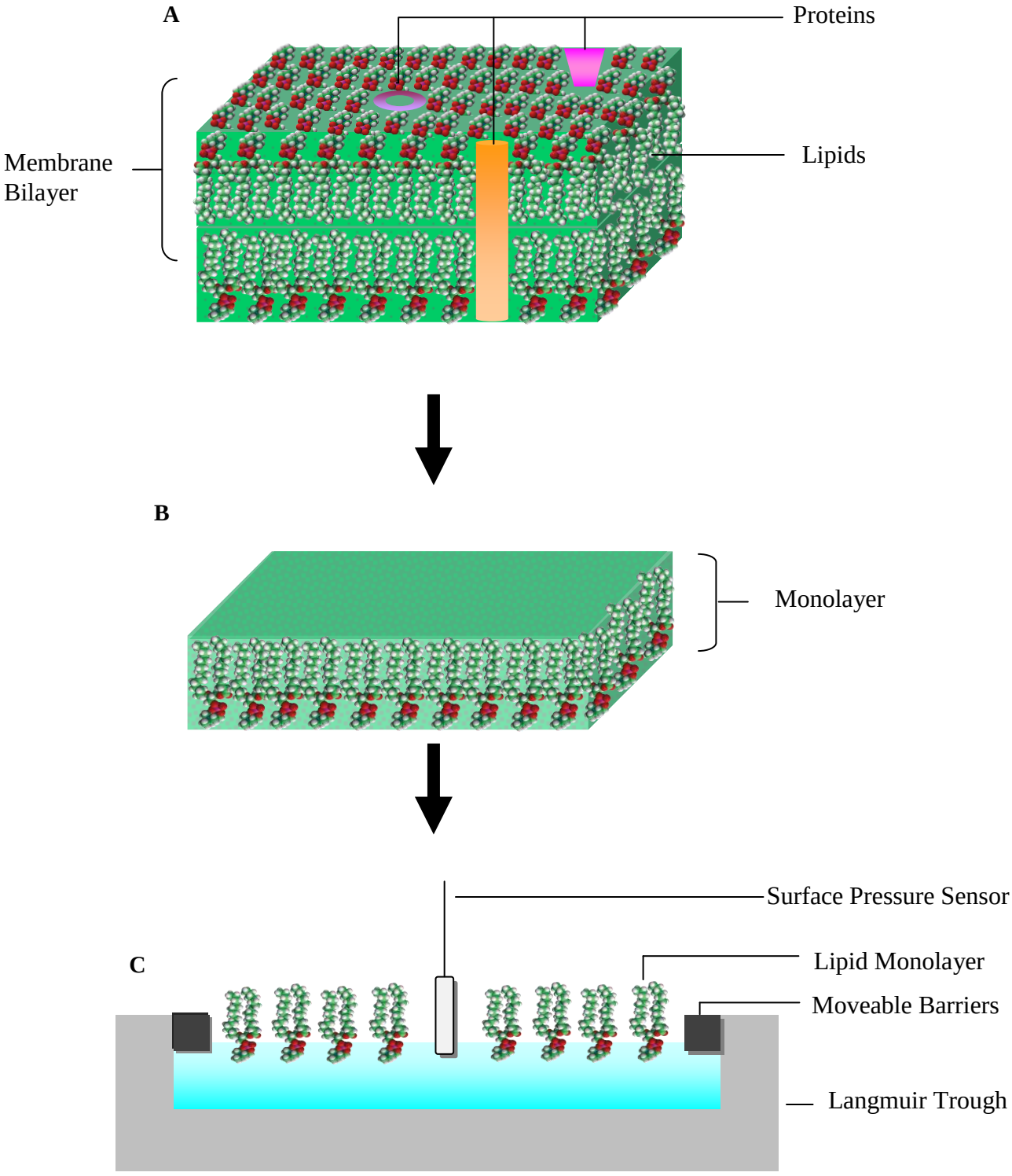

Figure 1.3: Schematics illustrating **(A)** a sketch of a typical biological membrane bilayer with lipids and different types of proteins embedded in the membrane, **(B)** a single layer of the membrane (monolayer) and **(C)** a lipid monolayer at the air/aqueous interface on the Langmuir trough mimicking the membrane. Sketches made are based on Li 2014 and Avanti Polar.

1.8.1.2. Unilamellar Vesicle as a Membrane Model.

Unilamellar phospholipid vesicle has been widely studied as a membrane model to elucidate various properties of membranes including lateral structure, phase behavior, packing order, as well as mechanical properties [Akashi 1996; Bagatolli 2000; Bagatolli 2006; Juhasz 2012; Mathievet 1996; Peterca 2011; Wesolowska 2009]. A schematic diagram of a unilamellar vesicle is illustrated in Figure 1.4. The formation of a phospholipid vesicle is considered to be a two-step self-assembly process [Antonietti 2003]. In the first step, phospholipids form a bilayer, which subsequently closes up to form a vesicle in order to avoid its hydrophobic regions exposed to aqueous media at its edges [Antonietti 2003; Collier 2011; Walde 2001]. However, vesicles do not form spontaneously as they are not usually thermodynamically stable. The formation of stable and monodisperse vesicles greatly depends on the physical properties of the amphiphiles as well as the experimental conditions [Peterca 2011; Walde 2001]. Several methodologies are utilized in order to generate vesicles with high stability and properties of interest such as size, polydispersity, morphology and etc. This includes electroformation, solvent evaporation, and gentle hydration method [Akashi 1996; Bagatolli 2000; Bagatolli 2006; Bozzuto 2015; Korlach 1999; Manley 2008; Moscho 1996; Wesolowska 2009]. Although electroformation is considered by far to be the most successful method used to obtain high yield of giant unilamellar vesicles (GUVs); we have utilized the latter two protocols to produce PEGylated GUVs, as discussed in detail in Chapter 6. This is due to the buffer, salts and other constituents used in the

experiments that may potentially interfere with the electric field and produce artifacts in the vesicle membrane [Manley 2008].

The terms liposome (from the Greek, the body of lipids) and vesicle (from the Latin, small bubble) are used interchangeably in biomaterial research [Antonietti 2003; Walde 2001]. This is due to the fact that unilamellar vesicles, in particular GUVs, are only greater in magnitude as compared to liposomes, with an average size of a few tens of micrometers [Bagatolli 2000; Bagatolli 2006; Korlach 1999; Suga 2013; Walde 2001; Wesolowska 2009]. It is their greater size, similar to the range of the membrane of a cell, which makes GUVs an excellent membrane model system because single vesicles can be directly visualized using different microscopy techniques. Some of these techniques include phase contrast, immunoelectron, fluorescence, and confocal fluorescence microscopy [Bagatolli 2000; Bagatolli 2006; Juhasz 2012; Kalvodova 2005; Korlach 1999; Morales-Penningston 2010; Veatch 2003; Wesolowska 2009]. Therefore, vesicles have been extensively studied as a membrane model to comprehend the mechanistic nature of lipid – lipid, lipid – DNA, lipid – RNA, and lipid – protein interactions [Bagatolli 2006; Korlach 1999; Kalvodova 2005; Nunes 2011; Suga 2013; Wesolowska 2009]. Another notable advantage of using vesicles as a membrane model system lies in the ability to control the mixture composition, PEG content as well as experimental conditions such as temperature, pH, osmotic pressure, and etc. [Akashi 1996; Bagatolli 2006; Korlach 1999; Mathivet 1996; Nunes 2011; Veatch 2003; Wesolowska 2009]. Hence, this report will include the complete preparation protocols of PEGylated phosphocholine giant and small unilamellar vesicles membrane models (GUVs and

SUVs) as well as their use to understand various properties of membrane and protein/membrane interactions.

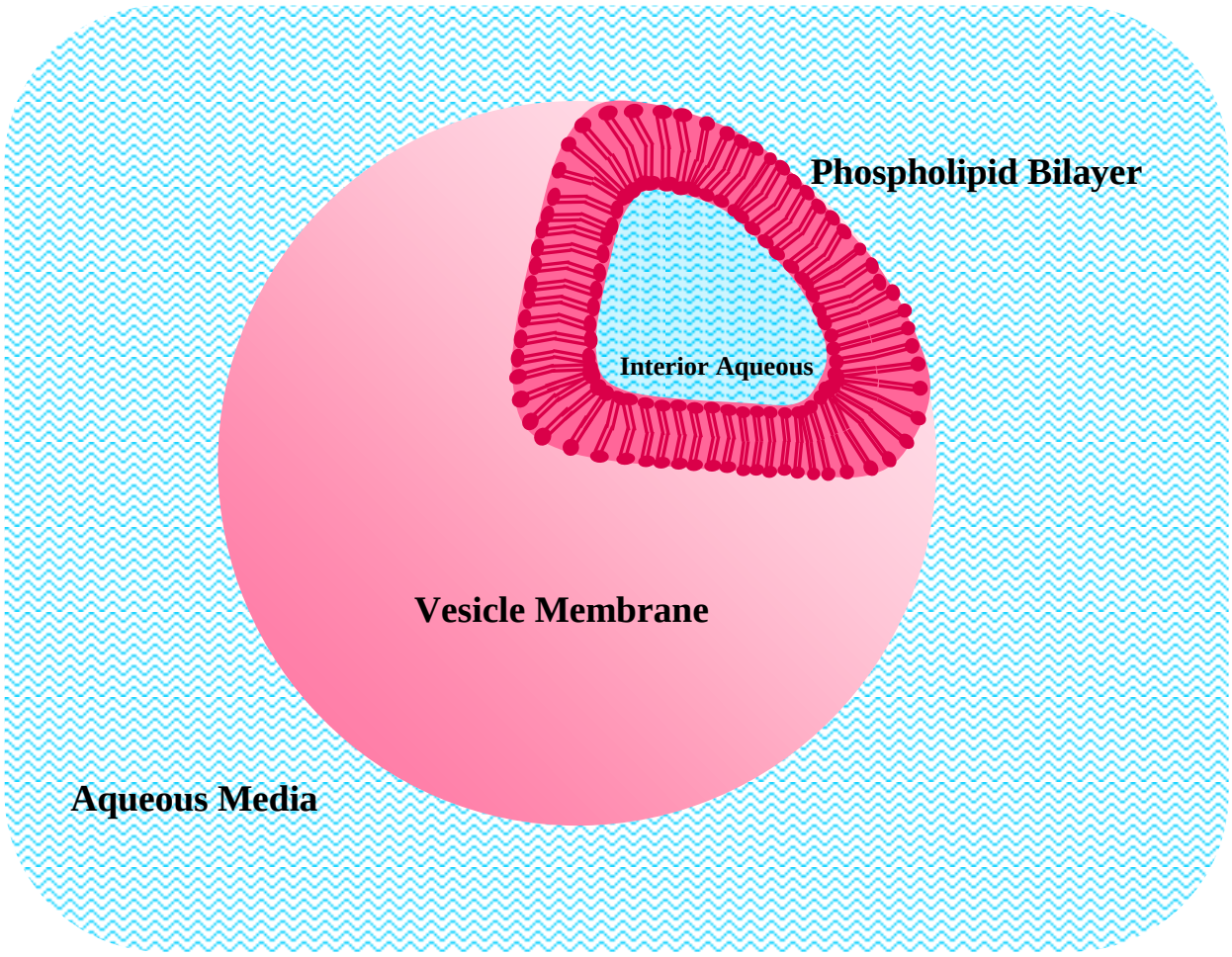

Figure 1.4: Cartoon sketch of phospholipid unilamellar vesicle as a membrane model in aqueous media. Sketch is constructed based on information from Bozzuto 2015; Collier 2001 and Kneidl 2014.

1.8.2. Selection of Matrix Phospholipid for Membrane Models.

Two disaturated phospholipids bearing either C_{16} (DPPC) or C_{18} (DSPC) aliphatic chains have been selected as the host matrix phospholipids in this study. Both synthetic phospholipids, dipalmitoyl phosphocholine (DPPC) and distearoyl phosphocholine (DSPC) are zwitterionic with a difference of only 2 CH_2 groups in their aliphatic chain, as can be seen in Figure 1.5 [Lewis 2000]. Zwitterions generally contain both negatively and positively charged groups thus making them overall neutral phospholipids [Lewis 2000]. Phosphatidylcholines (PC) have been found to be one of the most abundant phospholipids in natural plasma membranes, in particular in the exterior layer of the erythrocytes [Conde 2011; Lewis 2000; Li 2015; Nunes 2011]. In fact, lipid components, in particular zwitterionic phosphatidylcholines, comprising the exterior surface of the erythrocytes membrane are known to be non-thrombogenic [Lewis 2000]. This phenomenon leads to the distinct development of membrane-mimetic surfaces containing phosphocholine phospholipids and their structural analogues [Lewis 2000]. Indeed, reports show that liposomes resembling the outer layer of erythrocytes are more resistant to clearance by mononuclear phagocyte system (MPS) [Lewis 2000; Nunes 2011]. Hence, PC-based surfaces have been successfully used in many biomedical applications including soft contact lenses due to high water and oxygen transmissibility as well as low fouling properties [Chou 2002; Conde 2011; Lewis 2000]. Zwitterionic phosphocholine phospholipids, with even numbers of carbons, have also been used widely in several biomedical studies due to their favorable characteristics including stability, low surface tension, lateral rigidity, non-toxicity, biodegradability, and low fouling properties [Bedu-

Addo 1996; Belsito 2000; Chou 2002; Dos Santos 1999; Ickenstein 2003; Kim 2004; Li 2015; Lozano 2009a; Lozano 2009b; Maruyama 1997; Papahadjopoulos 1973; Stepniewski 2011; Walde 2001; Vermette 2003]. Thus, phosphocholines, with C_{16} or C_{18} acyl chain length, grafted with PEG-phospholipids have been used in this study to comprehend the phase states and various other aspects to aid in improving the efficiency of membrane-mimetic surfaces, in particular under physiological conditions.

(a)

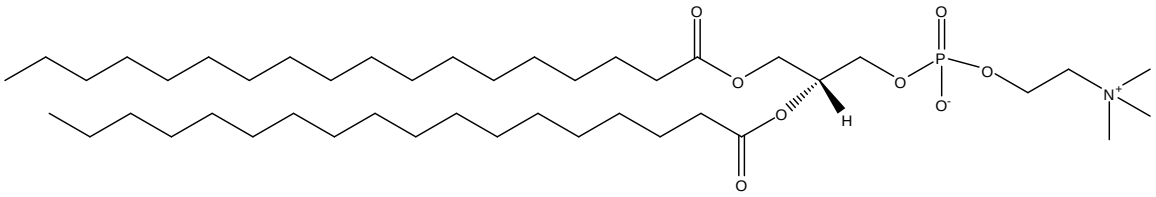

(b)

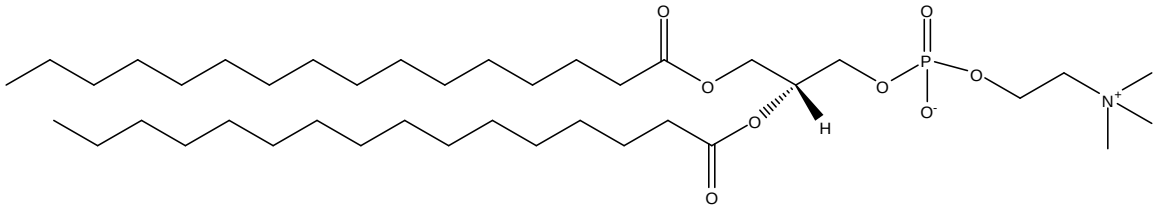

Figure 1.5: Chemical structures of (a) DSPC and (b) DPPC. Structure is made based on information from Kneidl 2014; Lewis 2000; Luna 2011; and Stepniewski 2011.

1.8.3. Selection of PEG-Phospholipid Conjugate for Membrane Models.

Two PEG-phospholipid conjugates, DPPE-PEG2000 and DSPE-PEG2000, have been selected to be introduced in the host phosphocholine membrane models in this study. DPPE-PEG2000 and DSPE-PEG2000 contain C_{16} and C_{18} aliphatic chains, respectively, with a phosphoethanolamine headgroup bearing poly(ethylene glycol) of 45 PEG monomers with a molecular mass of 2000 g/mol (Figure 1.6). PEGylated phospholipids, in particular DSPE-PEG2000 and DPPE-PEG2000, have been widely used in various biomedical formulations due to low toxicity, biocompatibility, bio-non-fouling as well as ease of excretion properties [Belsito 1998; Janout 2012; Luna 2011; Maruyama 1997; Pappalardo 2005; Vukovic 2011]. These formulations include micelles, immunoliposomes, vesicles, and ultrasound contrast reagents. Most importantly, DSPE-PEG2000 is a key component in a U.S. FDA approved pharmaceutical formulation, known as Doxil [Janout 2012; Jin 2014; Li 2015]. Doxil is a PEGylated liposomal carrier loaded with an anti-cancer drug (doxorubicin) for the treatment of various diseases including ovarian cancer and AIDS-related Kaposi sarcoma. PEG-phospholipids have also been studied for cell-specific targeting where a target-specific ligand is covalently attached to the distal end of PEG molecule to allow active targeting via receptor mediated endocytosis [Maruyama 1997; Morille 2008]. Moreover, PEG-phospholipid (DPPE-PEG or DSPE-PEG) has also been successfully used *in vitro* to conjugate anti-thrombogenic enzyme (urokinase) on the islets' cell surface in order to control thromobosis formation and improve the treatment of type I diabetes [Takemoto 2011]. Over the years, numerous studies have been carried out to explore different aspects of phospholipid membranes

grafted with DPPE-PEG2000 or DSPE-PEG2000 in order to improve the performance of membrane-mimetic surfaces [Belsito 1998; Chou 2002; Janout 2012; Kneidl 2014; Lozano 2009a; Luna 2011; Maruyama 1997; Pappalardo 2005; Stepniewski 2011; Walde 2001; Vermette 2003; Vukovic 2011]. However, the effect of PEG-phospholipids and its lateral distribution on the phase behavior of phosphocholine membrane, in physiological conditions, have not been deeply explored [Kim 2004]. Hence, one of the main objectives of this study is to probe the effect of PEG-phospholipid on the phase behavior of phosphocholine membranes under physiological conditions relevant to *in vivo* applications including phosphate buffered saline (PBS) at 20 ^{o}C. The results obtained can serve as a guideline in interpreting and tuning the properties of PEGylated membrane-mimetic surfaces.

(a)

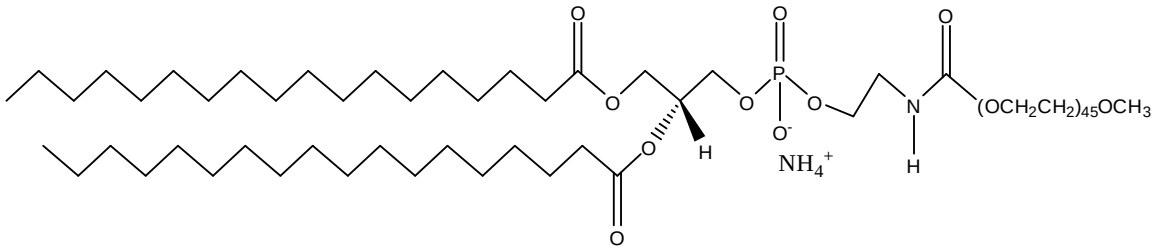

(b)

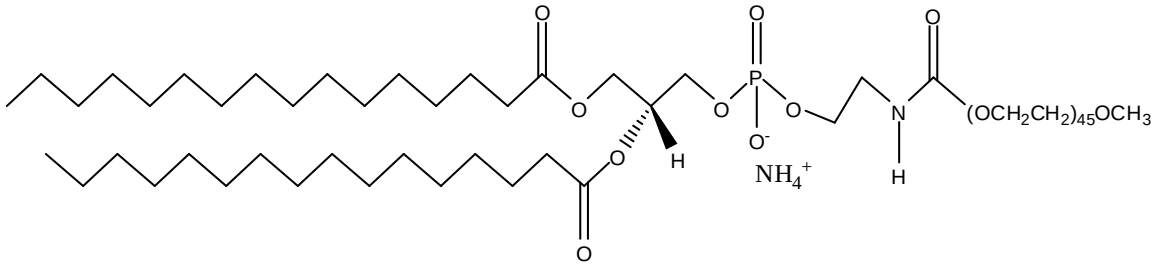

Figure 1.6: Chemical structures of (a) DSPE-PEG2000 and (b) DPPE-PEG2000. Chemical structures are drawn based on Kneidl 2014; Luna 2011; and Stepniewski 2011.

1.8.4. Selection of Insulin as a Model Protein.

Human insulin has been chosen as a representative of small size proteins for this study to understand the non-specific interactions of proteins with membrane models (Figure 1.7). The reason for selecting a small protein is due to the fact that non specific interactions of large proteins (such as bovind serum albumin (BSA)) and PEGylated membrane models have been studied extensively [Rahmati 2008; Vermette 2003; Zhao 2002]. Additionally, PEG chains on the surfaces have shown significant steric repulsion towards large proteins but might not experience the compression and do not efficiently reduce the penetration of small proteins and hence has been the focus of our study [Rahamati 2008; Vermette 2003]. Insulin is a small protein with 51 amino acids and bears an overall negative charge, –2 per monomer, in the presence of PBS subphase with a pH of about 7.4 [Farias 1989; Henry 2008]. The hydrodynamic diameter of zinc-free human insulin monomer has been approximated to be 3 nm with molecular dimensions of 2 x 2.5 x 2 nm^3 [Liu 2002; Henry 2008]. The interaction surface of insulin is comprised of two segments including a hydrophobic binding core and a hydrophilic surface [Liang 1994]. Insulin is also considered to be a protein, which can promote the hydrophobic interactions in order to avoid exposure to the aqueous environment by inserting its hydrophobic residues into the aliphatic region of the phospholipid membrane [Birdi 1976; Farias 1989; Grudzielanek 2007; Kadima 1993; Liang 1994; Liu 2002; Nieto-Suarez 2008; Rand 1972; Vermette 2002; Yang 2011]. Few reports have also suggested that insulin changes its conformation by partially submerging its hydrophilic residues in to the subphase [Nieto-Suarez 2008]. Although bearing an overall net negative charge, insulin has shown

attractive electrostatic interactions towards negatively charged surfaces, depending on its orientation [Nylander 1994; Vermette 2003]. Hence, it is of great interest to obtain a sound understanding of such unique and complex interactions of insulin with PEGylated membranes. The findings of such a study can aid to improve the quality and performance of various bio-non-fouling membrane-mimetic surfaces.

Figure 1.7: The structure of human insulin (**PDB ID: 2JV1;** Bocian et. al. 2008).

1.9. Methodology.

A comprehensive analysis of PEGylated phosphocholine membranes models has been carried out by utilizing different methodologies under various experimental conditions, as outlined below.

1.9.1. Surface Characterization of Monolayer Model at Air/PBS Interface.

Mixed monolayers of a matrix phosphocholine and a PEG-phospholipid grafted with a PEG chain of molecular weight 2000 (PEG2000) were formed on PBS subphase at 20 ^{o}C. Two types of binary mixtures selected for this study include DPPC/DPPE-PEG2000 and DSPC/DSPE-PEG2000 with a PEG content of 1, 3, 6, and 9 mol%. Analysis of phase behavior in terms of phase state and phase transitions was performed by π – A isotherm measurements. These measurements were further used for miscibility, PEG conformational, and compressibility analyses at physiological conditions including temperature and PBS subphase, pH ~7.4.

1.9.1.1. Surface (Lateral) Pressure – Area, π – A, Isotherm.

When a Langmuir monolayer is compressed, change in surface (lateral) pressure is recorded with respect to the change in area per phospholipid molecule. This produces a π – A isotherm (Figure 1.9) [Dhruv 2009; Gaines 1966; Li 2014]. Changes in the slope of the isotherm can reveal crucial information about the phospholipid packing, phase state,

etc. In particular, as shown in the Figure 1.9, when the phospholipid solution is spread on to the aqueous subphase, all the phospholipids are apart from each other and are in a disordered phase. This phase is referred to as the gaseous phase (G). Upon compression, the molecules start to come close to each other and this phase is known as the liquid expanded phase (LE). A plateau may emerge, which corresponds to the coexistence of the liquid expanded and liquid condensed phase. At this point, half of the phospholipid molecules are believed to be in a random orientation while others begin to align close to each other. Further compression leads to a steep straight line after the plateau, known as a low-compressibility region in the π – A isotherm [Mohwald 1990]. This refers to a liquid condensed (LC) phase of the monolayer. Eventually, the isotherm reaches a point where the monolayer collapses [Gaines 1966; Nakahara 2014]. A collapse point (C) corresponds to a pressure where the monolayer loses it stability by disruption in the phospholipid packing [El-Khouri 2009; Gaines 1966]. Advantages of π – A isotherm also include determining the limiting area of a phospholipid molecule in a closely packed state. This is achieved by extrapolating the low-compressibility region of the π – A isotherm to $\pi = 0$ mN/m as indicated by the dashed line in Figure 1.9. π – A isotherm can, hence, be a very beneficial tool in order to understand the effect of different mixture compositions and packing states on monolayer phase behaviour.

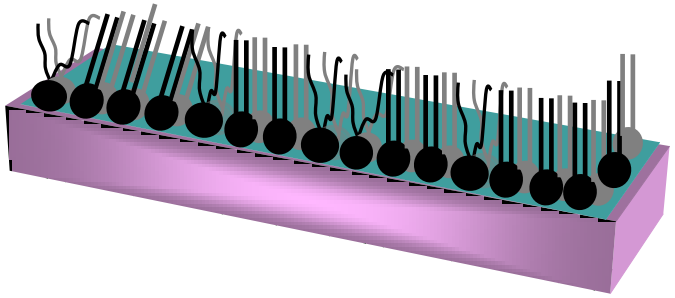

Figure 1.8: Cartoon sketch illustrating a phospholipid monolayer model at air/aqueous subphase on a trough. Cartoon is prepared based on Li et al. 2014.

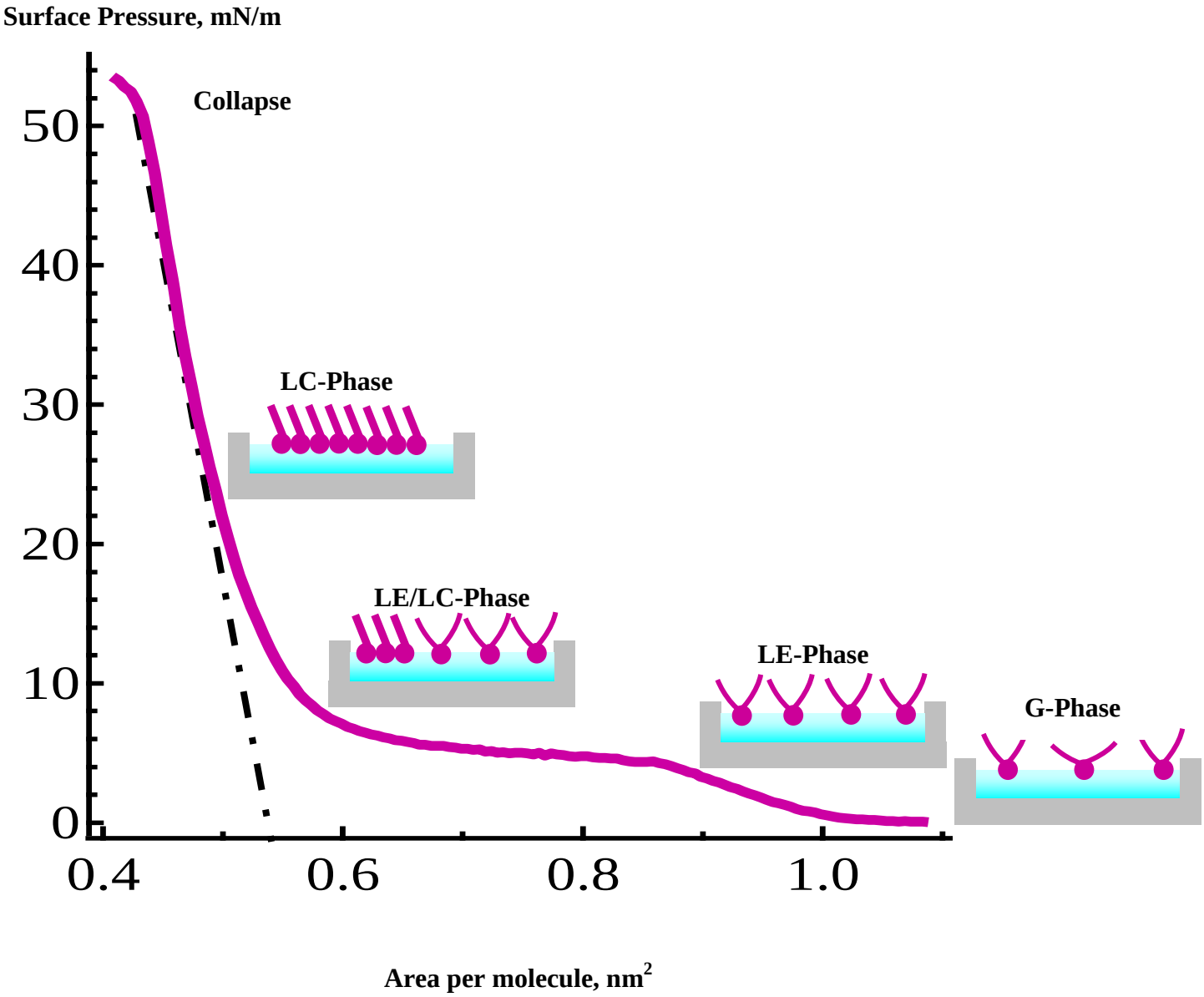

Figure 1.9.: A Schematic diagram of a typical phospholipid monolayer π – A isotherm at air/aqueous interface with cartoons depicting development of various unique phases during compression for illustration purpose. This includes gaseous phase depicted as a G phase in the diagram, liquid expanded phase represented as a LE phase, coexistence phase as LE/LC phase, liquid condensed phase shown as a LC phase and collapse point of the monolayer. Drawings made are based on Gaines 1966 and Dhruv 2009.

1.9.2. Monolayer Area Expansion Measurements.

Langmuir trough can also be used to monitor protein/membrane interactions by measuring the protein-induced expansion of monolayer area. The measurement is carried out by first preparing the monolayer compressing it to a preset surface pressure, π, value. The monolayer surface pressure is then kept constant while monolayer area is allowed to expand upon insulin injection in the subphase underneath the monolayer. The measurements afford the quantification of insulin/monolayer interactions including change in monolayer molecular area, ΔA, insulin penetration area, A_{ins}, and binding degree of insulin, χ_{ins} calculations. Details about carrying out the measurements and quantification of insulin/monolayer interactions are explained in Chapter 4.

1.9.3. In-Situ EFM Imaging.

The major goal of this study was to visualize different aspects of the monolayers including the morphology, coexisting phases as well as the lateral distribution of PEG-phospholipid in the phosphocholine matrix. For this, a unique two-channel epifluorescence microscopy (EFM) setup with the use of two different fluorescent probes has been utilized. This technique has been selected to simultaneously monitor both phase state and lateral distribution of PEG-phospholipid or protein binding under various experimental conditions.

The principle of fluorescence lies behind the emission of fluorescent light, usually within nanoseconds, after exciting the fluorophore [Lichtman 2005; Shahid 2013; Hou 2014]. The difference between the peaks of excitation and emission spectra is known as the Stokes shift [Lichtman 2005]. A better way to understand the phenomenon of fluorescence excitation and emission is through visualizing the Jablonski diagram sketched in Figure 1.10. Fluorophore resides in the ground state, S_o, and upon absorbing light, the fluorophore is excited to higher states (within femtoseconds) known as excited singlet states, S_1 and S_2. Most molecules usually return back to their S_o state within nanoseconds resulting in the emission of fluorescence at a specific wavelength, as displayed in Figure 1.10 [Lichtman 2005; Hou 2014].

Epifluorescence microscopy (EFM) has proven to be a powerful tool to image numerous aspects of living systems both at the cellular and molecular level [Gao 2014; Hou 2014; Lichtman 2005]. Epifluorescence microscopy has also been playing a key role in understanding the heterogeneity and phase behavior of various membrane models [Baumgart 2007; Lichtman 2005; Nag 1990; Veatch 2003]. This is due to the fact that it offers direct selection and specific detection of molecules of interest yet with a good signal to background ratio [Lichtman 2005; Yuste 2005]. Epifluorescence configured microscope is useful in a way that its objective not only serves for imaging the specimen but also plays a role as a condenser to illuminate it. One of the great advantages of epi-illumination lie in the possibility of blocking only a small amount of exciting light being reflected off the specimen in the return light path as compared to the transmitted or diascopic microscopes [Lichtman 2005]. A major obstacle with this configuration is the

overlap between the excitation light and fluorescence emissions, which is resolved by the use of beam splitters referred to as a dichroic mirror and filter sets as will be explained later in this section (Figure 1.11) [Cullander 1994; Koyama-Honda 2005; Lichtman 2005]. There are two types of epifluorescence microscopes available commercially and known as upright and inverted microscopes. Unlike upright microscope, inverted epifluorescence microscope has an objective at the bottom of the specimen and light is illuminated on the specimen from the top. For the purpose of our study, the inverted epifluorescence microscope was utilized for in-situ imaging of unilamellar vesicles. The upright epifluorescence microscope, on the other hand, was interfaced with the NIMA Trough for monolayer imaging, as illustrated in Figure 1.11 [Nag 1990; Plasencia 2005]. CCD camera was attached to both types of EFM for a direct in-situ imaging of membrane models.

The technical specification of EFM includes a light source which can be a halogen, mercury, or xenon lamp [Lichtman 2005]. The light reflects down where the fluorescence is collected from the surface by an objective and passes through the dichroic mirror (beamsplitter) and barrier/emission filter that blocks the excitation light and permits the emission light to reach towards the detector as shown in Figure 1.11 [Lichtman 2005]. Different kinds of optical filter sets with different wavelength ranges, depending on the choice of chromophore, are used for the excitation light to pass through the excitation bandpass filters. A CCD camera is used to capture the images from the membrane models and is also used to detect the difference in emission light intensities. Mostly low-light level cameras are used for high performance and maximum image

stability. The digital resolution of the images can be set to 3 pixels/μm or less for better images. The images can be recorded and stored directly to computer memory by an on-line image processor. The EFM setup is usually placed on an active vibration isolation table to avoid external vibrations which may cause discrepancy in the results [Lichtman 2005; Nag 1990].

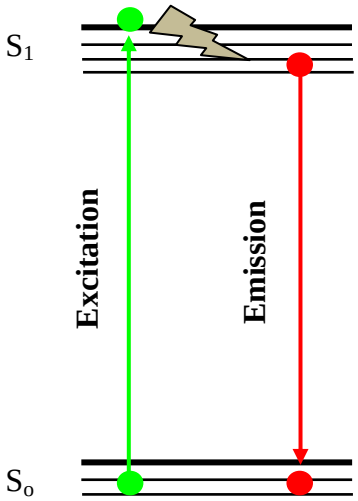

Phenomenon of Fluorescence

Figure 1.10: A Jablonski Diagram illustrating the phenomenon of fluorescence. Fluorophore in resting configuration reside at the lowest vibrational state known as ground state, S_o. Upon absorbing energy, the fluorophore gets excited to a higher singlet state, S_1. Most fluorophores would emit a photon in the form of fluorescence, upon relaxing back to the S_o state. Diagram sketched is based on Hou 2014 and Licthman 2005.

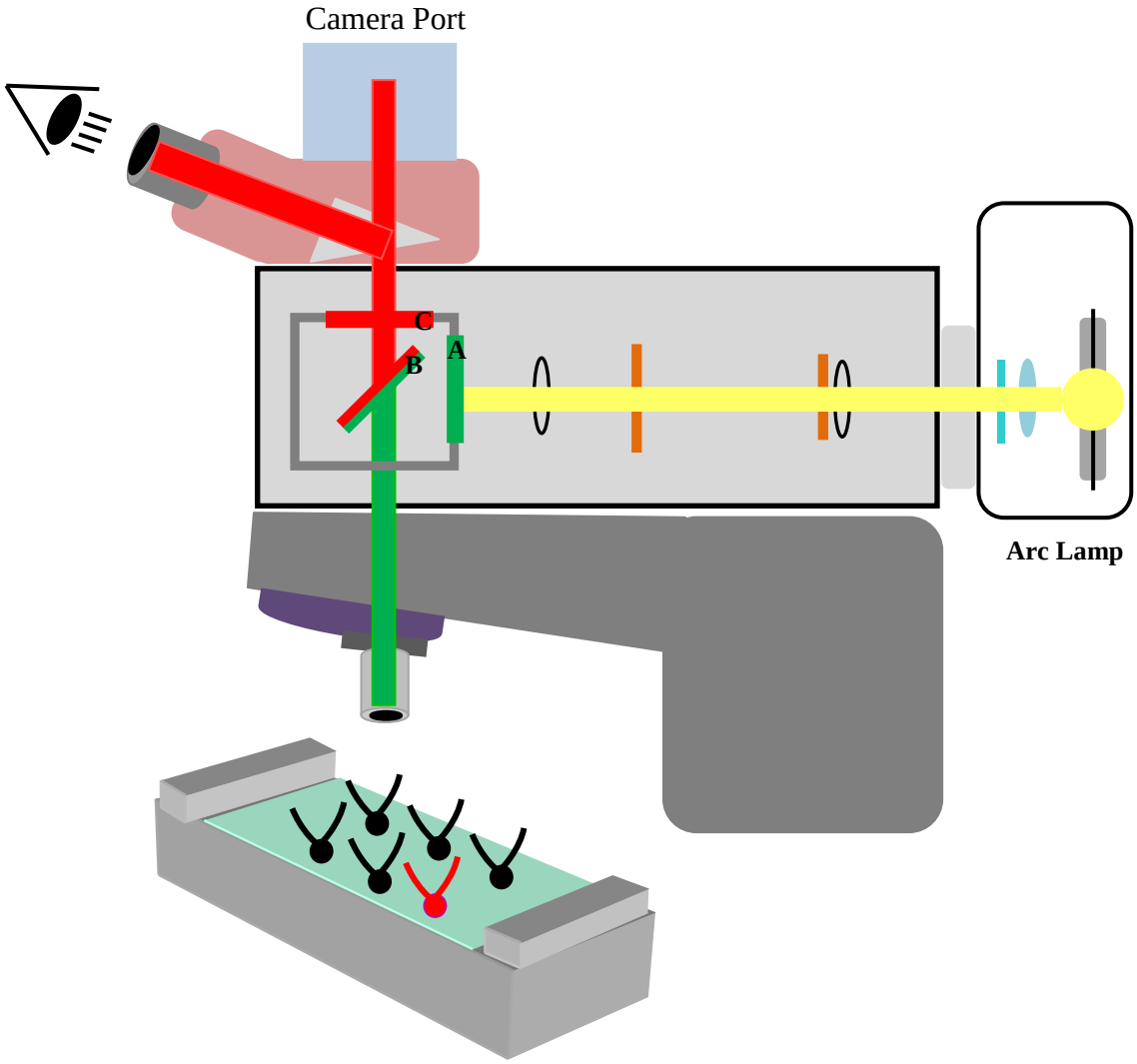

Figure 1.11: Cartoon of an upright epifluorescence microscope interfaced with a NIMA trough shown at the bottom. (A) Light from the source passes through the filter cube, in particular an exciter, that selectively excites the fluorophore at a specific wavelength (Green light in this particular example). (B) The dichroic mirror is a special type of beam splitter usually at a 45^{o} that separates excitation from the emission. (C) The barrier filter is used in EFM to allow the emitting light of a longer wavelength (red in this case) to pass and prevents the exciting light (green light) to reach the detector. The diagram is sketched based on the reference of Lichtman 2005.

1.9.4. Insulin Conformational Analysis upon Interactions with Vesicles by CD.

This study also examined the conformational changes of insulin upon non-specific interaction with the membrane model using circular dichroism, CD, spectroscopy. The small unilamellar vesicle (SUV) of PEGylated phosphocholine has been selected as a membrane model to probe the effect on insulin conformational structure during insulin/membrane interactions. The conformational changes of insulin upon interactions with the vesicle membrane will be evaluated in terms of α-helical content. The effect of varying PEG content in the vesicles on the insulin conformational structure as well as folding/unfolding state will also be examined. CD spectroscopy data analysis will be summarized in a CD phase diagram in order to determine the existence of different states of insulin species upon non-specific membrane interactions with varying PEG content.

Circular dichroism works on the principle of measuring the difference in absorbance between the left and right-handed circularly polarized light that arises from a chiral or optically active molecule [Greenfield 1996; Kelly 2005; Shahid 2013; Sreerama 2004]. CD spectroscopy has proven to be a remarkable tool to extract structural information about macromolecules, in particular proteins [Kelly 2009; Greenfield 1996; Sreerama 2004]. CD can provide dynamic information about proteins including secondary structure composition, tertiary structure, conformational changes, cofactor binding sites, protein-ligand interactions as well as protein folding [Ahmad 2004; Greenfield 1996; Kelly 2005; Kelly 2009; Kuznetsova 2002; Sreerama 2004; Tah 2014]. The molecule can be chiral for several reasons, in particular if it contains one or more

chiral centers, it is placed in an asymmetric environment, or it is covalently attached to a chiral center [Kelly 2009; Greenfield 1996]. In general, CD spectrometer operates on the same principle as demonstrated in Figure 1.12. Light from the source passes through the monochromator, which linearly polarizes light with respect to wavelength [Breeze 1972]. Light then enters photoelastic modulator where it splits into left and right circularly polarized light [Breeze 1972; DiNitto 2012; Kelly 2009]. The modulator is usually a piezoelectrical crystal whose unique axis is 45^{o} and it oscillates at a resonance frequency of about 50 kHz. The left and right circularly polarized light enters (LCP and RCP) the sample compartment [DiNitto 2012; Kelly 2009; Shahid 2013]. If there is no sample present in the compartment then the light hitting the detector (usually photomultiplier tube (PMT)) would be constant. However, if the chiral sample is present in the compartment then one of the circularly polarized lights will be absorbed more than the other and the resulting combined radiation will be elliptically polarized and thus the signals will get across the PMT (Figure 1.12) [Breeze 1972; DiNitto 2012; Kelly 2005; Kelly 2009]. The photomultiplier tube generates a signal comprised of a DC and AC component [Breeze 1972; DiNitto 2012]. A DC voltage corresponds to the average light intensity transmitted over time, which is usually held constant. AC component of the signal, on the other hand, refers to the intensity modulation resulting from the differential absorption of the sample, which is usually amplified and rectified with respect to DC component [Breeze 1972]. Hence, the ratio of AC and DC component (ignoring other factors) can be simply used to measure the CD signal and subsequently the molar ellipticity [Breeze 1972; DiNitto 2012]. The processed data is further applied to produce

a spectrum of the sample's ellipticity as a function of wavelength of light, as illustrated in Figure 1.12.

CD spectra can be used to obtain secondary structure information of proteins. For instance, proteins containing β-sheets will exhibit a CD spectrum with a positive band around 198 nm and a negative band around 215 nm [Greenfield 1996; Greenfield 2006; Kelly 2005; Sreerama 2004]. The CD spectrum of proteins with α-helical content can be characterized by one positive band at 192 nm and two negative bands of 208 and 222 nm. The two CD signals at 208 and 222 nm can also be further used in estimating the α-helical content of the protein [Greenfield 1969; Kelly 2005; Seelig 2000]. CD spectroscopy has been used in several studies to monitor the changes in the protein secondary structure, by estimating the α-helical content, upon interactions with membranes and various other molecules [Mollmann 2006; Nosrati 2009; Pal 2011; Seelig 2000; Shahid 2013; Tah 2014]. Hence, far-UV CD spectroscopy has been utilized in this study to assess the folding/unfolding states as well as conformational changes in the insulin's secondary structure, in terms of α-helical content, upon interactions with small unilamellar vesicles as membrane models.

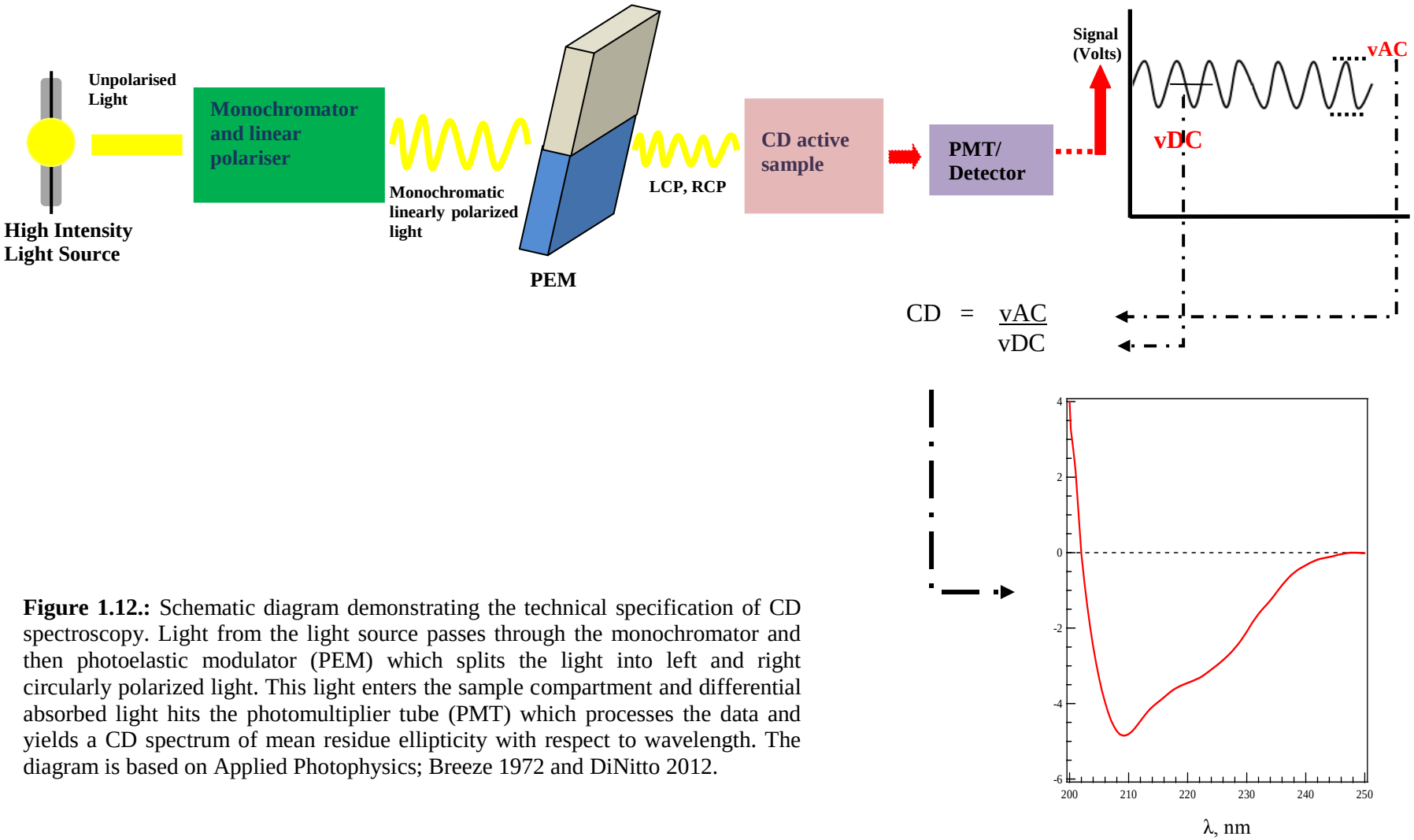

Figure 1.12.: Schematic diagram demonstrating the technical specification of CD spectroscopy. Light from the light source passes through the monochromator and then photoelastic modulator (PEM) which splits the light into left and right circularly polarized light. This light enters the sample compartment and differential absorbed light hits the photomultiplier tube (PMT) which processes the data and yields a CD spectrum of mean residue ellipticity with respect to wavelength. The diagram is based on Applied Photophysics; Breeze 1972 and DiNitto 2012.

1.10. References.

Ahmad, A.; Millett, I. S.; Doniach, S.; Uversky, V. N.; Fink, A. L. *The J. of Biol. Chem.*, **2004**, *279*, 14999 – 15013.

Akashi, K.; Miyata, H.; Itoh, H.; and Kinosita, K. *Biophys. J.* **1996**, *71*, 3242 – 3250.

Allen, C.; Santos, N. D.; Gallagher, R.; Chiu, G. N. C.; Shu, Y.; Li, W. M.; Johnstone, S. A.; Janoff, A. S.; Mayer, L. D.; Webb, M. S.; and Bally, M. B. *Biosci. Rep.* **2002**, *22*, 225 – 250.

Antonietti, M. and Forster, S. *Adv. Mater.* **2003,** *15*, 1323 – 1333.

Baekmark, T.R.; Elender, G.; Lasic, D.D.; and Sackmann, E. *Langmuir* **1995**, *11*, 3975 – 3987.

Bagatolli, L.A.; Parasassi, T.; and Gratton, E. *Chem. and Phys. of Lip.* **2000**, *105*, 135 – 147.

Bagatolli, L.A. *Biochim. et Biophys. Acta*, **2006**, *1758*, 1541–1556.

Barenholz, Y. Curr. *Opin. in Coll. & Interf. Sci.* **2001**, *6*, 66 – 77.

Baumgart, T.; Hunt, G.; Farkas, E. R.; Webb, W. W.; and Feigenson, G. W. *Biochim. et Biophys. Acta* **2007**, *1768*, 2182 – 2194.

Bedu-Addo, F. K.; Tang, P.; Xu, Y.; and Huang, L. *Pharm. Res.* **1996**, *13*, 710 – 717.

Belsito, S.; Bartucci, R.; Montesano, G.; Marsh, D.; and Sportelli, L. *Biophs. J.* **2000**, *78*, 1420 – 1430.

Bianco-Peled, H.; Dori, Y.; Schneider, J.; Sung, L-P.; Satija, S.; and Tirrell, M. *Langmuir* **2001,** *17*, 6931 – 6937.

Birdi, K. S. *J. Coll. and Inter. Sci.* **1976**, *57*, 228 – 232.

Bocian, W.; Sitkowski, J.; Bednarek, E.; Tarnowska, A.; Kawecki, R.; and Kozerski, L. *J. Biomol. NMR* **2008**, *40*, 55 – 64.

Bozzuto, G. and Molinari, A. *Intl J. of Nanomed.* **2015**, *10*, 975 – 999.

Boisselier, E.; Calvez, P.; Demers, E.; Cantin, L.; and Salesse, C. *Langmuir* **2012**, *28*, 9680 – 9688.

Breeze, R. H. and Ke, B. *Anal. Biochem.* **1972**, *50*, 281 – 303.

Castro, C. E.; Mattei, B.; Riske, K. A.; Jager, E.; Jager, A.; Stepanek, P.; and Giacomelli, F. C. *Langmuir* **2014**, *30*, 9770 − 9779.

Chou, T. H. and Chu, I. M. *Coll. Surf. A* **2002**, *211*, 267 – 274.

Chen, C. C. and Borden M. A. *Langmuir* **2010**, *26*, 13183 – 13194.

Chen, C. C.; Wu, S. Y.; Finan, J. D.; and Morrison III, B.; and Konofagou, E. E. *IEEE* **2013**, *60*, 524 – 534.

Cullander, C. *J. of Micro.* **1994**, *176*, 281 – 286.

Collier, J. H. and Messersmith, P. B. *Annu. Rev. Mater. Res.* **2001**, *31*, 237 – 63.

Conde, M. M.; Conde, O.; Trillo, J. M.; and Minones Jr., J. *Langmuir* **2011**, *27*, 3424 – 3435.

Damodaran, V. B.; Fee, C. J.; Ruckh, T.; and Popat, K. C. *Langmuir* **2010**, *26*, 7299 – 7306.

DeWolf, C.; Leporatti, S.; Kirsch, C.; Klinger, R.; Brezesinski, G. *Chem. and Phys. of Lip.* **1999**, *97*, 129 – 138.

Dhruv, H. D. PhD Dissertation, *Utah State University*, **2009**.

DiNitto, J. M. PhD Dissertation, *East Carolina University* **2012**.

Dos Santos, N. PhD Dissertation, *University of British Columbia*, **2004**.

Dos Santos, N.; Allen, C.; Doppen, A-M.; Anantha, M.; Cox, K. A. K.; Gallagher, R. C.; Karlsson, G.; Edwards, K.; Kenner, G.; Sameuls, L.; Webb, M. S., Bally, M. B. *Biochim. et Biophys. Acta* **2007**, *1768*, 1367 – 1377.

Efremova, N. V.; Sheth, S. R.; and Leckband, D. E. *Langmuir* **2001,** *17*, 7628 – 7636.

El-Khouri, R. J. PhD Dissertation, *University of California* **2009.**

Farias, R. N.; Vinals, A. E. L.; Posse, E.; and Morero, R. D. *Biochem. J.* **1989**, *264*, 285 – 287.

Greenfield, N. and Fasman, G. D. *Biochem.* **1969**, *8*, 4108 – 4116.

Greenfield, N. J. *Anal. Biochem.* **1996**, *235*, 1 – 10.

Gref, R.; Luck, M.; Quellec, P.; Marchand, M.; Dellacherie, E.; Harnisch, S.; Blunk, T.; and Muller, R. H. *Coll. and Surf. B: Biointerf.* **2000**, *18*, 301 – 313.

Gref, R.; Domb, A.; Quellec, P.; Blunk, T.; Muller, R. H.; Verbavatz, J. M.; and Langer, R. *Adv. Drug Del. Rev.* **2012**, *64*, 316 – 326.

Grudzielanek, S.; Smirnovas, V.; Winter, R. *Chem and Phys of Lip.* **2007**, *149*, 28 – 39.

Hadidi, M. and Zydney, A. L. *J. of Memb. Sci.* **2014**, *45*, 297 – 103.

Hasan, A. and Pandey L. *Poly.-Plas. Tech. and Eng.* **2015**, *54*, 1358 – 1378.

Hashizaki, K.; Taguchi, H.; Itoh, C.; Sakai, H.; Abe, M.; Saito, Y.; and Ogawa, N. *Chem. Pharm. Bull.* **2003**, *51*, 815 – 820.

Henry, M.; Dupont-Gillain, C.; and Bertrand, P. *Langmuir* **2008,** *24*, 458 – 464.

Hou, S. G.; Liang, L.; Deng, S. H.; Chen, J. F.; Huang, Q.; Cheng, Y.; and Fan, C. H. *Sci. China Chem.*, **2014**, *57*, 100 – 106.

Hristova, K.; Kenworthy, A.; and McIntosh, T. J. *Macromolecules* **1995**, *28*, 7693 – 7699.

Ickenstein, L. M.; Arfvidsson, M. C.; Needham, D.; Mayer, L; and Edwards, K. *Biochim. et Biophys. Acta* **2003**, *1614*, 135 – 138.

Immordino, M. L.; Dosio, F.; and Cattel, L. *Intl. J. of Nanomed.* **2006**, *1*, 297.

Janout, V.; Daly, T. A.; Cline, L. L.; Kulp, L. J.; and Regen, S. L. *Bioconj.Chem.* **2012**, *23*, 336 − 339.

Jebrail, M. MSc Dissertation, *York University* **2008**.

Jebrail, M.; Schmidt, R.; DeWolf, C. E.; Tsoukanova, V. *Coll. and Surf. A: Phys. and Eng. Asp.* **2008**, *321*, 168 – 174.

Jin, S-E.; Jin, H-E.; and Hong, S-S. *Hindawi: BioMed. Res. Intl.* **2014**, *2014*, 1 – 23.

Juhasz, J.; Davis, J. H.; Sharom, F. J. *Biochim. et Biophys. Acta* **2012**, *1818*, 19 – 26.

Kalvodova, L.; Kahya, N.; Schwille, P.; Ehehalt, R.; Verkade, P.; Drechsel, D.; and Simons, K. *The J. of Biol. Chem.* **2005**, *280*, 36815 – 36823.

Karatekin, E. and Rothman, J. E. *Nat Protoc.* **2012**, *7*, 903 – 920.

Kelly, S. M.; Jess, T. J.; and Price, N. C. *Biochimic. et Biophys. Acta* **2005**, *1751*, 119 – 139.

Kelly, S. M. and Price, N. C. *Encyclo. of Life Sci.;* John Wiley & Sons Ltd: Chichester, **2009.**

Kenworthy, A. K.; Hristova, K.; Needham, D.; and McIntosh, T. J. *Biophys. J.* **1995**, *68*, 1921 – 1936.

Kim, A.; Yun, M-I.; Oh, Y-K.; Ahn, W-S.; Kim, C-K. *Intl. J. of Pharma.* **1999**, *180*, 75 – 81.

Kim, K.; Shin, K.; Kim, H.; Kim, C.; and Byun, Y. *Langmuir* **2004**, *20*, 5396 – 5402.

Kneidl, B.; Peller, M.; Winter, G.; Lindner, L. H.; and Hossann, M. *Intl. J. of Nanomed.* **2014**, *9*, 4387 – 4398.

Korlach, J.; Schwille, P.; Webb, W.W.; and Feigenson, G.W. *PNAS* **1999**, *96*, 8461– 8466.

Koyama-Honda, I.; Ritchie, K.; Fujiwara, T.; Iino, R.; Murakoshi, H.; Kasai, R. S.; and Kusumi, A. *Biophys. J.* **2005**, *88*, 2126 – 2136.

Kuznetsova, I. M.; Stepanenko, O. V.; Turoverov, K. K.; Zhu, L.; Zhou, J. M.; Fink, A. L.; Uversky, V. N. *Biochim. et Biophys. Acta* 2002, *1596*, 138 – 155.

Lasic, D. D.; Woodle, M. C.; Martin, F. J.; and Valentincic, T. *Periodic. Biol.* **1991**, *93*, 287 – 290.

Lasic, D. D. and Needham, D. *Chem. Rev.* **1995**, *95*, 2601 – 2628.

Lee, H. and Larson, R. G. *Biomacromole.* **2016**, *17*, 1757 − 1765.

Lewis, A. L. *Coll. and Surf. B: Biointerf.* **2000**, *18*, 261 – 275.

Li, S. and Leblanc, R.M. *J. Phys. Chem. B* **2014**, *118*, 1181 − 1188.

Li, J.; Wang, X.; Zhang, T.; Wang, C.; Huang, Z.; Luo, X.; and Deng, Y. *Asian J. of Pharma. Sci.* **2015**, *10*, 81 – 98.

Lichtman, J. W. and Conchello, J-A. *Nat. Meth.* **2005**, *2*, 910 – 919.

Liu, X.; Kaczmarski, K.; Cavazzini, A.; Szabelski, P.; Zhou, D.; and Guiochon, G. *Biotechnol. Prog.* **2002,** *18*, 796 – 806.

Liu, Y.; Hu, Y.; and Huang, L. *Biomater*. **2014**, *35*, 3027 – 3034.

Lozano, M. M. and Longo, M. L. *Soft Matter* **2009a**, *5*, 1822 – 1834.

Lozano, M. M. and Longo, M. L. *Langmuir* **2009b**, *25*, 3705 – 3712.

Luna, D. M. N., Falcao, E. P. S., Melo, S. J., and Andrade, C. A. S. *Coll. Surf. A* **2011**, *373*, 22 – 28.

Manley, S. and Gordon, V. D. *Curr. Proto. in Cell Biol.*; John Wiley & Sons Inc.: USA, **2008.**

Maier, O.; Oberle, V.; and Hoekstra, D. *Chem. and Phys. of Lip.*, **2002**, *116*, 3 – 18.

Mathivet, L., Cribier, S., Devaux, P.F., *Biophys. J.* **1996**, *70*, 1112 – 1121.

McConnell, H. M. *Annu. Rev. Phys. Chem.* **1991**, *42*, 171 – 195.

Mfuh, A. M.; Mahindaratne, M. P. D.; Quintero, M. V.; Lakner, F J.; Bao, A.; Goins, B. A.; Phillips, W. T.; and Negrete, G. R. *Langmuir* **2011**, *27*, 4447 – 4455.

Moghimi, S. M.; Hunter, C.; and Murray, J. C. *Pharmacol. Rev.* **2001**, *53*, 283 – 318.

Mohwald, H. *Annu. Rev. Phys. Chem.* **1990**, *41*, 441 – 476.

Mollmann, S. H. Jorgensen, L.; Bukrinsky, J. S.; Elofsson, U.; Norde, W.; and Frokjaer, S. *Europ. J. of Pharma. Sci.* **2006**, *27*, 194 – 204.

Morales-Penningston, N. F.; Wu, J.; Farkas, E. R.; Goh, S. L.; Konyakhina, T. M.; Zheng, J. Y.; Webb, W. W.; and Feigenson, G. W. *Biochim. et Biophys. Acta* **2010**, *1798*, 1324 – 1332.

Morille, M.; Passirani, C.; Vonarbourg, A.; Clavreul, A.; and Benoit, J-P. *Biomater.* **2008**, *29*, 3477 – 3496.

Moscho, A.; Orwar, O.; Chiu, D. T.; Modi, B. P.; and Zare, R. N. *PNAS* **1996**, *93*, 11443 – 11447.

Nag, K.; Boland, C.; Rich, N. H.; and Keough, K. M. W. *Rev. Sci. Instrum.* **1990**, *61*, 3425 – 3430.

Nakahara, H. and Shibata, O. *J. of Oleo Sci.* **2014**, *63*, 1159 – 1168.

Naumann, C. A.; Brooks, C. F.; Fuller, G. G.; Knoll, W.; and Frank C. W. *Langmuir* **1999**, *15*, 7752 – 7761.

Naumann, C. A.; Brooks, C. F.; Wiyatno, W.; Knoll, W.; Fuller, G. G.; and Frank, C. W. *Macromole.* **2001**, *34*, 3024 – 3032.

Needham, D. and Kim, D. H. *Coll. and Surf. B: Biointerf.* **2000**, *18*, 183 – 195.

Netz, R. R.; Andelman, D.; and Orland, H. *J. Phys. II (France)* **1996**, *6*, 1023 – 1042.

Nosrati, N. MSc Dissertation, *York University* **2009**.

Nunes, C.; Brezesinski, G.; Pereira-Leite, C.; Lima, J. L. F. C.; Reis, S.; and Lucio, M. *Langmuir* **2011**, *27*, 10847 – 10858.

Nylander, T.; Kekicheff, P.; and Ninham, B. W. *J. of Coll. and Interf. Sci.* **1994**, *164*, 136 – 150.

Pal, P.; Mahato, M.; Kamilya, T.; and Talapatra, G. B. *Phys. Chem. Chem. Phys.* **2011**, *13*, 9385 – 9396.

Pallua, N. and Suschek, C. V. *Springer*, Berlin, **2011**.

Pappalardo, M.; Milardi, D.; Grasso, D.; and La Rosa, C. *J. of Therm. Anal. and Calorim.* **2005**, *80*, 413 – 418.

Peterca, M.; Percec, V.; Leowanawat, P.; and Bertin, A. *JACS* **2011**, *133*, 20507 – 20520.

Popovska, O.; Simonovska, J.; Kavrakovski, Z.; and Rafajlovska, V. *Intl. J. of Pharm. and Phyto. Res.* **2013**, *3 (3)*, 182 – 189.

Rahmati, K.; Koifman, J.; and Tsoukanova, V. *Coll. and Surf. A: Physicochem. Eng. Asp.* **2008**, *321*, 181 – 188.

Reulen, S. W. A. and Dankers, P. Y. W.; Bomans, P. H. H.; Meijer, E. W.; and Merkx, M. *J. Am. Chem. Soc.* **2009**, *131*, 7304 – 7312.

Savva, M. PhD Dissertation, *University of Pittsburgh* **1998**.

Seelig, A; Blatter, X. L.; Frentzel, A.; Isenberg, G. *The J. of Biol. Chem.* **2000**, *275*, 17954 – 17961.

Seth, M.; Ramachandran, A.; and Leal, L. G. *Langmuir* **2013**, *29*, 14057 − 14065.

Sezgin, E. and Schwille, P. *Molec. Memb. Biol.* **2012,** *29*, 144 – 154.

Shahid, M. N. and Tsoukanova, V. *The J. of Phys. Chem. B* **2011**, *115*, 3303.

Shahid, M. N. PhD Dissertation, *York University* **2013**.

Silpe, J. E.; Sumit, M.; Thomas, T. P.; Huang, B.; Kotlyar, A.; van Dongen, M. A.; Banaszak Holl, M. M.; Orr, B. G.; and Choi, S. K. *ACS Chem. Biol.* **2013**, *8*, 2063 − 2071.

Sreerama, N. and Woody, R. W. *Meth. in Enzym.* **2004**, *383*, 318 – 351.

Stefaniu, C. and Brezesinski, G. *Adv. in Coll. and Interf. Sci.* **2014a**, *207*, 265 – 279.

Stefaniu, C.; Brezesinski, G.; and Möhwald, H. *Adv. in Coll. and Interf. Sci* **2014b**, *208*, 197 – 213.

Stepniewski, M.; Pasenkiewicz-Gierula, M.; Rog, T.; Danne, R.; Orlowski, A.; Karttunen, M.; Urtti, A.; Yliperttula, M.; Vuorimaa, E.; and Bunker, A. *Langmuir* **2011**, *27*, 7788.

Suga, K.; Tanabe, T.; and Umakoshi, H. *Langmuir* **2013**, *29*, 1899 − 1907.
Sung, H-W. sonaje, K.; Liao, Z-X.; Hsu, L-W.; and Chuang, E-Y. *Acc. of Chem. Res.* **2012**, *45*, 619 – 629.

Tah, B.; Pal, P.; and Talapatra, G. B. *J. of Luminesci.* 2014, *145*, 81–87.

Takemoto, N.; Teramura, Y.; and Iwata, H. *Bioconj. Chem.* **2011**, *22*, 673 – 678.

Tanwir, K.; Shahid, M. N.; Thomas, A.; and Tsoukanova, V. *Langmuir* **2012**, *28*, 14000 – 14009.

Taylor, W. and Jones, R. A. L. *Langmuir* **2013**, *29*, 6116 − 6122.

Torchilin, V. and Trubetskoy, V. S. *Adv. Drug Deliv. Rev.* **1995**, *16*, 141 – 155.

Veatch, S. L. and Keller, S. L. *Biophys. J.* **2003,** *85*, 3074 – 3083.

Vermette, P. and Meagher, L. *Coll. Surf. B* **2003**, *28*, 153 – 198.

Vukovic, L. Khatib, F. A.; Drake, S. P.; Madriaga, A.; Brandenburg, K. S.; Kral, P. and Onyuksel, H. *J. Am. Chem. Soc.* **2011**, *133*, 13481 – 13488.

Walde, P. and Ichikawa, S. *Biomole. Eng.* **2001**, *18*, 143 – 177.

Wattendorf, U. and Merkle, H. P. *J. of Pharma. Sci.* **2008**, *97*, 4655 – 4669.

Wesołowska, O; Michalak, K.; Maniewska, J. and Hendrich, A. B. *Acta Biochim. Polon.* **2009**, *56*, 33 – 39.

Wisniewski, N. and Reichert, M. *Coll. and Surf. B: Biointerf.* **2000**, *18*, 197 – 219.

Yang, G. and Xu, Y. *Top. Curr. Chem.* **2011**, *298*, 189 – 236.

Yen, C.; He, H.; Fei, Z.; Zhang, X.; Lee, L. J.; Ho, W. S. W. *Intl. J. of Polym. Mater.* **2010**, *59*, 943 – 957.

Ziblat, R.; Leiserowitz, L.; and Addadi, L. *Angew. Chem. Int. Ed.* **2011**, *50*, 3620 – 3629.

Zhai, Y. and Zhai, G. *J. of Control. Rel.* **2014**, *193*, 90 – 99.

Zhao, H.; Dubielecka, P. M.; Soderlund, T.; and Kinnunen, P. K. J. *Biophys. J.* **2002**, *83*, 954 – 967.

Chapter 2: Experimental.

The main focus of this study was to assess different aspects of PEGylated phosphocholine membrane models including phase state, miscibility, morphology, composition, aliphatic chain length, as well as PEG distribution and its conformations. Two types of PEGylated phospholipid membrane models were selected (i) Langmuir monolayers as well as (ii) giant (GUV) and small unilamellar vesicles (SUV). The binary mixtures of PEG-grafted phospholipids and host matrix of phosphocholine selected were DPPC/DPPE-PEG2000 and DSPC/DSPE-PEG2000. The binary mixtures of PEG-grafted phospholipids and phosphocholine possessed same aliphatic chain length, C_{18}/C_{18} and C_{16}/C_{16}. Human insulin was chosen as a model protein in order to understand the mechanisms involved in the non-specific interactions of PEG-grafted phospholipid membrane models with small proteins. The techniques used in this study include Langmuir technique, epifluorescence microscopy (EFM) as well as circular dichroism spectroscopy (CD). A variety of fluorescent probes were used in membrane models for EFM imaging including (i) DOPE-Rh for phase behavior imaging, (ii) fluorescent analogues of the PEG-phospholipids, DPPE-PEG2000-FITC and DSPE-PEG2000-FITC, for PEG distribution imaging and (iii) FITC-insulin for imaging the protein binding.

2.1. MATERIALS.

All phospholipids and fluorescent probes were purchased from Avanti Polar Lipids and used as received. This includes poly(ethylene glycol)-grafted phospholipid with a PEG average

molecular weight of 2000, 1,2-distearoyl-*sn*-glycero-3-phosphoethanolamine-*N*-[poly(ethylene glycol)2000] (DSPE-PEG2000), its fluorescent analog, 1,2-distearoyl-*sn*-glycero-3-phosphoethanolamine-*N*-[poly(ethylene glycol)2000-*N*′-carboxyfluorescein] (DSPE-PEG2000-FITC), poly(ethylene glycol)-grafted phospholipid with a PEG average molecular weight of 2000, 1,2-dipalmitoyl-*sn*-glycero-3-phosphoethanolamine-*N*-[poly(ethylene glycol)2000] (DPPE-PEG2000), a fluorescent probe, rhodamine-dioleoyl-phosphatidylethanolamine labeled at the headgroup 1,2-dioleoyl-*sn*-glycero-3-phosphadtidylethanolamine-*N*-(lissamine rhodamine B sulfonyl) (DOPE-Rh), 1,2-dipalmitoyl-*sn*-glycero-3-phosphocholine (DPPC), and 1,2-distearoyl-*sn*-glycero-3-phosphocholine (DSPC). The fluorescent analog of DPPE-PEG2000, DPPE-PEG2000-FITC, was synthesized in the present study as will be discussed in Chapter 3. For this, a Boc-protected NHS-ester, α-Nhydroxysuccinimidyl-ω-tert-butoxycarbonyl [poly(ethylene glycol)2000] (NHS-PEG2000-Boc) was obtained from JenKem. Human insulin was purchased from Sigma Aldrich. Fluorescein isothiocyanate (FITC) fluorophore to label insulin was obtained from Molecular Probes. HPLC grade chloroform and methanol were purchased from Fisher Scientific and used as received. Phosphate-buffered saline (PBS) from Sigma containing 0.01 M phosphate salt, 0.12 M NaCl, and 0.0027 M KCl at pH 7.4 was used as the subphase. Deionized water produced by a Milli-Q Synthesis water purification system was used in all experiments. The specific resistivity of water was 18×10^6 Ω·cm (pH 6.2 in equilibrium with atmospheric carbon dioxide). All solutions were stored in the dark at 4 °C.

Stock solutions of DPPC, DSPC, and PEG2000-grafted phospholipids and fluorescent probes were typically prepared at concentrations of 0.1 – 0.5 mg/mL by dissolution in chloroform for monolayer studies. The concentrations of the mixtures for unilamellar vesicles

were 20 mg/mL for phosphocholine and 2 mg/mL, for PEG-phospholipid. The stock solutions were prepared in chloroform/methanol mixture (60:40 v/v). Stock solutions were mixed in various molar ratios to obtain spreading solutions containing 1, 3, 6, and 9 mol% PEG-phospholipid. Insulin solutions were prepared at a concentration of ~0.3 mg/mL (~0.5 μM) by dissolving in phosphate buffer pH ~7.4 containing 0.009 M KH_2PO_4 and 0.03 M Na_2HPO_4.

2.2. EXPERIMENTAL TECHNIQUES.

Monolayer studies were carried out in a Langmuir trough using different methodologies. This includes surface pressure, compressibility analysis, area expansion measurements and epifluorescence microscopy (EFM). The experimental techniques used for studying unilamellar vesicles (GUV and SUV) as membrane models include optical and epifluorescence microscope as well as circular dichroism spectroscopy (CD).

2.2.1. Preparation of Langmuir Monolayers for $\pi - A$ Isotherm Measurements.

Two types of custom made Langmuir troughs, KSV2000SP and NIMA, were utilized to study the phospholipid monolayers at the air/aqueous interface. A KSV2000SP Langmuir trough (KSV Instruments Ltd., Finland) was used to study the phase transition, lateral organization and protein-membrane interactions of mixed monolayers whereas NIMA trough (NIMA technology Ltd., UK) was employed to image the morphology of monolayers upon compression simultaneously by EFM. KSV Langmuir trough has an effective surface area of 75 × 760 mm

and NIMA trough has an effective area of 70 x 460 mm. Both troughs are equipped with two moveable barriers to compress or decompress the amphiphilic monolayers, as illustrated in Figure 2.1. The monolayers were compressed at a constant speed of 10 and 7 mm/min, respectively, to ensure equilibrium surface pressure values at each molecular area [Nakahara 2014]. A filter paper, Wilhelmy plate, was used to measure the surface pressure, π, of the monolayer to an accuracy of 0.1 mN/m. The trough was thermostated to maintain the subphase temperature with an accuracy of ± 1 °C.

The troughs were cleaned by ethanol and milli-Q water before spreading the monolayers. A reference run of milli-Q water was conducted without phospholipids to ensure cleanliness of the subphase. The cleaning of the trough was repeated if the surface pressure rose above 0.2 mN/m. After the cleaning procedure, the phospholipids solubilized in chloroform were slowly spread drop wise on the trough subphase to prevent unwanted surface pressure change. The chloroform was allowed to evaporate for 15 min and the compression commenced by two barriers to record the surface pressure – area ($\pi - A$) isotherms. Each isotherm was repeated at least three times.

To study the monolayer – protein interactions area expansion measurements were performed. The monolayer was prepared by spreading the PEGylated phospholipid binary mixtures with appropriate molar ratios on the trough and allowed to compress to a preset surface pressure, π, value using the barriers. The π was kept constant throughout the experiment using an electronic feedback device. The insulin solution at a desired concentration was injected in the subphase underneath the monolayer. The monolayer area expansion was then measured with

respect to time. The technical details of area expansion measurements are described in detail in Chapter 4.

2.2.2. Epifluorescence Microscopy (EFM) Imaging of Monolayer Models.

EFM images of monolayers were acquired by using a custom designed NIMA trough (NIMA Technology Ltd., U.K.) interfaced with an upright Nikon Eclipse FN1 Epifluorescence microscope (Nikon, Japan). The π - A isotherm measurement parameters were adjusted to precisely match those of the KSV2000SP trough. To observe the fluorescence from the fluorescein fluorophore attached to the distal end of the PEG2000 chain on the DPPE-PEG2000-FITC and DSPE-PEG2000-FITC molecule, Nikon CFI infinity optics, a blue excitation filter set (B-1E filter combination, 480CWL excitation filter, 505LP dichroic mirror, and 540CWL barrier filter) was used. On the other hand, a green excitation filter set (TRITC HYQ filter combination, 545CWL excitation filter, 570LP dichroic mirror and 620CWL barrier filter) was utilized to detect the fluorescence from the DOPE-Rh molecule. Each of the two channels was equipped with a 10x objective (Nikon CFIPlan 10) to enable imaging. The images were captured by a Hamamatsu CCD camera, ORCA ER(AG) (Hamamatsu, Japan) and visualized directly onto a computer screen using an advanced Simple PCI 6 software (Compix Inc., PA).

The main goal of our study was to simultaneously visualize changes in the membrane morphology and insulin/membrane interactions. Hence, a two channel EFM (TRITC and FITC channels) was utilized, which afforded the use of two fluorophores of different spectral profiles,

to achieve our goals. A rhodmine-labelled phospholipid probe, DOPE-Rh, and fluorescein-isothiocyanate (FITC) conjugated with either PEG-phospholipid or insulin are the two types of fluorescent probes used for our membrane models studies (Figure 2.1). This is due to the fact that their excitation and emission wavelengths are different from each other and hence, can be selectively detected through the use of different filter sets in two channel EFM [Cullander 1994; Licthman 2005; Shahid 2013]. For instance, the excitation range of rhodamine lies in the range between 530 – 560 nm with its absorption maximum of about 545 nm which is far from excitation range of FITC from 470 – 490 nm with its absorption maximum of about 488 nm, as described in detail elsewhere [Shahid 2013; Tanwir 2012]. Similarly, the emission intensity range of rhodamine is between 590 – 650 nm which is different from the range of FITC from 510 – 560 nm [Shahid 2013; Tanwir 2012]. In this case, TRITC channel detects fluorescence from rhodamine fluorophore while cutting off FITC fluorescence whereas FITC channel detects fluorescence from FITC while cutting off rhodamine fluorescence. A sophisticated approach of switching between TRTIC and FITC channels in EFM can make the use of two fluorophores possible for the purpose of our study. Hence, in-situ imaging of phase state and lateral PEG distribution was performed by using DOPE-Rh as well as DPPE-PEG2000-FITC and DSPE-PEG2000-FITC. The insulin/membrane interactions study, on the other hand, was carried out by using DOPE-Rh and FITC-insulin.

The phase state imaging of membrane models was performed by using a headgroup-labelled phospholipid probe, DOPE-Rh. Headgroup-labelled phospholipids are usually used for phase state imaging since bulky fluorophore attached to the aliphatic chain may disrupt the lipid packing in the membrane model [Manley 2008]. DOPE-Rh is comprised of two unsaturated

aliphatic chain and a headgroup with a bulky fluorophore attached to it due to which it preferentially partitions into liquid expanded/liquid disordered (LE or L_d) phase and is mainly excluded from the liquid condensed/gel (LC or $L_{\beta'}$) phase [Baumgart 2007; Klymchenko 2014; Samsonov 2001]. The bright regions represent the LE phase which is rich in DOPE-Rh fluorophore whereas the dark region in the membrane model corresponds to the DOPE-Rh excluded area or LC phase [Klymchenko 2014; Tsoukanova 2008]. This property makes DOPE-Rh useful for the phase state imaging to visualize LE and LC coexisting phase in the membrane at various surface pressure and PEG content.

The lateral distribution of PEG-phospholipid in the host phosphocholine matrix was carried out by detecting fluorescence from a FITC fluorescent probe attached at the distal end of the PEG2000 chain. DSPE-PEG2000-FITC is readily available commercially but DPPE-PEG2000-FITC was synthesized in our lab due to lack of commercial availability. Both fluorescent analogues, DSPE-PEG2000-FITC and DPPE-PEG2000-FITC mix well and stay with their counterparts, DSPE-PEG2000 and DPPE-PEG2000 in the membrane models. Hence, use of both fluorophores can aid in locating the DSPE-PEG2000 and DPPE-PEG2000 molecules as well as make that region appear green in the EFM images. The FITC analogue of each PEG-phospholipid was added together with the DOPE-Rh in order to study the lateral PEG distribution as well as phase behaviour of binary mixtures of phosphocholine and PEG-phospholipid, simultaneously. This was done by capturing images through both TRITC and FITC channel from the same area of the membrane model. Comparative analysis of TRITC and FITC images then afforded determining the distribution of PEG-phospholipid between the LE and LC phase [Tanwir 2012].

Two channel EFM has also been employed to monitor the interactions between insulin and membrane models. This was executed by adding one type of fluorophore in the membrane model to monitor changes in the membrane morphology whereas attaching the FITC or rhodamine fluorophore to insulin to visualize the insulin binding. Insulin has been labelled with FITC and characterized for numerous applications in many reports [Gok 2004; Hentz 1997; Shahid 2013]. Insulin labelled with FITC is a mono-substituted species which is modified at the N-terminus of the B-chain. The substitution made on B-chain of insulin molecule has shown to retain similar biological activity as compared to unlabelled insulin molecule [Gok 2004; Hentz 1997]. Thus, in this study, FITC-insulin and Rh-insulin were prepared in our lab as will be described in Chapter 5. To achieve our goal, FITC channel was used to visualize FITC-insulin binding whereas TRITC channel was employed to image the changes in LE/LC of membrane model upon insulin binding using DOPE-Rh. The above procedure was also performed by using Rh-insulin and FITC-labelled PEG-phospholipid but no noticeable differences were observed in the results. Hence, the results provided herein will only be discussed for DOPE-Rh and FITC-insulin in the membrane models.

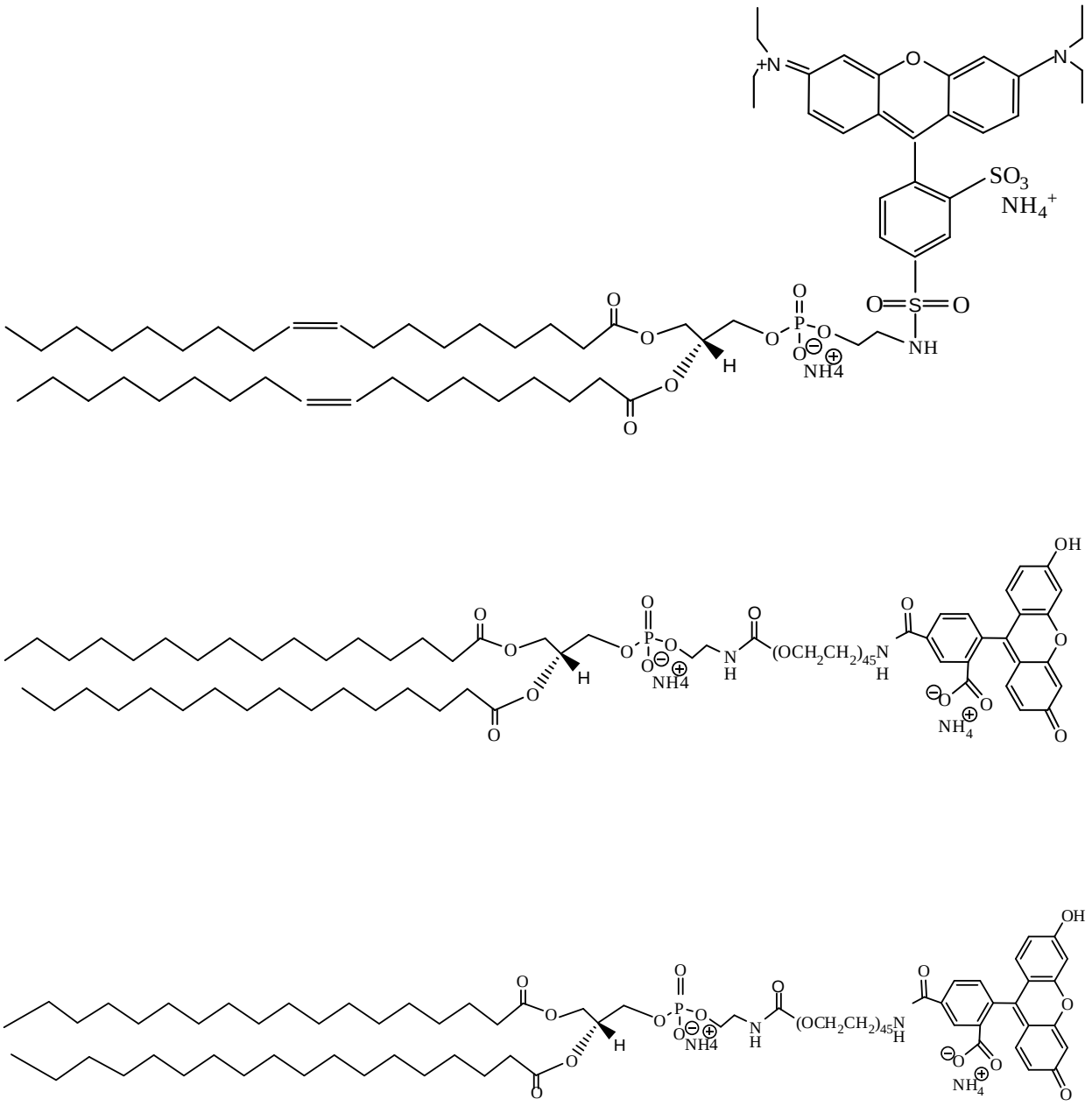

Figure 2.1.: The chemical structures of fluorescently labelled phospholipids (A) DOPE-Rh, (B) DPPE-PEG2000-FITC, and (C) DSPE-PEG2000-FITC.

2.2.2.1. Enhancement of Low-Resolution FITC Imaging.

The major obstacle associated with the HBO mercury lamp supplied by Nikon was the poor contrast and low resolution imaging in the FITC channel. This is due to the fact that mercury lamp, in the visible range, has all its major bands positioned at 365, 405, 436, 546, and 579 nm. The band at 546 nm is positioned right in the excitation window of the TRITC filter set resulting in the optical output power of 76 mW/cm^2. This produces high contrast images due to optimum fluorescence emission from the rhodamine probe. However, the mercury band closest to the FITC range is 436 nm, which falls outside the excitation window resulting in a low optical output power of 20 mW/cm^2. This produces very low contrast and low intensity monolayer images through FITC channel. Hence, an innovative scheme was designed to improve the sharpness and resolution of FITC channel without compromising that of TRITC channel.

A HBO lamp was first replaced by a X-Cite technology Hg lamp (120 W) from EXFO Photonic Solutions Inc. This lamp improved the FITC optical output power to about 34.8 mW/cm^2 but with a slightly reduced power of about 67.4 mW/cm^2 in TRITC channel. This lamp offered a considerable improvement in the FITC images without compromising the resolution of TRITC images. However, a power of 34.8 mW/cm^2 was still not sufficient enough to produce a high FITC fluorescence for which the acquisition time had to be raised. This made the monolayers move faster throughout the image frame while making it difficult to obtain high quality images. Hence, the EFM setup was further aligned with a laser to improve the contrast and sharpness of images in the FITC channel. The laser was purchased from Laser Glow Technology Inc., ON and had an excitation output power of about 100 mW at 473 nm for FITC.

The laser has the capacity to excite the fluorophore directly at the desired wavelength in order to provide maximum excitation and high fluorescence emission. The setup was further aligned with a convex lens in order to focus all of the 100 mW output power of the laser at a certain focal point of the monolayer covering a diameter of about 500 μm, and has been discussed in detail elsewhere [Shahid 2013]. This has reduced the acquisition time and enhanced the contrast and crispiness of the FITC images.

2.2.3. EFM Imaging of GUV Models.

GUV imaging was performed in an imaging cell with a glass bottom, a diameter of ~15 mm, using an inverted Nikon Eclipse TE2000 microscope (Nikon, Japan) through visible and two channel EFM (TRITC and FITC channel). The technical specifications of two channel EFM used for GUV imaging is the same as those of monolayer EFM imaging (described above). Vesicle dispersions were prepared at a concentration of ~3 mg/mL and hydrated with a swelling solution of either 0.1 M NaCl containing 1 vol% glycerol or PBS. The vesicle dispersion was gently transferred in the cell and visualized using inverted Nikon Eclipse TE2000 microscope (Nikon, Japan) through TRITC, FITC and visible channel. TRITC channel was used to image the morphology of the vesicles with a DOPE-Rh fluorophore whereas the insulin binding on the vesicle was monitored by the FITC channel using FITC labeled insulin, FITC-insulin. The visible channel was used to monitor the size and lamellarity.

2.2.4. CD Spectroscopy of SUV Models.

CD spectroscopy was used to study the conformational changes in insulin upon non-specific interactions with PEGylated phosphocholine vesicle membranes. The CD measurements were performed using a Jasco J-180 spectropolarimeter, which is equipped with a temperature controlled holder. Prior to the measurements, nitrogen gas was purged for about 10 minutes to eliminate oxygen and ozone formation from the instrument. The CD measurements of insulin were performed with SUV membrane models. The SUV solution for each binary mixture was prepared in PBS. Vesicle dispersion was visualized with visible microscopy to ensure the formation of vesicles as discussed in detail in Chapter 6. Vesicle dispersion was then transferred into a rectangular cell with a path length of 10 mm. After measuring the CD of vesicles, insulin solution was injected and the measurements were performed. The Far-UV CD spectrum was recorded between 260 – 200 nm with a scan rate of 10 nm/min and 1 nm bandwidth at 20 ^{o}C. All spectra were collected by averaging the signal at every 0.5 nm for 2 s. The PBS baseline was also measured to be used to subtract from all the average CD scans. Moreover, the spectra of insulin interacting with SUVs were obtained by subtracting the spectra of vesicles alone in PBS. Each plot shows the average of three spectra. Every measurement was carried out three times. The data analysis is discussed in detail in Chapter 6.

2.3. REFERENCES.

Bagatolli, L. A. *Biochim. et Biophys. Acta* **2006**, *1758*, 1541 – 1556.

Baumgart, T.; Hunt, G.; Farkas, E. R.; Webb, W. W.; and Feigenson, G. W. *Biochim. et Biophys. Acta* **2007**, *1768*, 2182 – 2194.

Black, S. L.; Stanley, W. A.; Filipp, F. V.; Bhairo, M.; Verma, A.; Wichmann, O.; Sattler, M.; Wilmanns, M.; and Schultza, C. *Bioorg. & Med. Chem.* **2008**, *16*, 1162 – 1173.

Chong, P. L-G. and Sugar, I. P. *Chem. and Phys. of Lip.* **2002**, *116*, 153 – 175.

Cullander, C. J. *of Micros.* **1994**, *176*, 281 – 286.

Dhruv, H. D. PhD Dissertation, *Utah State University* **2009**.

DiNitto, J. M. PhD Dissertation, *East Carolina University* **2012**.

Gaines, G. L. Jr. *Insoluble monolayers at liquid-gas interfaces;* Wiley: New York **1966.**

Gok, E. and Olgaz, S. *J. of Fluor.*, **2004**, *14*, 203 – 206.

Haas, H. and Mohwald. H. *Thin Sol. Film.* **1989**, *180*, 101 – 110.

Hentz, N. G.; Richardson, J. M.; Sportsman, J. R.; Daijo, J.; and Sittampalam, G. S. *Anal. Chem.* **1997,** *69*, 4994 – 5000.

Immordino, M. L. Dosio, F.; and Cattel, L. *Intl. J. of Nanomed.* **2006**, *1 (3)*, 297 – 315.

Klymchenko, A. S. and Kreder R. *Chem. & Biol.* **2014**, *21*, 97 – 113.

Li, S. and Leblanc, R. *J. of Phys. Chem. B.* **2014**, *118*, 1181 – 1188.

Lichtman, J. W. and Conchello, J-A. *Nat. Meth.* **2005**, *2*, 910 – 919.

Maier, O.; Oberle, V.; and Hoekstra, D. *Chem. and Phys. of Lip.*, **2002**, *116*, 3 – 18.

Manley, S. and Gordon, V. D. *Curr. Proto. in Cell Biol.*; John Wiley & Sons Inc.: USA, **2008.**

Nakahara, H. and Shibata, O. *J. of Oleo Sci.* **2014**, *63*, 1159 – 1168.

Samsonov, A. V.; Mihalyov, I.; and Cohen F. S. *Biophys. J.* **2001**, *81*, 1486 – 1500.

Sezgin, E. and Schwille, P. *Mole. Memb. Biol.* **2012,** *29*, 144 – 154.

Shahid, M. N. PhD Dissertation, *York University* **2013**.

Stefaniu, C.; Brezesinski, G.; and Mohwald, H. *Adv. in Coll. and Inter. Sci*. **2014**, *208*, 197 – 213.

Tanwir, K.; Shahid, M. N.; Thomas, A; and Tsoukanova, V. *Langmuir* **2012**, *28*, 14000 – 14009.

Tsoukanova, V. and Salesse, C. *Langmuir* **2008**, *24*, 13019 – 13029.

Chapter 3: Examining the Lateral Distribution of PEG-Grafted Phospholipids and Phase Behavior of Phosphocholine Membranes.

In this study, a comparative analysis of binary mixtures of phosphocholine, DPPC and DSPC, and PEG-phospholipids including DPPE-PEG2000 and DSPE-PEG2000 with varying PEG-phospholipid content is performed to systematically examine the effect of PEG-phospholipids on the lateral organization and phase behavior of the phospholipid membranes. All studies have been carried out in the aqueous media of physiological relevance (PBS) at 20 ^{o}C. Two channel epifluorescence microscopy imaging has been used to directly image the lateral distribution of PEG-phospholipid and its effect on the phase behavior of the binary mixtures. With the help of phase drawings and phase diagrams, it can be suggested that there is a complex relationship between the PEG-phospholipid lateral distribution and the membrane phase behavior. This may aid in developing a fundamental knowledge on non-specific interactions of dissolved proteins with PEG-grafted membranes which will allow us to develop general guidelines to the rational design of bio-nonfouling membrane-mimetic surfaces.

3.1. RESULTS.

In this study, several types of mixed monolayers were used as model membranes. All the monolayers were comprised of a matrix phosphocholine component (DSPC or DPPC) and a PEG-phospholipid (DSPE-PEG2000 or DPPE-PEG2000). However, for EFM imaging, three types of mixtures compositions containing different fluorescent probes were prepared. These include (i) mixtures labeled with 0.5 mol% of DOPE-Rh, (ii) mixtures in which 0.5 mol% of the entire PEG content was replaced with PEG fluorescent probe (DSPE-PEG2000-FITC or DPPE-PEG2000-FITC), and (iii) mixtures labeled with both DOPE-Rh and PEG fluorescent probes. DOPE-Rh was used to image the phase state of the binary mixtures. This specifically includes analyzing the liquid-expanded (LE) and liquid-condensed (LC) phases of the mixtures [Discher 1999; El-Khouri 2011; Shahid 2011]. In a typical membrane, the LE phase corresponds to the liquid-disordered (L_d) phase whereas the LC packing refers to the gel phase (L_β or $L_{\beta'}$) [Kenworthy 1995; Ickenstein 2003; Eeman 2010; Tenchov 2001]. The term $L_{\beta'}$ is usually used for DPPC and DSPC membrane as they both are known to form the tilted gel phase [Kenworthy 1995; Ickenstein 2003; Eeman 2010; Tenchov 2001]. In contrast, PEG fluorescent probes (DSPE-PEG2000-FITC and DPPE-PEG2000-FITC) were used to enable imaging the lateral distribution of the PEG-phospholipids in the phosphocholine matrix [Kinsinger 2010; Tanwir 2008]. The imaging was performed simultaneously with both DOPE-Rh and PEG fluorescent probes to determine the composition of coexisting phases in the binary mixtures as discussed below.

3.1.1. $\pi - A$ Isotherms of DPPE-PEG2000 and DSPE-PEG2000.

$\pi - A$ isotherms have been used as a simple yet efficient tool to characterize and understand the phase and conformational transitions in PEG-grafted phospholipid monolayers [Baekmark 1995; El-Khouri 2011; Lozano 2009a; Nunes 2011; Naumann 2001; Shahid 2011; Tanwir 2008; Tanwir 2012; Vermette 2003; Zhao 2002]. The isotherms of PEG-phospholipids, DPPE-PEG2000 and DSPE-PEG2000, on PBS at 20 $^{\circ}$C are presented in Figure 3.1. The lift-off (the area per molecule wherein the neighboring phospholipid molecules start to interact with each other) in DPPE-PEG2000 and DSPE-PEG2000 isotherms was observed at ~17 nm^2/molecule. Both isotherms exhibit a pseudoplateau with a midpoint at ~12 mN/m. This region corresponds to the conformational transition in the grafted PEG2000 chains, $\pi_{t,PEG}$ [Shahid 2011]. The plateau is described as a conformational transition from pancake to pseudobrush in the polymeric moiety [Tsoukanova, 2008, Arhens, 2000]. A second change in the slope is also observed in the isotherms at high surface pressures and will be referred to as a high-pressure transition, $\pi_{t,high}$. DPPE-PEG2000 isotherm exhibits the second change in slope, $\pi_{t,high}$, with a midpoint at ~42 mN/m (solid curve in Figure 3.1A). The high-pressure transition in DSPE-PEG2000 might be occurring at ~26 mN/m but does not appear to be very prominent in the isotherm (solid curve in Figure 3.1B). Lateral compressibility analysis can be very helpful in detecting even a slight change in the isotherm [Baekmark 1995; Naumann 2001; Shahid 2011; Tanwir 2012]. Hence, the $\pi - A$ isotherms of DPPE-PEG2000 and DSPE-PEG2000 monolayers were analyzed in terms of lateral area compressibility, *C,* to better identify such transitions [Baekmark 1995; Gaines 1966;

Lozano 2009a; Naumann 2001; Shahid 2011; Tanwir 2012; Yu 2002]. The insets present in Figure 3.1 show the lateral compressibility plot with respect to surface pressure, which is obtained by numerical differentiation of π – A isotherm values using the equation shown below

$$C = -\left(1/A\right)\left(\partial A/\partial p\right)_T \qquad 3.1$$

The C – π plot for DSPE-PEG2000 at 20 ^{o}C indeed shows a peak at ~26 mN/m which can be referred to as a high-pressure transition, $\pi_{t,high}$ (solid curve in inset of Figure 3.1B) [Baekmark 1995; Naumann 2001; Shahid 2011; Tanwir 2012].

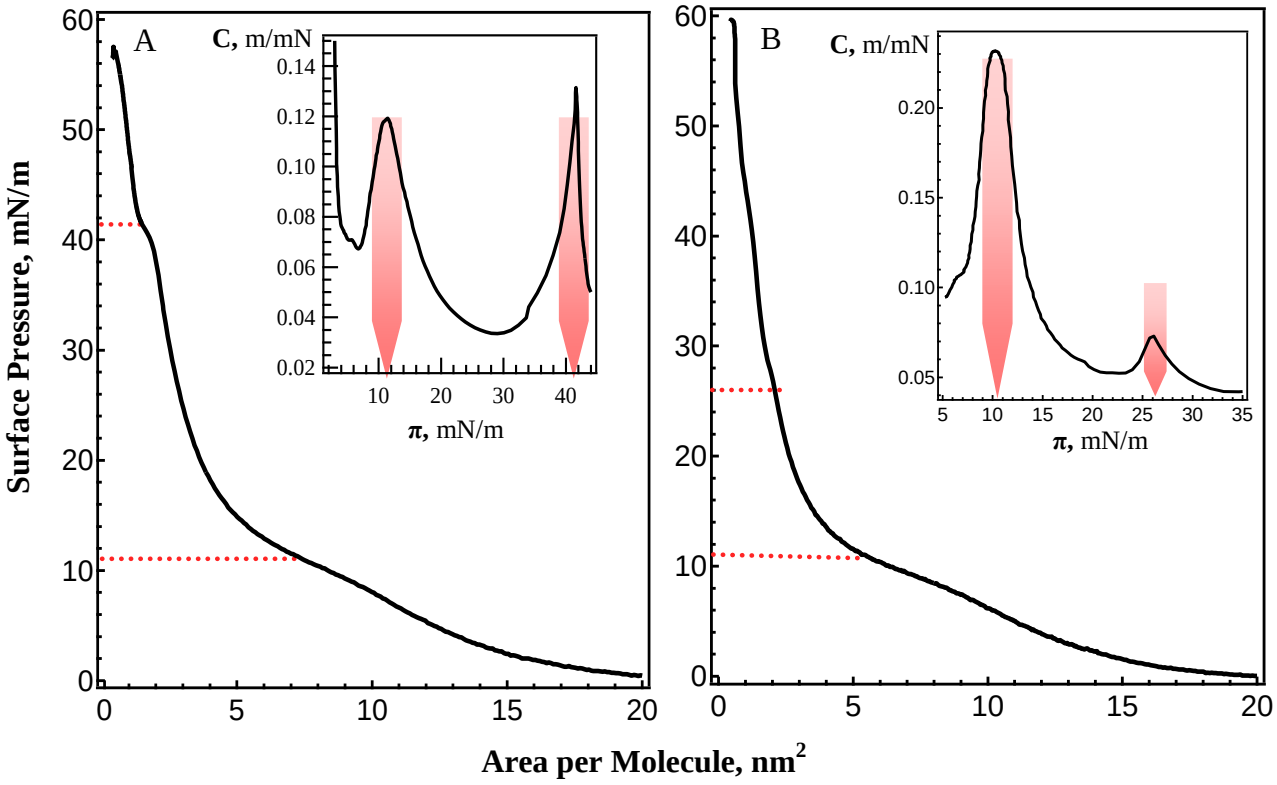

Figure 3.1. $\pi - A$ isotherms of (A) DPPE-PEG2000 and (B) DSPE-PEG2000 on PBS at 20 ° C (solid curve). Insets display the $C - \pi$ plots obtained using numerical differentiation of the $\pi - A$ isotherms. Red arrows display the peaks in the $C - \pi$ plots corresponding to the conformational transition of PEG2000, $\pi_{t,PEG}$ and the high-pressure transition, $\pi_{t,high}$. The $\pi_{t,PEG}$ and $\pi_{t,high}$ values determined from the $C - \pi$ plots are also indicated on the $\pi - A$ isotherms as red dotted lines.

3.1.2. Fluorescent Probes for PEG-Phospholipids.

DSPE-PEG2000-FITC is commercially available and has been used as a fluorescent probe for DSPE-PEG2000 previously [Borden 2006; Kinsinger 2010; Tanwir 2008]. The fluorescent probe for DPPE-PEG2000, DPPE-PEG2000-FITC, was synthesized in our lab to examine the lateral distribution of PEG-phospholipid in the phosphocholine matrix. The synthesis was performed by reacting dipalmitoylphosphatidylethanolamine (DPPE) with an excess of NHS-PEG2000-Boc but with little modifications in the procedure from the previously reported data [Mattson 1993; Miura 2006]. An *N-hydroxysuccinimidyl* (NHS) is an ester activated group to react with the amino group of DPPE whereas Boc is a protective group for an amino group of PEG, which was removed to label the distal end of the PEG chain with the FITC fluorophore [Mattson 1993; Miura 2006]. First, DPPE (42 mg, 0.06 mmol) was dissolved in 3 ml of chloroform containing 15% of methanol by heating for 30 min at ~30 °C. Further, 20 μL of basic medium, Triethylamine, and NHS-PEG2000-Boc (148 mg, 0.074 mmol) in 2 ml of dichloromethane were added [Miura 2006; Slaughter 2007; Sorgi 2001]. The reaction mixture was stirred for 4 h at 60 °C and then left overnight at 30 °C. Afterwards, 2 mL of Trifluoroacetic acid (TFA) was added to the reaction mixture at ~4 °C to remove the protecting Boc group [Miura 2006; Martin 1994]. The solution was stirred for 30 min and then the mixture was extracted into chloroform. The excess solvent was removed under reduced pressure, and the crude was precipitated into cold diethyl ether [Miura 2006; Sukhishvili 2002]. The crude product was further washed with ether to remove the excess unbound NHS-PEG2000-Boc [Sukhishvili 2002]. After drying in vacuum, a PEG-phospholipid conjugate, DPPE-

PEG2000-NH_2, was obtained as a white solid with a mass of 118 mg and a yield of 69%. Peaks in ^1H NMR (CD_2Cl_2, 600 MHz, δ ppm) are categorized as; 0.85 (t, 6H, $–CH_3$), 1.23 (br, 56H, $–CH_2–$), 3.65 (br, 218H, PEG). MS ($C_{128}H_{58}N_3O_{54}P$, turbo spray, positive): M + H^+ = 2749.8 g/mol. To label PEG-lipid with fluorescent probe (FITC), DPPE-PEG2000-NH_2 (20 mg, 0.007 mmol) was dissolved in 1 mL of dicholormethane and reacted with 0.5 mL of ethanol solution containing FITC (3 mg, 0.008 mmol) [Miura 2006]. The reaction mixture was stirred overnight at ~40 °C. DPPE-PEG2000-FITC mixture was then precipitated into cold diethyl ether. The precipitate was washed with ether to remove any unbound FITC [Sukhishvili 2002]. After drying in vacuum, a yellow-orange solid (16 mg, yield 83%) was obtained. The product was used without further purification in our imaging study.

To test the properties of DPPE-PEG2000-FITC as a probe for DPPE-PEG2000, the $\pi - A$ isotherm was recorded. The isotherm of DPPE-PEG2000-FITC appeared virtually identical to that of DPPE-PEG2000 (data not shown). This implies that FITC fluorophore attached to the PEG2000 chain is not likely to affect the intermolecular interactions and conformational behavior of PEG-phospholipid molecules to any significant extent. To verify the miscibility, mixtures of DPPE-PEG2000 and DSPE-PEG2000 containing 1 mol% of their fluorescent probes were also prepared and imaged using EFM (data not shown). EFM imaging displayed uniform fluorescent monolayers without any artifacts thus confirming their ideal miscibility. Hence, DPPE-PEG2000-FITC and DSPE-PEG2000-FITC fluorescent probes can be used to investigate the phase state properties of membrane models.

3.1.3. Surface Pressure – Area ($\pi - A$) Isotherms of DPPC and DSPC.

The $\pi - A$ isotherm of DPPC on PBS at 20 ^{o}C is demonstrated in Figure 3.2A. The lift-off of the DPPC isotherm is observed at ~1 nm^2/molecule as can be seen by the black curve in Figure 3.2A. The plateau depicting the LE – LC transition of DPPC phospholipids develops at about 5 mN/m, which appears as a peak in $C - \pi$ plot in the figure inset. The monolayer of DPPC collapses at ~52 mN/m. The data is in good agreement with the reported literature values [Albrecht 1978; Chou 2000; Discher 1999; Kinsinger 2010; Luna 2011; Yu 2002].

Figure 3.2B shows the isotherm of DSPC on PBS at 20 °C. DSPC forms a condensed type monolayer, as can be seen from the figure. The isotherm lift-off was observed at ~0.65 nm^2/molecule followed by a steep rise in surface pressure until the monolayer collapsed at A ~0.4 nm^2/molecule and π ~58 mN/m, which is in good agreement with literature [Chou 2002; Chou 2003; Tanwir 2008]. The inset in Figure 3.2B displays the compressibility plot of DSPC. The DSPC $C - \pi$ plot does not exhibit any LE-LC transition peak, as compared to the one seen in DPPC compressibility plot (Figure 3.2B).

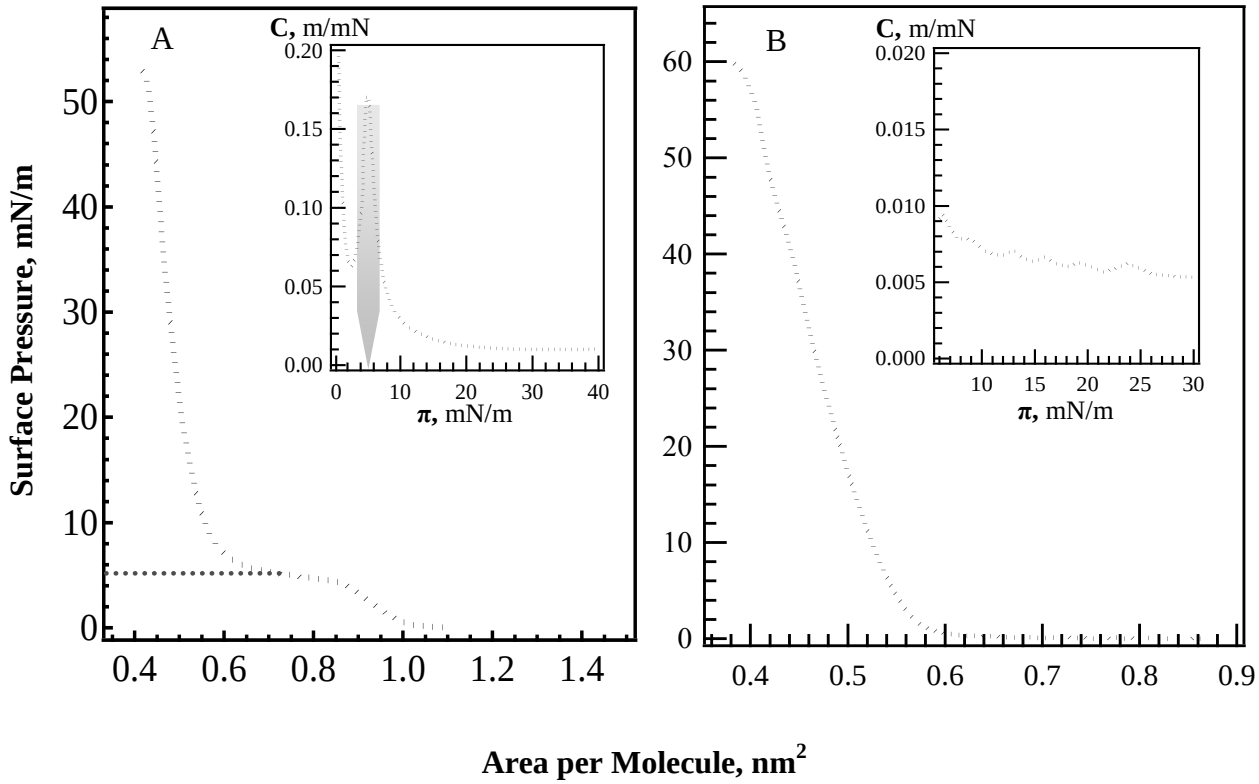

Figure 3.2. $\pi - A$ isotherms of (A) DPPC and (B) DSPC on PBS at 20 °C. Insets display the $C - \pi$ plots obtained using numerical differentiation of the $\pi - A$ isotherms. Peaks in the $C - \pi$ plots correspond to the LE – LC transition of DPPC, $\pi_{t,DPPC}$.

3.1.4. π – A Isotherms of Mixed DPPC/DPPE-PEG2000 Monolayers on PBS at 20 ^{o}C.

Figure 3.3 shows the π – A isotherms of mixed DPPC/DPPE-PEG2000, C_{16}/C_{16}-PEG2000, monolayers containing 1 – 9 mol % PEG2000-phospholid on PBS subphase. As seen in the figure, the isotherms of mixed DPPC/DPPE-PEG2000 monolayers show features of both components at 20 ^{o}C. The plateau depicting the LE – LC transition of DPPC phospholipids develops at about 5 mN/m. This data is in good agreement with reported literature values [Albrecht 1978; Chou 2000; Discher 1999; Kinsinger 2010; Luna 2011; Yu 2002]. The isotherms shifted to the right towards more expanded phase with increasing PEG2000-phospholipid content in the mixed monolayers. The effect of PEG2000 content in the low-compressibility region, however, disappears since all the mixed monolayers almost converge very close to each other. The collapse pressure of all DPPC/DPPE-PEG2000 mixtures is observed at ~52mN/m. It is also observed that with increasing PEG content, the LE – LC transition plateau in the isotherms becomes less noticeable. To substantiate this trend, the isotherms of DPPC/DPPE-PEG2000 mixtures were further analyzed in terms of lateral area compressibility, C – π, format (inset of Figure 3.3). As seen in the figures, the C – π plots predominantly exhibit two peaks. One of the peaks aligns well with peak in DPPC monolayers' C – π plots (green dotted curve in Figure 3.3). This peak can be attributed to the LE – LC phase transition, which is associated with the ordering of DPPC aliphatic chains in all-trans conformation [Albrecht 1978]. The second peak, however, appears in the range of surface pressures that corresponds to the $\pi_{t,PEG}$ in the compressibility plots of PEG-phospholipids (red dotted

curve in inset of Figure 3.3). Thus, the second peak seen in the $C - \pi$ plots of binary mixtures can be attributed to the conformational transition in the grafted polymer chains.

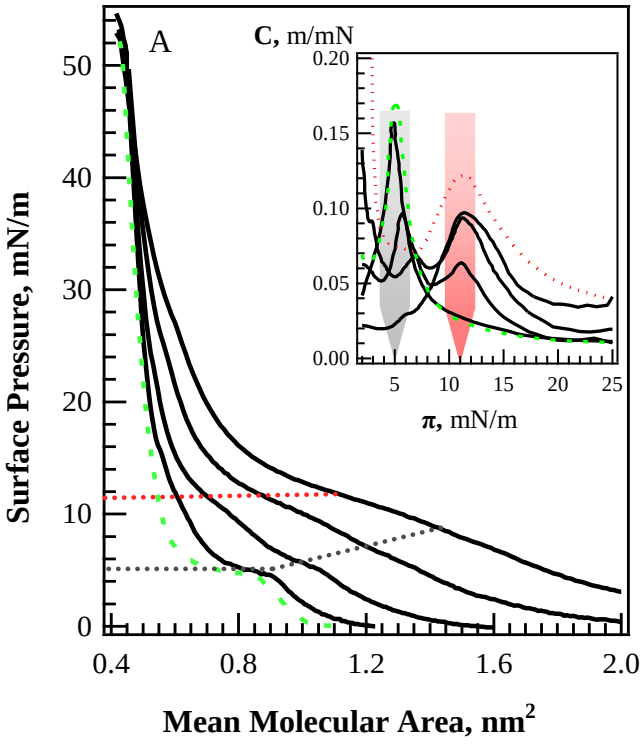

Figure 3.3.: $\pi - A$ isotherms of DPPC and DPPE-PEG2000 binary mixtures containing 1, 3, 6, and 9 mol % PEG2000-phospholipid spread on PBS subphase at 20 ^{o}C. Insets show the $C - \pi$ plots obtained by numerical differentiation of the $\pi - A$ isotherms. Green curves represent DPPC alone, whereas red curve is for DPPE-PEG2000. Peaks in the $C - \pi$ plots correspond to DPPC LE – LC phase transition, $\pi_{t,DPPC}$, whereas the PEG2000 conformational transition, $\pi_{t,PEG}$. Both transitions, $\pi_{t,DPPC}$ and $\pi_{t,PEG}$, are also highlighted by corresponding color dotted lines in the isotherms.

3.1.5. Surface Pressure (π – A) Isotherms of Mixed DSPC/DSPE-PEG2000 Monolayers on PBS at 20 ^{o}C.

The π – A isotherms of mixed DSPC/DSPE-PEG2000, C_{18}/C_{18}-PEG2000, monolayers containing 1 – 9 mol % of the PEG2000-phospholid on the PBS subphase at 20 ^{o}C are demonstrated in Figure 3.4. As presented in the figure, all isotherms show three major regimes: (i) an expanded region below ~8 mN/m, (ii) a pseudo-plateau between 9 – 18 mN/m, and (iii) a low-compressibility region above ~20 mN/m. The isotherms shifted to the right into more expanded phase with increased mean molecular area upon increasing PEG2000-phospholipid content in the mixed monolayers. The effect of PEG2000 content in the low-compressibility region, however, disappears since all the mixed monolayers almost converge very close to each other. The collapse pressure of the binary mixtures increased from ~60 mN/m at 1 mol% PEG2000-phospholipid in the host DSPC monolayer to ~67 mN/m at 9 mol %.

All the binary mixtures containing DSPC overall show condensed type isotherms as opposed to the ones of DPPC (cf. isotherms in Figures 3.3, 3.4). Indeed, this behavior correlates well with the properties of DSPC matrix. DSPC bears C_{18} aliphatic chains and predominantly forms the LC ($L_{\beta'}$) phase [Ducharme 1990; Petriat 2004; Stepniewski 2011; Suzuki 1985; Tanwir 2008; Tenchov 2001]. Thus, the transitions seen in the isotherms of DSPC and PEG2000 binary mixtures are mainly associated with the PEG-phospholipids (Figure 3.4). The C – π plots in the insets of Figure 3.4 yield better understanding about the transitions. The peaks in the C – π plots of binary mixtures appear in the same range of surface pressures corresponding to the conformational

transitions of PEG ($\pi_{t,\ PEG}$) and the high-pressure transition ($\pi_{t,high}$) seen in the isotherms of pure PEG-phospholipids (cf. Figure 3.1 and 3.4). Interestingly, the $\pi_{t,high}$ peak is only observed in the DSPC/DSPE-PEG2000 mixture containing 9 mol% PEG2000. Hence, the miscibility of all the binary mixtures was further investigated at 20 °C in order to obtain clear results about the mixing behavior of all binary mixtures.

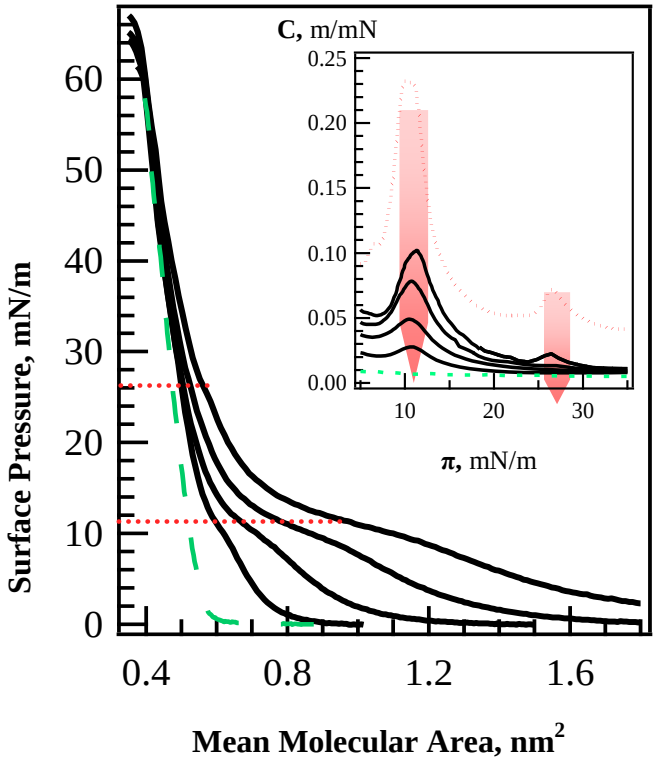

Figure 3.4.: $\pi - A$ isotherms of DSPC and DSPE-PEG2000 binary mixtures containing 1, 3, 6, and 9 mol % PEG2000-phospholipid spread on PBS subphase at 20 ^{o}C. Insets show the $C - \pi$ plots obtained by numerical differentiation of the $\pi - A$ isotherms.

3.1.6. Miscibility in Phosphocholine and PEG-Phospholipids Mixtures.

Miscibility between the matrix phosphocholine and PEG-phospholipids was assessed by analyzing the $\pi - A$ isotherms in terms of excess area, A_{exc}, of the mixture [Chou 2002; Chou 2003; Shahid 2011; Tanwir 2008]. As described in the literature, if the matrix phosphocholine and PEG-phospholipids behave immiscibly or form a complete ideal binary mixture, the mean molecular area, $A_{id/im}$, of the mixed monolayers should then be the sum of areas of separated individual components [Chou 2002; Chou 2003; Shahid 2011; Tanwir 2008].Thus, the relation between the $A_{id/im}$, and mol fractions of the individual components, at any given surface pressure, should obey the equation below

$$A_{id/im} = \chi_{PC} A_{PC} + \chi_{PEG-phospholipid} A_{PEG-phospholipid} \qquad 3.2$$

In equation 3.2, χ_{PC} and $\chi_{PEG\text{-}phospholipid}$ are the mol fractions of components and A_{PC} and $A_{PEG\text{-}phospholipid}$ represent the molecular areas of each component in their pure monolayers at the same surface pressure [Chou 2002; Chou 2003; Gaines 1966; Tanwir 2008]. However, if the binary mixtures do not obey equation above, then any deviation from the rule can be quantitatively defined as A_{exc} using equation

$$A_{exc} = A - A_{id/im} = A - (\chi_{PC} A_{PC} + \chi_{PEG-phospholipid} A_{PEG-phospholipid}) \qquad 3.3$$

where A is the mean molecular area in the $\pi - A$ isotherms at any given surfaces pressure. By definition, if the two components are completely immiscible or form an ideal mixture

then the A_{exc} would be zero, whereas any deviation from zero, either negative or positive, would indicate the nonideal miscibility in the mixed monolayers. Immiscible mixture refers to a mixture where both components do not mix with each other and stay heterogeneous. In this case, the monolayer of two immiscible components will exhibit the properties of two separate individual component monolayers [Gaines 1966]. Miscible mixture refers to a mixture where both components mix homogeneously. However, miscible mixtures can behave ideally or non-ideally. The term ideal mixture is used where the interaction between two different components is similar to the interactions between identical molecules. In contrast, non-ideal mixture has dissimilar interactions between both components of the mixture and would be observed as two different phases in the monolayer [Luna 2011]. The A_{exc} calculations in this study were performed between 15 – 35 mN/m, which is relevant to the lateral pressures of a typical membrane, as estimated in the literature [Lozano 2009a; Konttila1988]. The values for A_{exc} calculated for all the binary mixtures are summarized in Tables 3.1 and 3.2. As can be seen, most of the A_{exc} values are negative suggesting a nonideal miscibility in the mixtures. The negative deviations of A_{exc} seem to be more pronounced with an increase in surface pressure and PEG content in all the binary mixtures.

Another supportive argument for the nonideal miscibility in the mixtures arises from the surface phase rule. According to the rule, if two components are miscible then the mixed monolayer collapse point will vary based on the composition [Chou 2002; Chou 2003; Gaines 1966; Tanwir 2008]. Conversely, if two components are immiscible, then the monolayers will have two different collapse points, each at their own surface

pressures, regardless the composition [Chou 2002; Chou 2003; Gaines 1966; Tanwir 2008]. As can be seen in Figures 3.3 and 3.4, the collapse pressures of all mixtures changed with an increase in PEG content from 1 mol% to 9 mol%. This change in collapse point clearly indicates a nonideal mixing for most of the phosphocholine and PEG-phospholipid mixtures. Although miscibility analysis clearly points towards the nonideal mixing behavior in the mixed monolayers but "immiscible mixed phases" of different compositions may coexist in the mixtures [Baekmark 1995; Tanwir 2008]. Hence, EFM imaging of the binary mixtures was performed to further investigate the mixing behavior of phosphocholine and PEG-phospholipids on PBS at 20 °C.

Table 3.1.

Excess Area, A_{exc}, Calculated for Binary Mixtures of DPPC/DPPE-PEG2000 at 20 ^{o}C.

	A_{exc}, nm^2			
π, mN/m	1 mol% PEG	3 mol% PEG	6 mol%	9 mol% PEG
15	-0.03	-0.06	-0.09	-0.10
25	-0.02	-0.06	-0.09	-0.10
35	-0.02	-0.04	-0.08	-0.12

Each value of A_{exc} calculated is an average of three isotherm measurements. Standard deviations calculated for A_{exc} are based on a series of three measurements are within ± 0.01 nm^2.

Table 3.2.

Excess Area, A_{exc}, Calculated for Binary Mixtures of DSPC/DSPE-PEG2000 at 20 ^{o}C.

	A_{exc}, nm^2			
π, mN/m	1 mol% PEG	3 mol% PEG	6 mol%	9 mol% PEG
15	0.03	-0.03	-0.05	-0.08
25	0.02	-0.02	-0.04	-0.06
35	0.02	-0.01	-0.03	-0.04

Each value of A_{exc} calculated is an average of three isotherm measurements. Standard deviations calculated for A_{exc} are based on a series of three measurements and within ± 0.01 nm^2.

3.1.7. EFM Imaging of DPPC and DPPE-PEG2000 Mixtures.

The coexistence of phospholipid phases and formation of liquid condensed (LC) phase in DPPC/DPPE-PEG2000 binary mixtures was visualized by introducing DOPE-Rh as a fluorescent probe. DOPE-Rh, like many other dyes, is known to possess high affinity towards LE phase due to its unsaturated aliphatic chains [Sezgin 2012; Shahid 2011; Tsoukanova 2008]. Thus, the red stain of DOPE-Rh chromophore in the TRITC channel indicated the LE phase while the dark background represented the LC phase of the mixtures. Conversely, the lateral distribution of PEG in the phosphocholine matrix was monitored using the FITC channel by detecting the fluorescence from DPPE-PEG2000-FITC, which bears a fluorescein fluorophore at the distal end of the PEG2000 chain. The green stain of FITC fluorophore in the FITC channel corresponds to the areas where PEG-phospholipid molecules were present [Borden 2006; Kinsinger 2010; Tanwir 2008].

The EFM imaging was performed throughout the monolayer compression. Monolayers of type (i) containing DOPE-Rh probe and (ii) containing FITC labelled PEG-phospholipid showed the same imaging sequence as the monolayers of type (iii) containing both probes using two channel EFM. The two channel imaging, thus, did not produce any artifacts. Hence, for the clarity of discussion, this study will only include results obtained by two channel EFM imaging. The EFM images shown in the present study is limited to the typical range of membrane pressures as discussed above, which is

15 – 35 mN/m. The images obtained through FITC and TRITC channel are displayed from the same patch of the monolayer for a better comparison, whenever possible.

Figure 3.5 displays the LE/LC phases and lateral distribution of DPPE-PEG2000-FITC in DPPC matrix at 15, 25, and 35 mN/m. The binary mixtures of DPPC/DPPE-PEG2000 showed dark domains that began nucleating above π ~4 mN/m (images not shown). At about 15 mN/m, both TRITC and FITC images displayed a great proportion of dark domains for the mixed DPPC/DPPE-PEG2000 monolayers (Figure 3.5). In the low-compressibility region, the TRITC channel showed the fusion of dark domains for DPPC/DPPE-PEG2000 mixtures (image B1 and C1 in Figure 3.5) and then all the mixtures converted to a continuous dark LC phase with very small fluorescent spots of DOPE-Rh chromophore at π above 35 mN/m (images not shown). Conversely, FITC channel had a somewhat different sequence as compared to the TRITC channel. The green stained areas, containing DPPE-PEG2000-FITC, started to expand above 20 mN/m, as shown in images B2 and C2 in Figure 3.5. Moreover, the DPPE-PEG2000-FITC excluded domains were observed in the FITC channel but getting significantly smaller above 35 mN/m (images not shown).

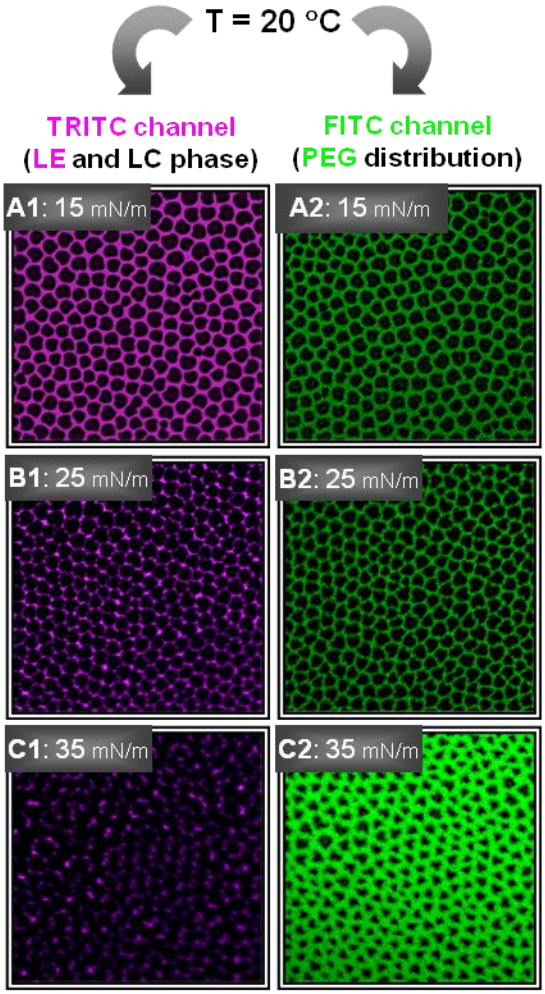

Figure 3.5: Epifluorescence microscopy images of mixed DPPC/DPPE-PEG2000 monolayers containing 3 mol% PEG2000 content at 15, 25, and 35 mN/m, at 20 ^{o}C. Red Fluorescent background represents LE phase and dark domains show the LC phase whereas green fluorescent in the images show the distribution of PEG containing DSPE-PEG2000FITC and dark domains represent the PEG-FITC excluded domains. Image size is 250 × 250 μm^2. Based on our study [Tanwir et. al. 2012].

3.1.8. EFM Imaging of Binary Mixtures of DSPC and DSPE-PEG2000.

In the TRITC images, the binary mixtures containing DSPC as matrix phospholipids exhibited more dark LC phase as compared to the DPPC mixtures at 20 °C. The dark circular LC phase domains in the fluorescent background began to nucleate at ~4 mN/m for DSPC/DSPE-PEG2000 mixtures. Most of the binary mixtures of DSPC DSPC-PEG2000 converted into a continuous dark LC phase above 15 mN/m, as seen in the images in Figure 3.6. Moreover, the size of LC phase domains in DSPC mixtures appeared smaller than those in DPPC mixtures. As seen in the FITC images, the domain boundaries started to "melt" continually in the DSPC/DSPE-PEG2000 mixtures and the monolayer morphology changed to a single homogeneous fluorescent phase upon compression (cf. images A2, B2 and C2 in Figure 3.6). The surface pressure at which the morphology changed varied depending on the PEG2000-phospholipid concentration in the mixtures. A single homogeneous florescent phase was achieved for 1 mol % at ~ 48 mN/m and for 9 mol % at ~ 13 mN/m. Surprisingly, mixed monolayers containing 6 and 9 mol % PEG2000-FITC had few irregular shaped fluorescent DSPE-PEG2000FTC-rich domain that appeared in the low-compressibility region at π above 30 mN/m (images not shown). These irregular shaped domains were not observed in other type of mixed monolayers at 20 ^{o}C.

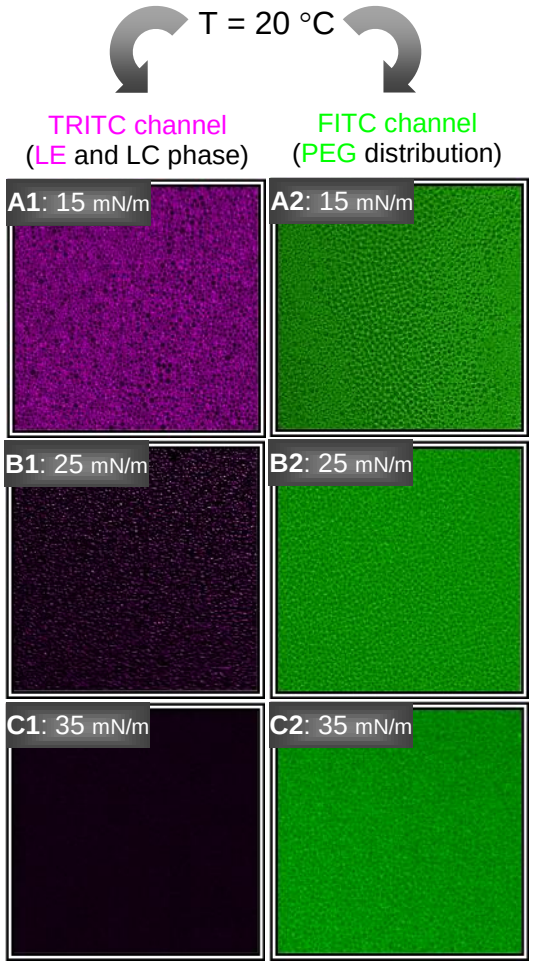

Figure 3.6.: Epifluorescence microscopy images of mixed DSPC/DSPE-PEG2000 monolayers containing 6 mol% PEG2000 content at 15, 25, and 35 mN/m, at 20 ^{o}C. Image parameters are as same as in Figure 3.7. Image size is 250 × 250 μm^2. Based on our study [Tanwir et. al. 2012].

3.2. DISCUSSION.

The mixing behavior of phosphocholine matrix with PEG2000-grafted phospholipids has been studied extensively at different temperatures at air/water interface [Borden 2006; Heeb 2009; Lozano 2009]. The main goal of this study was to analyze the effect of PEG content on the morphology and phase behavior of phosphocholine membrane on air/PBS interface. By analyzing the $\pi - A$ isotherms at 20 ^{o}C, it can be elucidated that PEG has a profound impact on the binary mixtures of phosphocholine and PEG-phospholipid. This can be seen from the development of a pseudo-plateau at ~10 mN/m, which was broadened upon increasing PEG2000 content in the mixtures. This pseudo-plateau is considered as a unique property of the conformational transition in grafted PEG chains ($\pi_{t,PEG}$) and usually termed as a change from pancake to pseudo-3D conformation. The latter has been described in the literature as a mushroom, a cigar, and a brush conformation [Backmann 2010; Baekmark 1995; El-Khouri 2011; Kinsinger 2010; Luna 2011; Majewski 1998; Naumann 2001; Vermette 2003; Zhao 2002]. At low surface grafting density, PEG chains form a pancake like structure by spreading on the surface and do not interact with each other [Baekmark 1995]. With increasing the surface grafting density, PEG chains begin to form mushroom structure with coil dimension to avoid interactions with each other [Backmann 2010; Baekmark 1995; Kato 2003]. Upon further increase in the grafting density, PEG chains are forced to stretch away from the surface by forming elongated brushes to avoid overlapping and in turns play a key role in optimal protein repellence [Backmann 2010; Baekmark 1995; Dhruv 2009; Kato 2003; Zhao 2000]. These terms mainly apply to the PEG conformation at the air/water

interface. However, we are not presenting any experimental data in this report that could enable us to conclude about the most adequate model in describing conformation of the PEG2000 chains in the binary mixtures of phosphocholine and PEG-phospholipids. Thus, the term "pseudo-3D conformation" will be used throughout this study to refer to the PEG conformation adopted upon the transition at $\pi \sim 10$ mN/m. This simply suggests that grafted PEG chains largely squeeze out of the phospholipid headgroup region and extend away from the membrane during its conformational transition [Baekmark 1995; Majewski 1998; Naumann 1999; Naumann 2001; Shahid 2011; Stepniewski 2011; Tanwir 2008; Vermette 2003; Zhao 2002]. As can be seen from the upper limit of the $\pi_{t,PEG}$ peak in the compressibility plots, the conformational transition is almost completed around 20 mN/m (insets of Figures 3.1, 3.3 and 3.4). Therefore, it is believed that the grafted PEG2000 chains are likely in the pseudo-3D conformation in a surface pressure range of 15 – 35 mN/m, which is relevant to the membrane lateral pressures.

Based on the DSPC/DSPE-PEG2000 mixtures at 20 °C, it can be suggested that excluded volume interactions between PEG2000 chains in the pseudo-3D conformation might force the PEG-phospholipid molecules to distribute uniformly throughout the membrane at higher PEG grafting densities [Tanwir 2008]. Indeed, these mixtures form a continuous LC phase with homogeneous distribution of DSPE-PEG2000 with increase in pressures and PEG contents (images C1 and C2 in Figure 3.6). Interestingly, previous studies on DSPC/DSPE-PEG2000 mixtures have also reported the coexistence of immiscible phases over a temperature range of 25 – 55 °C [Bedu-Addo 1996; Borden 2006]. Moreover, Borden et al. have reported an increase in the phase separation in

DSPC/DSPE-PEG2000 mixtures with increasing PEG content at 25 – 55 °C [Borden 2006]. However, this conclusion completely contradicts the trend observed at 20 °C [Tanwir 2008; Kinsinger 2010]. This signifies towards a great need to develop a more comprehensive understanding of the phase behavior of PEGylated phosphocholine membranes and construct phase diagrams. The first step to construct such diagrams is to identify the coexisting phases. This is usually done by a comparative analysis of $\pi - A$ isotherms and EFM images obtained with a single fluorescent probe to stain the LE phase [Lozano 2009a; Shahid 2011]. In this study, the lateral distribution of PEG was also determined by using an additional fluorescent probe (DPPE-PEG2000-FITC or DSPE-PEG2000-FITC) in EFM imaging. This has allowed us locating the PEG-phospholipid molecules in the coexisting phases of the mixtures. Using this unique approach, we have found a more complex and intricate behavior of PEGylated phosphocholine membranes than previously comprehended. Hence, our major goal will be to identify all possible coexisting phases in the model PEGylated phosphocholine membranes.

The mixing behavior, phase state, and morphology of phosphocholine and PEG-phospholipid mixtures with different aliphatic chain length have also been studied in this project. These mixtures include DPPC/DSPE-PEG2000 (C_{16}/C_{18}) and DSPC/DPPE-PEG2000 (C_{18}/C_{16}). The π – A isotherms of binary mixtures bearing different aliphatic chain length (data not shown) appeared similar to those of mixtures bearing same aliphatic chain length. Some differences were observed in the morphology of DPPC/DSPE-PEG2000 mixtures as compared to DPPC/DPPE-PEG2000 mixtures as well as between the mixtures of DSPC/DPPE-PEG2000 and DSPC/DSPE-PEG2000 at

higher surface pressures (images not shown). However, this surface pressure range does not lie in the typical range of membrane surface (lateral) pressure. Hence, for the clarity of discussion, the results of DPPC/DSPE-PEG2000 and DSPC/DPPE-PEG2000 mixtures containing 1, 3, 6, and 9 mol% PEG will not be included in this report.

3.2.1. Coexisting Phases in Phosphocholine and PEG-Phospholipids Binary Mixtures.

The comparative analysis of EFM images obtained through TRITC and FITC channels has revealed several phases in the phosphocholine and PEG-phospholipid binary mixtures. Schematic diagrams depicting the coexisting phases in the binary mixtures are shown in Figure 3.7. These diagrams are constructed by superimposing the red and green fluorescent backgrounds seen in both TRITC and FITC channels.

EFM images of some of the binary mixtures at 20 °C often show the coexistence of two phases, where dark domains are present in a fluorescent background (Figures 3.6). Dark domains in the TRITC channel correspond to the LC phase of the phosphocholine matrix, LC_{PC}, which is nucleating out of the fluorescent background (LE_{mix} phase) [Baekmark 1995; El-Khouri 2011; Lozano 2009; Shahid 2011]. PEG-phospholipid molecules usually tend to reside outside the LC phase domains and this correlates well with the identical patterning of fluorescence observed in both TRITC and FITC images (cf. images A1 and A2 Figure 3.6). Hence, Figure 3.7A shows a coexistence of two phases displaying an identical non-homogeneous fluorescence in both images and can be

inferred as two immiscible phases: one refers to as LC phase of the DSPC matrix and the second one as a mixed LE phase containing both LC_{PC} and LE_{mix}.

Interestingly, binary mixtures of DPPC/DPPE-PEG2000 at 20 °C exhibit a somewhat more complex type of coexistence phase. For instance, the binary mixtures of DPPC/DPPE-PEG2000 images at $\pi \sim 15$ mN/m show identical fluorescence patterns of typical LC_{PC} + LE_{mix} phase coexistence in both TRITC and FITC channel (cf. images A1 and A2 in Figure 3.5). However, the fluorescent patterning in TRITC and FITC start to differ at higher surface pressures. The FITC images exhibit more fluorescent staining with respect to the TRITC images (cf. images C1 and C2 in Figure 3.5). This is suggestive of the infiltration of DPPE-PEG2000 molecules into the LC phase domains of DPPC, yet only at a minute level. Thus, it can be inferred that the coexistence phase that depicts a non-homogeneous fluorescence along with the non-identical patterning in both TRITC and FITC channel comprise of three phases LE_{mix} + LC_{PC} + LC_{mix} (Figure 3.7B). LE_{mix} phase is rich in the PEG-phospholipid, the LC_{PC} phase includes only phosphocholine LC phase, while mixed LC phase, LC_{mix}, is considered to be rich in both the phosphocholine and PEG-phospholipid molecules.

It has been seen that DPPC/DPPE-PEG2000 mixtures eventually form a continuous LC phase at higher pressures well above the membrane pressure range. These mixtures show an almost complete dark field in the TRITC images but still show DPPE-PEG2000-FITC excluded domains in the FITC images (images not shown). This type of pattern refers to a non-uniform distribution of PEG chains throughout the LC DPPC

matrix [Tanwir 2008]. Thus, DPPC/DPPE-PEG2000 mixtures at higher pressures contain two phases in the LC state: (i) LC_{PC} phase and (ii) a mixed LC phase, LC_{mix} as sketched in Figure 3.7C.

Binary mixtures of DSPC/DSPE-PEG2000 have shown a remarkable homogeneous mixing of the two components in the LC state at 20 ^{o}C. This can be seen in the images in Figure 3.6 that features a "miscibility transition" at intermediate pressures. Indeed, TRITC image in B1 of Figure 3.6 exhibits two phases, LE and LC, whereas the FITC image in B2 of Figure 3.6 display a uniform fluorescence field. This observation points towards an almost homogeneous distribution of DSPE-PEG2000 molecules between these phases. This suggests that both phases are mixed phases and can be recognized as the LE_{mix} + LC_{mix} coexistence phase (Figure 3.7D). Furthermore, the dark field seen in TRITC image C1 in Figure 3.6, at higher pressures, corresponds to the formation of a continuous LC phase whereas, FITC image C2 in Figure 3.6 displays a uniform distribution of DSPE-PEG2000-FITC molecules. Therefore, this phase refers to as a single mixed LC phase, LC_{mix}, and is schematically shown in Figure 3.7E.

The phases identified in our model study correlate well with the literature data for PEGylated phosphocholine membranes [Bedu-Addo 1996; Borden 2006; Kenworthy 1995; Pu 2005; Tanwir 2008]. However, a direct comparison is not always possible due to a limited literature data for PEGylated phosphocholine model membranes. For instance, a study by Kenworthy et al. has reported a single $L_{\beta'}$ phase for the DSPC/DSPE-PEG2000 bilayer membranes, at low PEG grafting densities [Kenworthy 1995]. On the

other hand, Bedu-Addo et al. reports on the coexistence of two immiscible phases, L_d and $L_{\beta'}$ for membranes of liposomal drug carriers [Bedu-Addo 1996]. This coexistence phase resembles the LC_{PC} + LE_{mix} phase depicted in Figure 3.7A in the present study. The presence of two immiscible (L_d and $L_{\beta'}$) phases as well as three phase coexistence has also been reported in phospholipid-coated microbubble membranes for implications in diagnostic agent delivery [Borden 2006; Pu 2005].

A

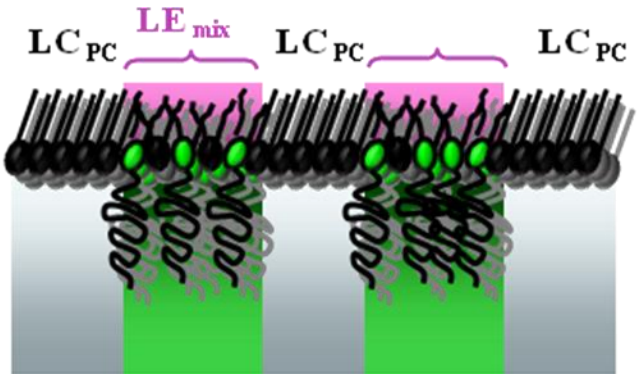
LC PC
LE mix
LC PC
LC PC

B

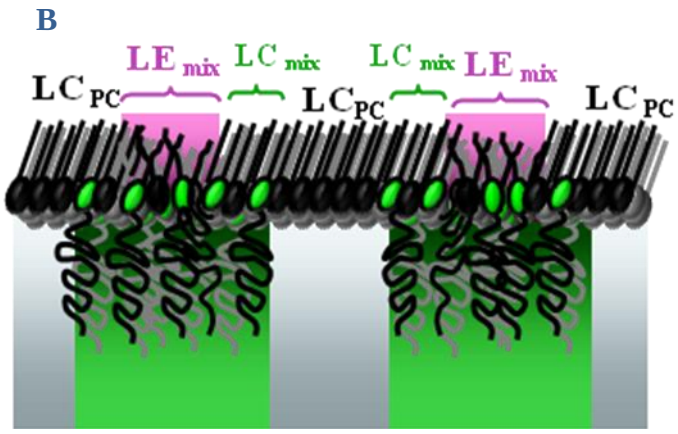
LE mix
LC mix
LC mix
LE mix
LC PC
LC PC
LC PC

C

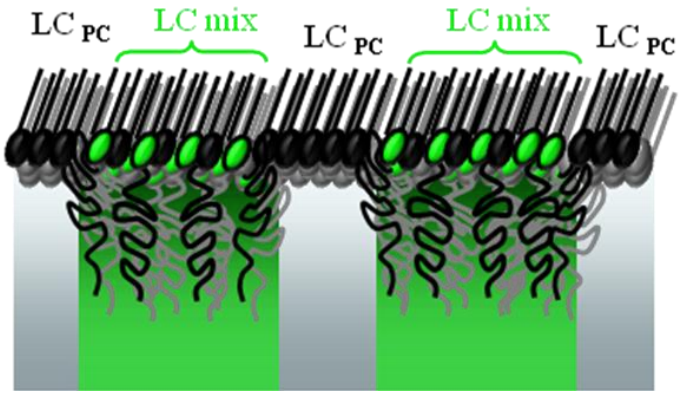
LC PC
LC mix
LC PC
LC mix
LC PC

D

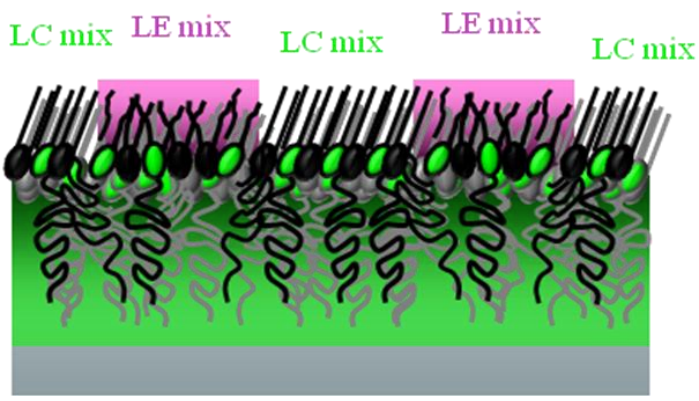
LC mix
LE mix
LC mix
LE mix
LC mix

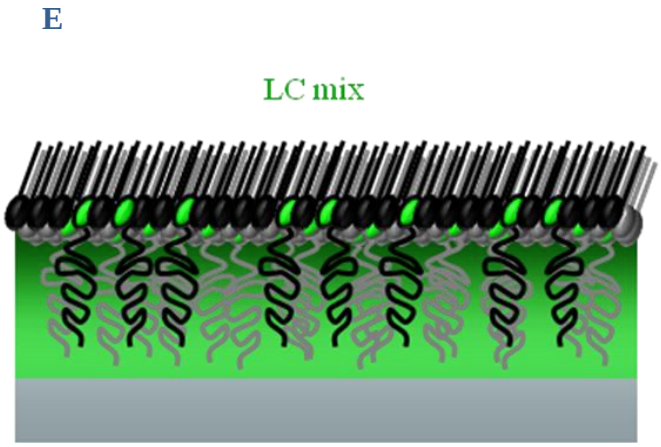

Figure 3.7: Schematic diagrams depicting the coexistence phases in the binary mixtures of phosphocholine and PEG-phospholipids. (A) the coexistence of two immiscible phases, LE_{mix} + LC_{PC}, (B) three phase coexistence, LE_{mix} + LC_{PC} + LC_{mix}, (C) coexistence of two immiscible LC phases, LC_{PC} + LC_{mix}, (D) the coexistence of two immiscible mixed phases, LE_{mix} + LC_{mix}, (E) the mixed LC phase, LC_{mix}. Phosphocholine and PEG-phospholipid molecules are drawn with black and green headgroups. Red and green fluorescent areas show fluorescence staining observed in TRITC and FITC channel, respectively. The diagrams are based on our study [Tanwir et. al. 2012].

3.2.2. Phase Diagrams of Phosphocholine and PEG-Phospholipid Binary Mixtures.

To better demonstrate the phase behavior of phosphocholine and PEG-phospholipid binary mixtures, phase diagrams are constructed over a wide range of surface pressures using $\pi - A$ isotherms and EFM image analysis (Figure 3.8 and 3.9). The data in the diagrams are shown for a range of PEG contents of 1 – 9 mol% for the clarity of the presentation. In the figures, black curves depict the onset (lower pressures) and completion (higher pressures) of the LC phase formation [Lozano 2009]. These curves make the upper limit boundary for the LE state, seen as the white area at the bottom of the diagram, and also mark the lower limit of the LC phase, which is shown as the grey area in the phase diagram (Figure 3.8 and 3.9). The solid grey line in the diagram indicates the collapse point of all the monolayers. The dashed curve in Figure 3.8 depicts the surface pressures where fluorescence staining in both TRITC and FITC images started to diverge. In DSPC/DSPE-PEG2000 mixtures, this trend corresponds to the miscibility transition. However, in DPPC/DPPE-PEG2000 mixtures, this curve indicates the infiltration of DPPE-PEG2000 molecules into the LC_{PC} domains. The pink shaded area represents the two immiscible phases, LE_{mix} and LC_{PC}. The light green area either depicts the two immiscible, LE_{mix} + LC_{mix}, or three immiscible phase coexistence, LE_{mix} + LC_{mix} + LC_{PC}. The area shaded with grey color depicts the LC_{mix} and LC_{PC} phase coexistence whereas a single mixed LC phase, LC_{mix}, is displayed as a green color. The PEG-phospholipid conformational transitions are shown as dotted curves using π values from the $C - \pi$ peaks, which correspond to the $\pi_{t,PEG}$ at ~12 mN/m and $\pi_{t,high}$ above 20 mN/m.

Phase diagram for DSPC/DSPE-PEG2000 mixtures mainly shows the phase coexistence of LE_{mix} + LC_{PC}. For DSPC/DSPE-PEG2000 mixtures, the LE_{mix} + LC_{PC} phase coexistence appears at low surface (lateral) pressures but these mixtures begin to undergo the miscibility transition. At 3 – 9 mol% PEG, the onset of the miscibility transition (dashed curve in Figure 3.9) correlates well with the completion of the PEG conformational transition (Dotted curve in Figure 3.9). The mixtures eventually form a single LC_{mix} phase where the two components mix homogeneously (green area in Figure 3.9).

Furthermore, as can be seen in the phase diagrams, PEG-phospholipids and phosphocholine tend to mix in the LE state as opposed to the LC state. This is in good agreement with previous studies [Bedu-Addo 1996; Naumann 2001]. However, a closer look at the diagrams in Figure 3.8 and 3.9 reveal a homogeneous mixing of PEG-phospholipids and phosphocholine in the LC state for some mixtures as well. For instance, a unique mixture composition of DSPC/DSPE-PEG2000 containing 3 mol% PEG-phospholipid exhibits a single LC_{mix} phase above 20 mN/m (lower π edge of the green shaded area in Figure 3.9). The π at which single LC_{mix} phase was achieved in the rest of the DSPC/DSPE-PEG2000 mixtures differ, as can be seen in Figure 3.9. Identifying such mixture compositions that form a complete LC ($L_{\beta'}$) state along with a homogeneous PEG-phospholipid distribution can be of great importance in various biomedical applications including therapeutic delivery systems.

DPPC mixtures also exhibit different coexisting phases in the diagram in Figure 3.8 shows the most interesting phase diagram of DPPC/DPPE-PEG2000 at 20 °C. The diagram shows three different stages throughout the compression. At lower pressures, binary mixtures of DPPC/DPPE-PEG2000 exhibits mixed LE phase. At intermediate pressures, mixtures display LE_{mix} + LC_{PC} phase due to phase separation which then changes to LE_{mix} + LC_{PC} + LC_{mix} due to partial re-mixing. The mixtures eventually convert to a LC phase containing two immiscible LC_{PC} + LC_{mix} phases, at higher pressures. A direct correlation between the onset of the steep portion of the isotherm (corresponds to the closest packing of phospholipid molecules) and the formation of a continuous LC phase, LC_{mix}, LC_{PC}, was observed for DPPC/DPPE-PEG2000 mixtures.

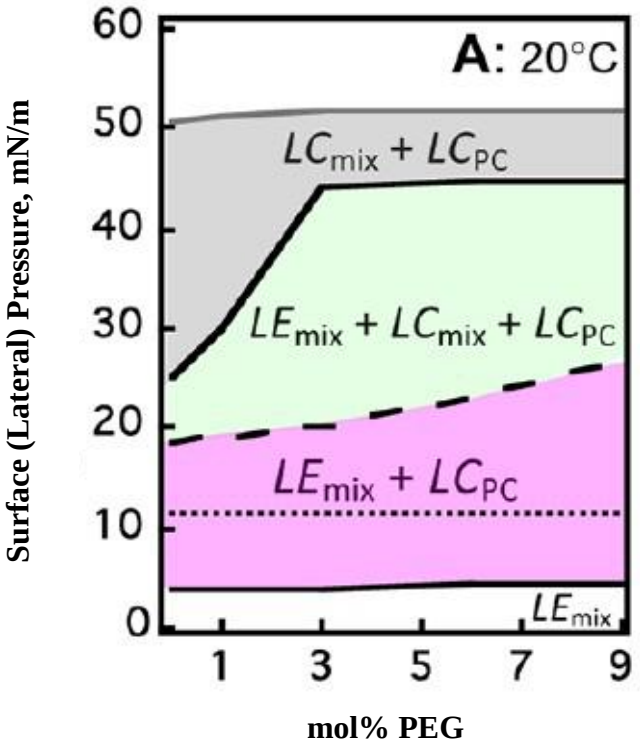

Figure 3.8: Phase diagrams for the binary mixtures of DPPC/DPPE-PEG2000 on PBS subphase at 20 °C. Details of diagram parameters are in the discussion. The diagram is based on our study [Tanwir et. al. 2012].

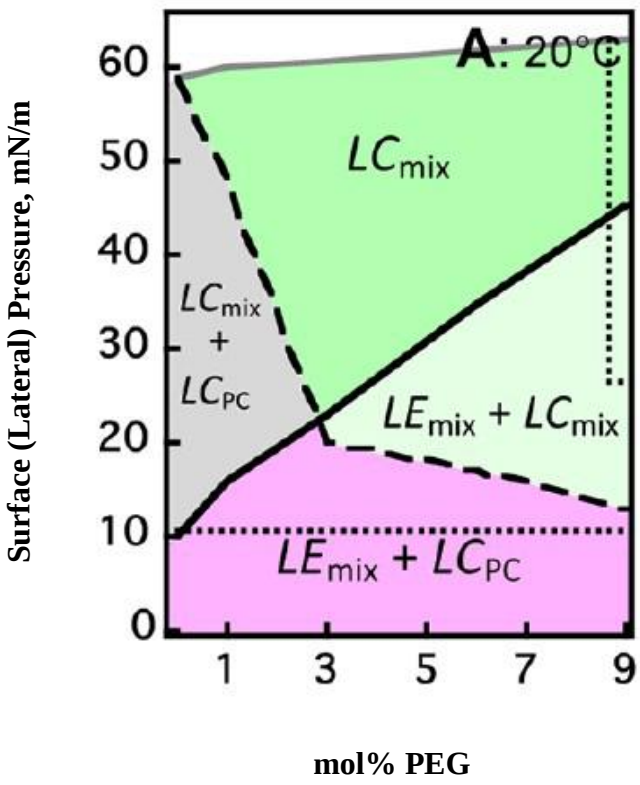

Figure 3.9: Phase diagrams for the binary mixtures of DSPC/DSPE-PEG2000 on PBS subphase at 20 °C. Details of diagram parameters are in the discussion. The diagram is based on our study [Tanwir et. al. 2012].

3.2.3. Implications in Designing the PEGylated Phosphocholine Membranes.

The results of the present study, in particular the phase diagrams, suggest an intricate interplay between the phase state of the mixtures and factors such as (i) PEG content and (ii) aqueous medium. Surface (lateral) pressure is another factor contributing towards the phase state of the binary mixtures. Based on the data analysis, several observations can be made about the factors influencing the phase behavior of PEGylated phosphocholine membranes, as stated below.

3.2.3.1. Effect of PEG Content on the Phase State of Phosphocholine Membranes.

An increase in PEG content in the phosphocholine membranes shifted both liquidus and solidus transitions to considerably high surface (lateral) pressures, as seen in the diagrams in Figure 3.8 and 3.9. This suggests that high PEG content introduces more disorder in the phosphocholine membranes, which may result in a significant change in the phase behavior of the membranes. For instance, DSPC/DSPE-PEG2000 mixtures containing 1 mol% PEG mainly exist as the LC ($L_{\beta'}$) state whereas mixtures containing more than 3 mol% PEG have appreciable amount of LE (L_d) phase for the range of membrane lateral pressures (Figure 3.9). Similarly, a coexistence of LE (L_d) and LC ($L_{\beta'}$) phase is suggested for the DPPC/DPPE-PEG2000 mixtures below 3 mol% PEG, but a single LE (L_d) phase is noticed for higher PEG densities (Figure 3.8). Moreover, the appearance of the phase coexistence (light green area), LE_{mix} + LC_{mix}, as well as a single LC_{mix} phase (green area) in the diagram in Figure 3.9 clearly indicates that DSPE-

PEG2000 becomes uniformly distributed throughout the DSPC matrix upon increasing PEG content.

3.2.3.2. Effect of Aqueous Medium on Phase State of Phosphocholine Membranes.

Aqueous medium, to which membrane is exposed, is also a key factor contributing towards the phase behavior of PEGylated phosphocholine membranes. Upon comparison with the data available in the literature, it is found that the diagrams obtained for the mixtures in Figure 3.9 on PBS subphase differ from the one reported previously on water [Lozano 2009]. In particular, the solidus transition in DSPC/DSPE-PEG2000 mixtures at 20 °C on PBS appear ~15 mN/m higher than those shown on water [Lozano 2009].

The above findings may play a pivotal role in understanding the phase state of PEGylated phosphocholine membranes in various biomedical applications. However, it is noteworthy that there might be a complex interplay between several factors governing the phase state of the model membranes. It is very essential to have a fundamental knowledge of these factors contributing towards the phase state of the model membranes. Therefore, the set of data obtained under identical experimental conditions on PBS may offer a new tool for the rational design of PEGylated phosphocholine membranes. This may help understanding and controlling the properties of model membranes in aqueous media of physiological relevance.

3.3. CONCLUSIONS.

Comprehensive analysis of phosphocholine and PEG-phospholipids binary mixtures has given a new insight on the mixing behavior of PEGylated phosphocholine membranes on PBS in a range of 1 – 9 mol% PEG. Depending on the composition, both homogeneous mixing and completely immiscible phases have been observed in the mixtures. For instance, remarkable changes in the phase behavior of DSPC/DSPE-PEG2000 mixtures have been observed upon increasing PEG content from 1 – 9 mol%. DSPC/DSPE-PEG2000 mixture containing 1 mol% PEG predominantly forms immiscible LC phase which turns to the coexistence of mixed LE and LC phases in mixture containing 9 mol%. In fact, there is a unique mixture composition seen at 3 mol% PEG, which features a single homogenously mixed phase in the LC state. This unique mixture exists is in a very small range of PEG content and hence was not identified in previous studies. These findings thus imply that the phase behavior of PEGylated phosphocholine membranes may significantly change in response to slight changes in composition which can be used for rational design of PEGylated membranes mimetic surfaces for various biomedical applications including diagnostic devices, exclusion filters for microfluidic devices, as well as nanocarriers for therapeutic and diagnostic agents.

3.4. REFERENCES.

Albrecht, O.; Gruler, H.; and Sackmann, E. *J. Phys.* **1978**, *39*, 301 – 313.

Allen, C.; Dos Santos, N.; Gallagher, R.; Chiu, G. N. C.; Shu, Y.; Li, W. M.; and Johnstone, S. A.; Janoff, A. S.; Mayer, L. D.; Webb, M. S.; Bally, M. B. *Biosci. Rep.* **2002**, *22*, 225 – 250.

Ahrens, H.; Baekmark, T. S.; Merkel, R.; Schmitt, J.; Graf, K.; Raiteri, R.; and Helm, C. A. *ChemPhysChem* **2000,** *2*, 101 – 106.

Backmann, N.; Kappeler, N.; Braun, T.; Huber, F.; Lang, H-P.; Gerber, C.; and Lim, R. Y. H. *Beils. J. Nanotechnol.* **2010,** *1*, 3 – 13.

Baekmark, T.R.; Elender, G.; Lasic, D.D.; and Sackmann, E. *Langmuir* **1995**, *11*, 3975 – 3987.

Bedu-Addo, F. K.; Tang, P.; Xu, Y.; and Huang, L. *Pharm. Res.* **1996**, *13*, 710 – 717.

Bianco-Peled, H.; Dori, Y.; Schneider, J.; Sung, L. P.; Sajita, S.; and Tirrell, M. *Langmuir* **2001**, *17*, 6931 – 6937.

Blummel, J.; Perschmann, N.; Aydin, D.; Drinjakovic, J.; Surrey, T.; Garcia, M. L.; Kessler, H.; and Spatz, J. P. *Biomater.* **2007**, *28*, 4739 – 4747.

Borden, M. A.; Matrinez, G. V.; Ricker, J.; Tsvetkova, N.; Longo, M.; Gillies, R. J.; Dayton, P. A.; and Ferrara, K. W. *Langmuir* **2006**, *22*, 4291 – 4297.

Chou, T. H. and Chang, C. H. *Langmuir* **2000**, *16*, 3385 – 3390.

Chou, T. H. and Chu, I. M. *Coll. Surf., A* **2002**, *211*, 267 – 274.

Chou, T. H. and Chu, I. M. *Coll. Surf., B* **2003,** *27*, 333 – 344.

Dhruv, H. D. PhD Dissertation, *Utah State University*, **2009**.

Discher, B. M.; Schief, W. R.; Vogel, V.; and Hall, S. B. *Biophys. J.* **1999**, *77*, 2051 2061.

Dos Santos, N.; Cox, K. A.; Mckenzie, C. A.; Baarda, F. V.; Gallagher, R. C.; Karlsson, G.; Edwards, K.; Mayer, L. D.; Allen, C.; and Bally, M. B. *Biochim. Biophys. Acta* **2004**, *1661*, 47 60.

Ducharme, D.; Max, J.-J.; Salesse, C.; and Leblanc, R. M. *J. Phys. Chem.* **1990**, *94*, 1925 – 1932.

El-Khouri, R. J.; Frey, S. L.; Szmodis, A. W.; Hall, E.; Kauffman, K. J.; Patten, T. E.; Lee, K. Y. C.; and Parikh, A. N. *Langmuir* **2011**, *27*, 1900 – 1906.

Ellison, E. H. and Castellino, F. J. *Biophys. J.* **1997**, *72*, 2605 – 2615.

Eeman, M. and Deleu, M. *Biotechnol., Agron., Soc. Environ.* **2010**, *14*, 719 – 736.

Gaines Jr., G.L. Wiley, New York, **1966**.

Ickenstein, L. M.; Arfvidsson, M. C.; Needham, D.; Mayer, L. D.; and Edwards, K. *Biochim. Biophys. Acta* **2003**, *1614*, 135 – 138.

Immordino, M. L.; Dosio, F.; and Cattel, L. *Intl. J. of Nanomed.* **2006**, *1*, 297 – 315.

Jebrail, M.; Schmidt, R.; DeWolf, C.E.; and Tsoukanova, V. *Coll.s and Surf. A* **2008**, *321*, 168 – 174.

Kato, K.; Uchida, E.; Kang, E-N.; Uyama, Y.; and Ikada, Y. *Prog. Polym. Sci.* **2003**, *28*, 209 – 259.

Kenworthy, A. K.; Simon, S. A.; and McIntosh, T. J. *Biophys. J.* **1995**, *68*, 1903 – 1920.

Keough, M. R. *Dissertation, North Carolina State University*, **2009**.

Kim, K.; Shin, K.; Kim, H.; Kim, C.; and Byun, Y. *Langmuir* **2004,** *20*, 5396 – 5402.

Kinsinger, M. I.; Lynn, D. M.; and Abott, N. L. *Soft Matter* **2010**, *6*, 4095 – 4104.

Konttila, R.; Salonen, I.; Virtanen, J. A.; and Kinnunen, P. K. *J. Biochem.* **1988**, *27*, 7443 – 7446.

Lozano, M. M. and Longo, M. L. *Soft Matter* **2009**, *5*, 1822 – 1834.

Luna, D. M. N.; Falcao, E. P. S.; Melo, S. J.; and Andrade, C. A. S. *Coll. Surf. A* **2011**, *373*, 22 – 28.

Luna, C.; Stroka, K. M.; Bermudez, H.; and Aranda-Espinoza, H. *Coll. Surf. B Biointerf.* **2011**, *85*, 293 – 300.

Majewski, J.; Kuhl, T. L.; Kjaer, K.; Gerstenberg, M. C.; Als-Nielsen, J.; Israelachvili, J. N.; and Smith, G. C. *JACS* **1998**, *120*, 1469 – 1473.

Martin, S. F.; Josey, J. A.; Wong, Y. -L.; and Dean, D W. *J. Org. Chem.* **1994**, *59*, 4805 – 4280.

Mattson, G.; Conklin, E.; Desai, S.; Nielander, G.; Savage, M. D.; and Morgensen, S. *Mol. Bio. Rep.* **1993,** *17*, 167 – 183.

Miura, S.; Teramura, Y.; and Iwata, H. *Biomater.***2006**, *27*, 5828 – 5835.

Mouritsen, O. G. Springer-Verlag: New York, **2005.**

Nunes, C.; Brezesinski, G.; Pereira-Leite, C.; Lima, J.L.F.C.; Reis, S. and Lucio, M. *Langmuir* **2011**, *27*, 10847 – 10858.

Naumann, C. A.; Brooks, C. F.; Fuller, G. G.; Knoll, W.; and Frank C. W. *Langmuir* **1999**, *15*, 7752 – 7761.

Naumann, C. A.; Brooks, C. F.; Wiyatno, W.; Knoll, W.; Fuller, G. G.; and Frank, C. W. *Macromole.***2001**, *34*, 3024 – 3032.

Petriat, F.; Roux, E.; Leroux, J. C.; and Giasson, S. *Langmuir* **2004**, *20*, 1393 – 1400.

Pu, G.; Longo, M. L.; and Borden, M. A. *JACS* **2005**, *127*, 6524 – 6525.

Rex, S; Zuckermann, M. J.; Lafleur, M.; and Silvius, J. R. *Biophys. J.* **1998,** *75*, 2900 – 2914.

Scott, M. D. and Murad, K. L. *Curr. Pharm. Des.* **1998**, *4*, 423 – 438.

Shahid, M. N. and Tsoukanova, V. *The J. of Phys. Chem. B* **2011**, *115*, 3303 – 3314.

Slaughter, J. N.; Schmidt, K. M.; Byran, J. L.; and Mecozzi, S. *Tetra. Lett.* **2007**, *48*, 3879 – 3882.

Sorgi, K. L. John Wiley & Sons, Ltd**.** Spring House, PA, **2001**.

Stepniewski, M.; Pasenkiewicz-Gierula, M.; Rog, T.; Danne, R.; Orlowski, A.; Karttunen, M.; Urtti, A.; Yliperttula, M.; Vuorimaa, E.; and Bunker, A. *Langmuir* **2011**, *27*, 7788 – 7798.

Sukhishvili, S. A.; Chen, Y.; Muller, J. D.; Gratton, E.; Schweizer, K. S.; and Granick, S. *Macromole.* **2002**, *35*, 1776 – 1784.

Suzuki, A. and Cadenhead, D. A. *Chem. Phys. Lip.* **1985**, *37*, 69 – 82.

Tanwir, K. and Tsoukanvoa, V. *Langmuir* **2008**, *24*, 14078 – 14087.

Tanwir, K.; Shahid, M. N.; Thomas, A; and Tsoukanova, V. *Langmuir* **2012**, *28*, 14000 – 14009.

Tenchov, B.; Koynova, R.; and Rapp, G. *Biophys. J.* **2001**, *80*, 1873.

Tsoukanova, V. and Christian, S. *Langmuir* **2008,** *24*, 13019.

Vermette, P. and Meagher, L. *Coll. Surf. B* **2003**, *28*, 153.

Yu, Z.-W.; Jin, J.; and Cao,Y. *Langmuir* **2002**, *18*, 4530.

Zhao, B. and Brittain, W. J. *Prog. Polym. Sci.* **2000**, *25*, 677 – 710.

Zhao, H.; Dubielecka, P. M.; Soderlund, T.; and Kinnunen, P. K. J. *Biophys. J.* **2002**, *83*, 954 – 967.

Chapter 4: Determining the Parameters of Insulin Binding with Phosphocholine and PEG-Phospholipids Binary Mixtures.

Understanding the effect of non-specific protein binding on the PEGylated membrane mimetic surfaces has been the key interest to the efficiency of numerous biomedical applications [Allen 2002; Takmoto 2011; Rahmati 2008; Ratner 2004; Shimanouchi 2014; Zhao 2002]. This chapter is exclusively devoted to gain insight into the mechanisms involved in the interactions of small protein, e.g. insulin, with the binary mixtures of phosphocholine and PEG-phospholipid. Monolayer has been used as a membrane model for this study. The binary mixtures of DPPC/DPPE-PEG2000 and DSPC/DSPE-PEG2000 containing 1, 3, and 6 mol% PEG2000 have only been used for this study. The conventional monolayer area expansion technique has been utilized for insulin monolayer interactions in the PBS subphase at 20 ^{o}C. The change in mixed monolayers induced by insulin has also been investigated upon varying the PEG content. The data obtained for DPPC/DPPE-PEG2000 and DSPC/DSPE-PEG2000 has been further analyzed in terms of insulin penetration area, A_{ins}, and binding degree, χ_{ins}. Most importantly, the analysis of various factors affecting the degree of insulin binding on the monolayers has also been performed. This knowledge can contribute immensely to understanding the interactions between small proteins and PEGylated phosphocholine membranes.

4.1. RESULTS.

4.1.1. Area Expansion Measurements of Monolayers upon Insulin Interactions.

Area expansion measurements is a unique approach to monitor changes in the monolayer induced by proteins e.g. insulin [Hanakam 1996; Seelig 1987]. It's a simple approach that can provide useful quantitative information about penetration area and binding degree of insulin in the mixed DPPC/DPPE-PEG2000 and DSPC/DSPE-PEG2000 monolayers containing 1, 3, and 6 mol% PEG. In this section, the methodology as well as the monolayer area expansion measurements upon insulin interaction will be described in detail.

4.1.1.1. Methodology for Area Expansion Measurement Studies.

The effect of insulin interactions on the monolayer mean molecular area was examined by area expansion, ΔA, measurements at different surface pressures [Seelig 1987; Shahid 2013; Hanakem 1996]. At first, the monolayer was prepared by spreading the phospholipid binary mixtures of 1, 3, and 6 mol% PEG with appropriate molar ratios on the trough and allowed to compress to a preset surface pressure, π, value using the barriers. The π was kept constant throughout the experiment using a unique electronic feedback device while the trough was thermostated to maintain the desired temperature of the subphase. The creep test was also performed since creeps in the monolayers may change the area of the monolayer, ΔA, due to conformational rearrangements of the

molecules or collapse of the monolayer over the period of time and hence, should be examined before/after the area expansion measurements [Gaines 1966; Rahmati 2008].

This was done by keeping the monolayer at a preset surface pressure for at least 20 min without the insulin injection to verify the stability of the monolayer over time. The monolayer ΔA of ~3% with respect to time infers monolayer to be stable. Hence, after verifying the stability of the monolayer, the insulin with a concentration of ~75 ng/mL was injected in the subphase underneath the monolayer to monitor the area expansion with respect to time. The measurements were usually conducted for a 2 – 6 h period. However, this report will only include the data for 2 h experiment time since ΔA of the monolayers usually remained unchanged after reaching the steady state. Besides the creep test, a reference run for each monolayer was also measured to account for any changes in the monolayer resulting from the creep in the monolayer over the 2 h period. The reference run was performed, at a preset π value, by recording the ΔA of the monolayer for 2 h experiment time without insulin injection. This reference run for each monolayer was further used for subtraction to obtain the corrected ΔA – t curves upon insulin interactions. Each measurement was performed three times and the difference in the ΔA values from a series of measurements lies within 10 – 15%.

4.1.1.2. Area Expansion Measurements of Phosphocholine and PEG-Phospholipid Binary Mixtures upon Insulin Interactions.

The mixed phosphocholine and PEG-phospholipid monolayers area expansion measurements upon insulin interactions were performed for a surface pressure range between 13 – 17 m/Nm with a surface pressure increment of 2 mN/m because the area expansion measurements above this range did not detect significant changes in the mean molecular area upon insulin interactions (data not shown). The area expansion for each mixed phosphocholine and PEG-phospholipid monolayer upon insulin injection was monitored over time shown as $\Delta A - t$ curve in Figure 4.1. Each measurement was repeated three times at each surface pressure. All three curves were then averaged as the one shown in Figure 4.1 for binary mixture of DPPC and DPPE-PEG2000 containing 1 mol% PEG at $\pi \approx 15$ mN/m. The reference run for each individual mixed monolayer was also measured to obtain the actual change in area, ΔA, upon insulin interactions as the one shown in Figure 4.1. The averaged and subtracted $\Delta A - t$ curves for all mixed DPPC/DPPE-PEG2000 monolayers containing 1, 3, and 6 mol% PEG at different surface pressures are presented in Figure 4.2 to 4.4. As seen in the figures, the molecular area of phospholipid monolayer changes, ΔA, immediately after the insulin injection at about $t \approx 0$ but then levels off at a steady state, ΔA_{ss}. The time it takes a given monolayer to attain the ΔA_{ss} varied upon the preset surface pressure value. The steady state value decreased with increasing the preset π value. This can be seen in Figure 4.2, where the ΔA_{ss} value for binary mixture of DPPC/DPPE-PEG2000 containing 1 mol% PEG is ~0.137 nm^2 at π = 13 mN/m which decreased to 0.014 nm^2 at π = 17 mN/m. Similar trends were observed for binary mixtures of DPPC/DPPE-PEG2000 containing 3 and 6 mol% PEG as well

where the ΔA_{ss} values at π = 13 mN/m are ~0.139 and 0.156 nm^2 that decreased to 0.0155 and 0.0132 nm^2 at π = 17 mN/m, respectively (Figure 4.3 and 4.4). The positive change in the molecular area of all the monolayers upon insulin injection in the surface pressure range between 13 – 17 mN/m indeed implies that the area expansion of the monolayer is due to the interactions between insulin and monolayer. Furthermore, change in the lateral surface pressure also has a great impact on the insulin/monolayer interactions. This effect was further investigated by obtaining the ΔA_{ss} values from the exponential fits of all ΔA – t curves (solid curves in Figure 4.2 – 4.4) and then plotted as a function of π. The $\Delta A_{ss} - \pi$ plot displayed in Figure 4.5 shows a significant expansion of monolayers upon insulin interactions below 17 mN/m. However, the ΔA_{ss} values vary depending on the PEG content of each binary mixture. This phenomenon can be grasped by relating the ΔA_{ss} of the monolayers containing 1 – 6 mol% PEG upon insulin interactions, 0.14 – 0.16 nm^2/molecule, with their mean molecular area, A, found between 0.58 – 0.78 nm^2/molecule, at 13 mN/m. This indeed exhibits a considerable monolayer expansion induced by insulin interactions from about 24% – 20% in the binary mixtures of DPPC and DPPE-PEG2000 containing 1 – 6 mol% PEG.

The area expansion measurements on binary mixtures of DSPC/DSPE-PEG2000 also exhibited similar behavior as binary mixtures of DPPC/DPPE-PEG2000 (cf. Figure 4.2 – 4.4 and Figure 4.6 – 4.8). The molecular area of phospholipid monolayer changes, ΔA, followed by insulin injection at about time ≈ 0 min, which then levels off at a steady state, ΔA_{ss}. The time it takes a given monolayer to obtain the ΔA_{ss} varied with respect to the preset surface pressure value. Similar to the binary mixtures of DPPC/DPPE-

PEG2000, the ΔA_{ss} value of mixed DSPC/DSPE-PEG2000 monolayers upon insulin injection decreased with increasing the preset π value. For instance, the ΔA_{ss} value for binary mixture of DSPC/DSPE-PEG2000 containing 1 mol% PEG is ~0.037 nm^2 at π = 13 mN/m which decreased to 0.0023 nm^2 at π = 17 mN/m. Similar behavior was seen for binary mixtures of DSPC/DSPE-PEG2000 containing 3 and 6 mol% PEG where the ΔA_{ss} values at π = 13 mN/m are ~0.046 and 0.090 nm^2 that decreased to 0.0036 and 0.0080 nm^2 at π = 17 mN/m, respectively (Figure 4.6 and 4.8). Interestingly, the ΔA_{ss} values of binary mixtures of DSPC and DSPE-PEG2000 are much lower than the ΔA_{ss} values obtained for the binary mixtures of DPPC and DPPE-PEG2000 (cf. Figure 4.2 – 4.4 with Figure 4.6 – 4.8). Most importantly, change in surface pressure also seems to have a greater effect on the insulin/monolayer interactions. The plot of ΔA_{ss} values as a function of π in Figure 4.9 reveals a noticeable monolayer area expansion induced by insulin molecules, which decreases with the increase of surface pressure.

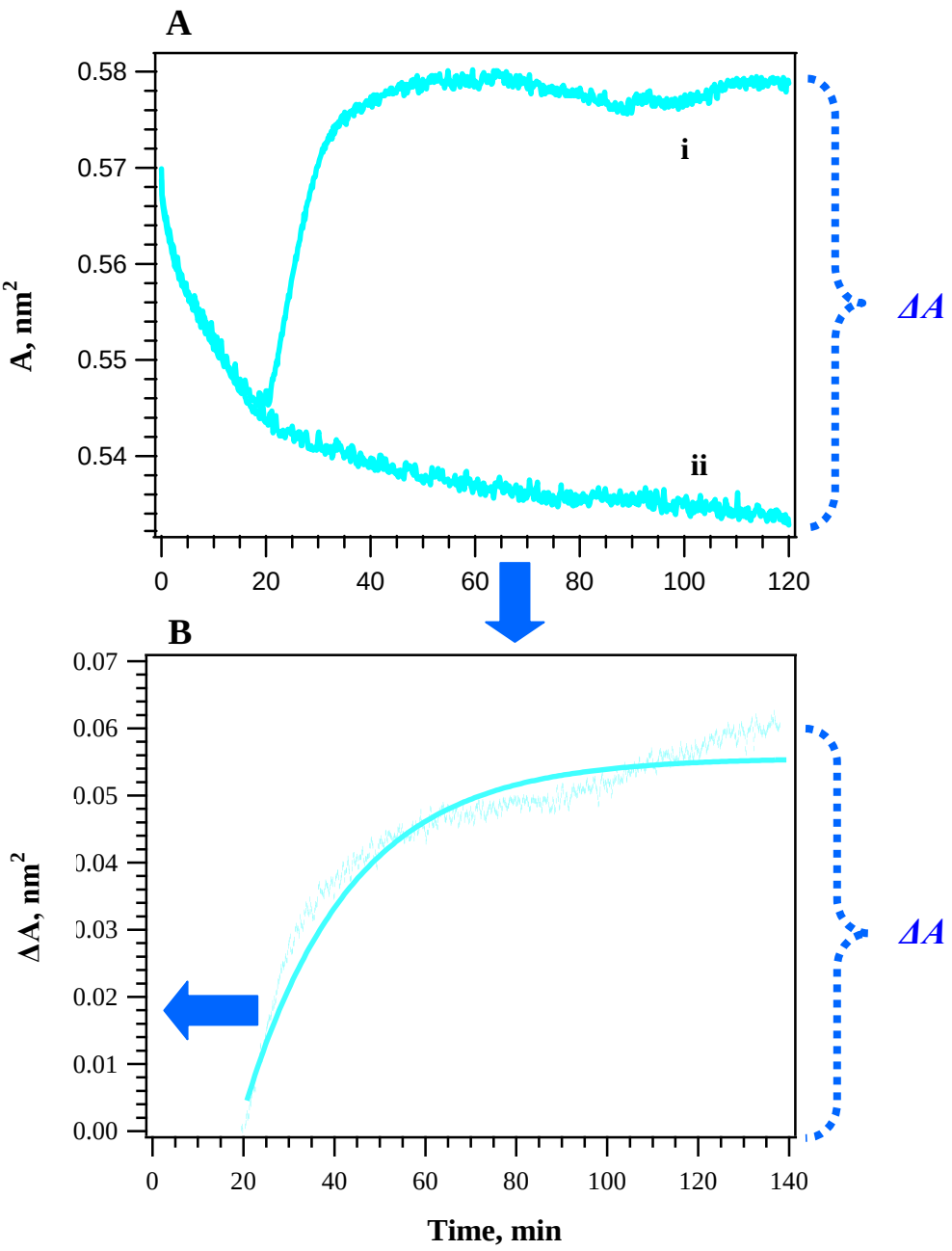

Figure 4.1. A schematics demonstrating the data analysis for area expansion measurements: (**A**) (i) *A* – *t* curves obtained for a monolayer upon insulin injection in the subphase (ii) without insulin, as a reference run. Both curves are obtained for a monolayer containing 1 mol% PEG held at a preset π of 15 mN/m. (**B**) *ΔA* – *t* curve is obtained by subtracting from the reference run depicted as (ii) from *A* – *t* curves for insulin/monolayer interactions represented as (i). Dotted curve is the subtracted curve whereas solid curve represents the exponential curve fit in order to determine the steady-state ΔA_{ss} values. For clarity, the creep test portion of the *ΔA* – *t* curve is removed and the insulin injection point at t= 20 min is shifted to t = 0 min as shown by the arrow in part B of the figure. Hence, *ΔA* – *t* curves in Figures 4.2 – 4.4 and Figures 4.6 – 4.8 illustrate *ΔA* rise at time of ≈ 0 min.

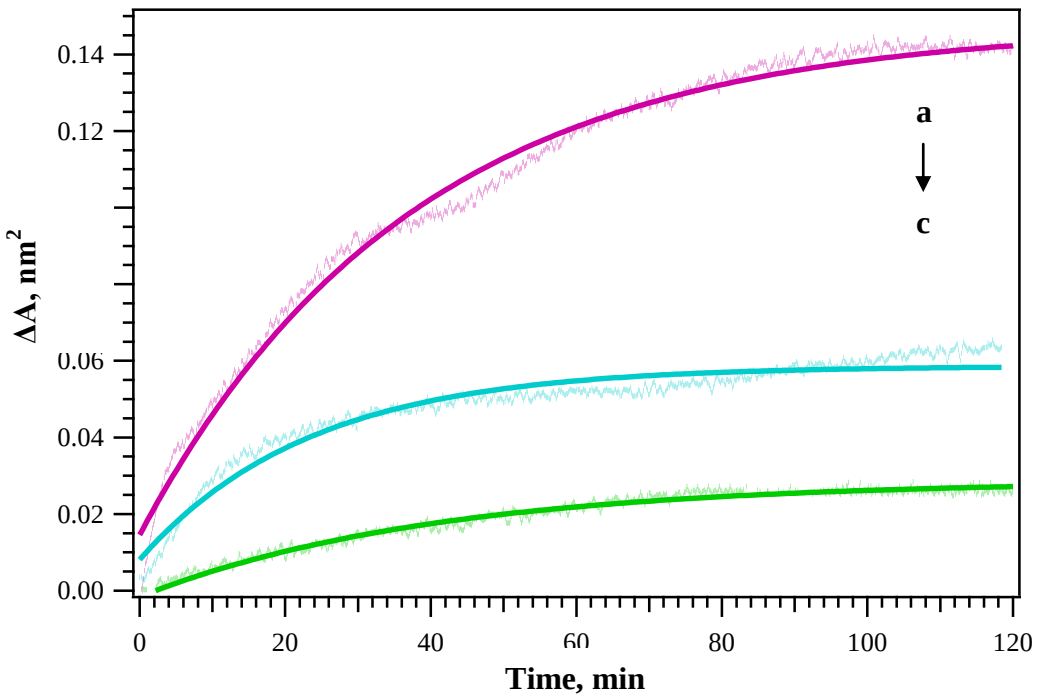

Figure 4.2. Change in mean molecular area, ΔA, of DPPC/DPPE-PEG2000 monolayer containing 1 mol% PEG induced by insulin with respect to time. Dotted curves represent the actual averaged and subtracted ΔA-t curves upon insulin injection at a predefined π of (**a**) 13, (**b**) 15, and (**c**) 17 mN/m whereas solid curves are the exponential fit to the actual measured ΔA-t curves.

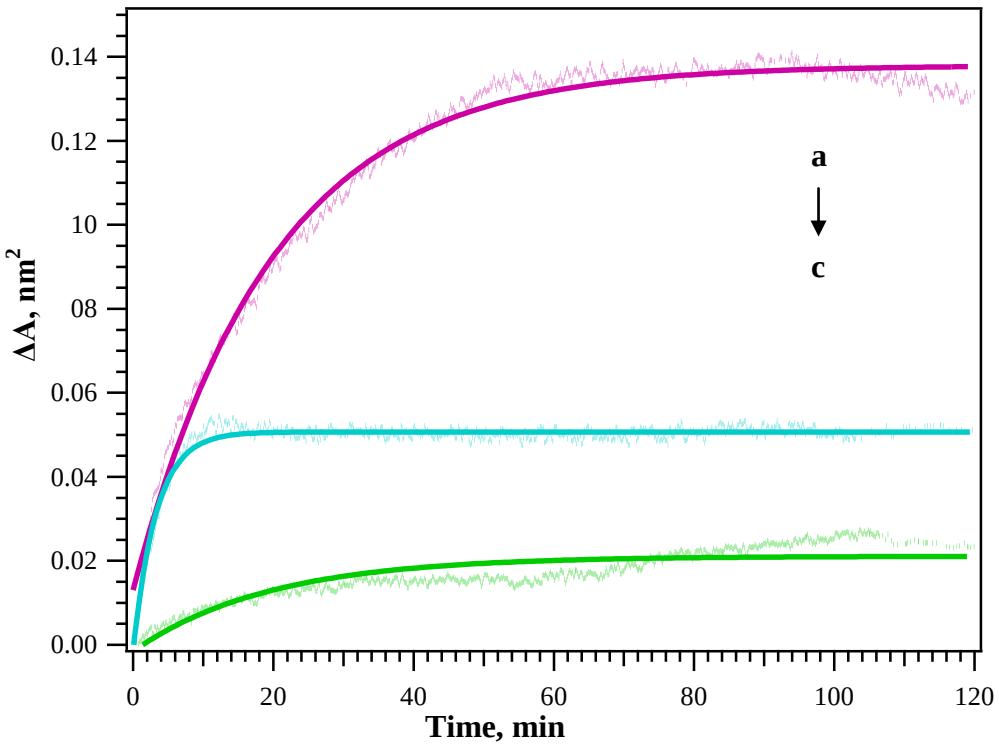

Figure 4.3. Change in mean molecular area, ΔA, of DPPC/DPPE-PEG2000 monolayer containing 3 mol% PEG induced by insulin as a function of time. Dotted curves represent the actual averaged and subtracted ΔA-t curves upon insulin injection at a predefined π of (a) 13, (b) 15, and (c) 17 mN/m whereas solid curves are the exponential fit to the actual measured ΔA-t curves.

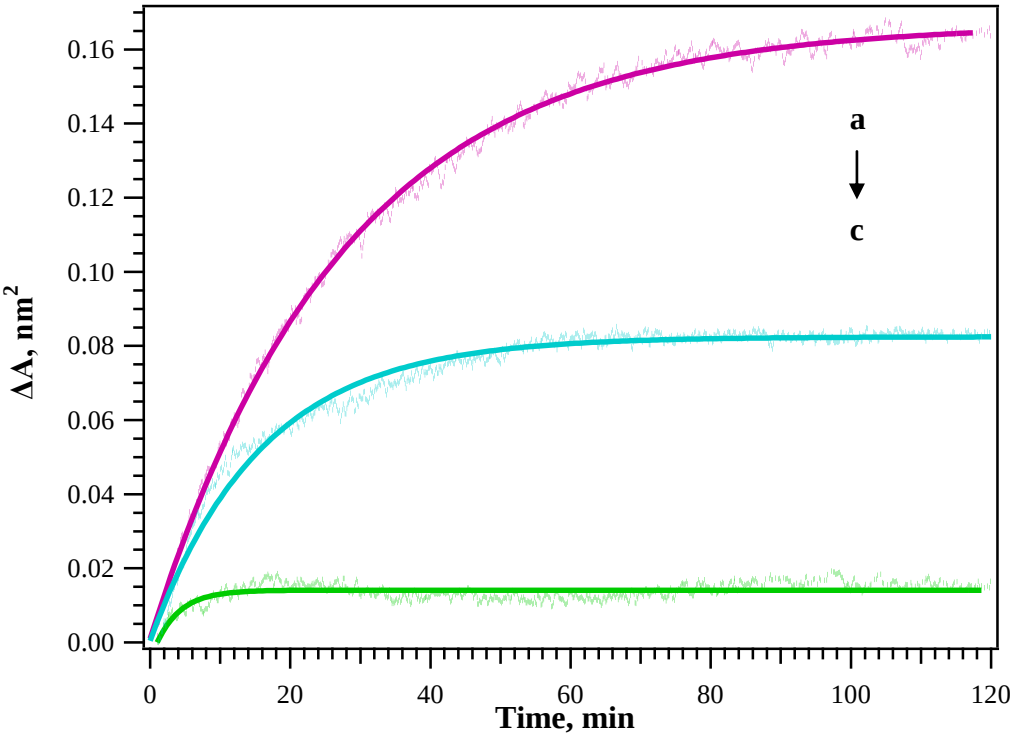

Figure 4.4. Change in mean molecular area, ΔA, of DPPC/DPPE-PEG2000 monolayer containing 6 mol% PEG induced by insulin as a function of time. Dotted curves represent the actual averaged and subtracted ΔA-t curves upon insulin injection at a predefined π of (a) 13, (b) 15, and (c) 17 mN/m whereas solid curves are the exponential fit to the actual measured ΔA-t curves.

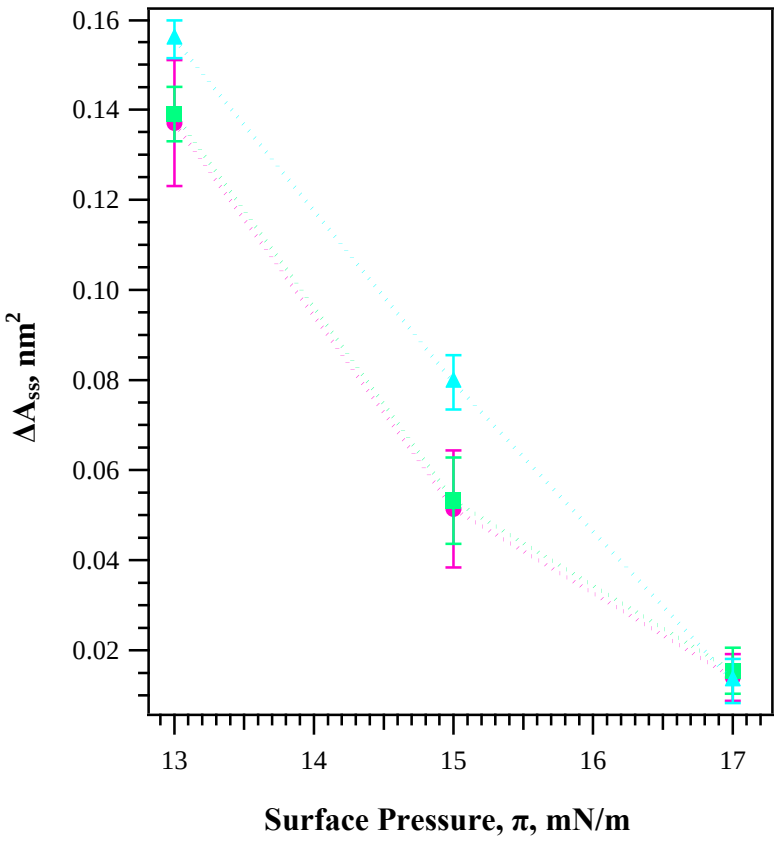

Figure 4.5. ΔA_{ss} values obtained for mixed DPPC/DPPE-PEG2000 monolayers plotted against surface pressure, π, containing different mol% PEG: (●) 1, (■) 3, (▲) 6 mol% PEG2000. Error bars indicate ± standard deviation.

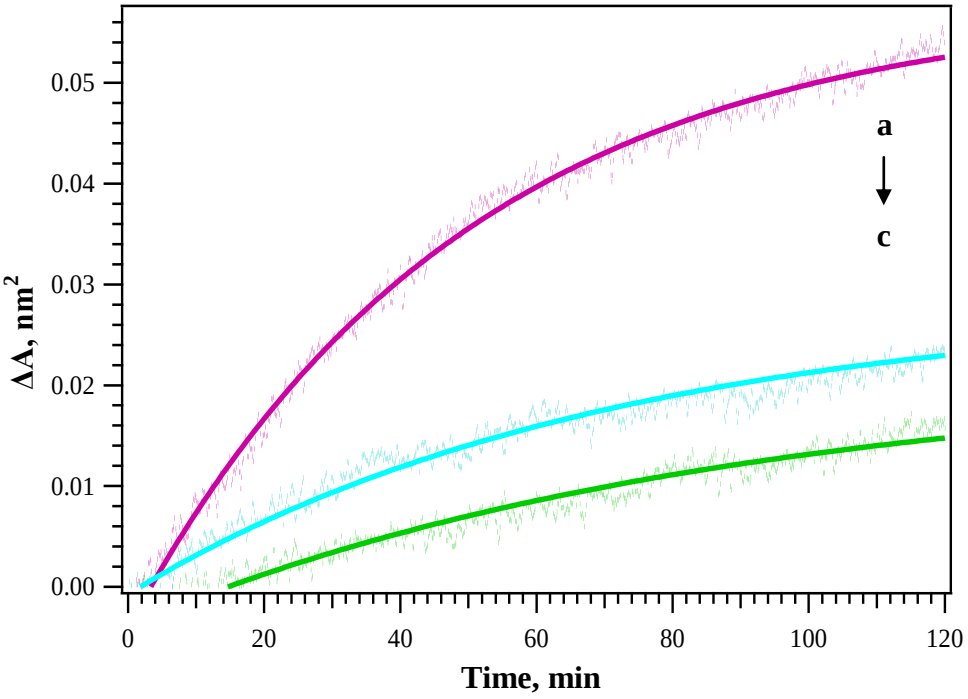

Figure 4.6. Change in mean molecular area, ΔA, of DSPC/DSPE-PEG2000 monolayer containing 1 mol% PEG induced by insulin as a function of time. Dotted curves represent the actual averaged and subtracted ΔA-t curves upon insulin injection at a predefined π of (a) 13, (b) 15, and (c) 17 mN/m whereas solid curves are the exponential fit to the actual measured ΔA-t curves.

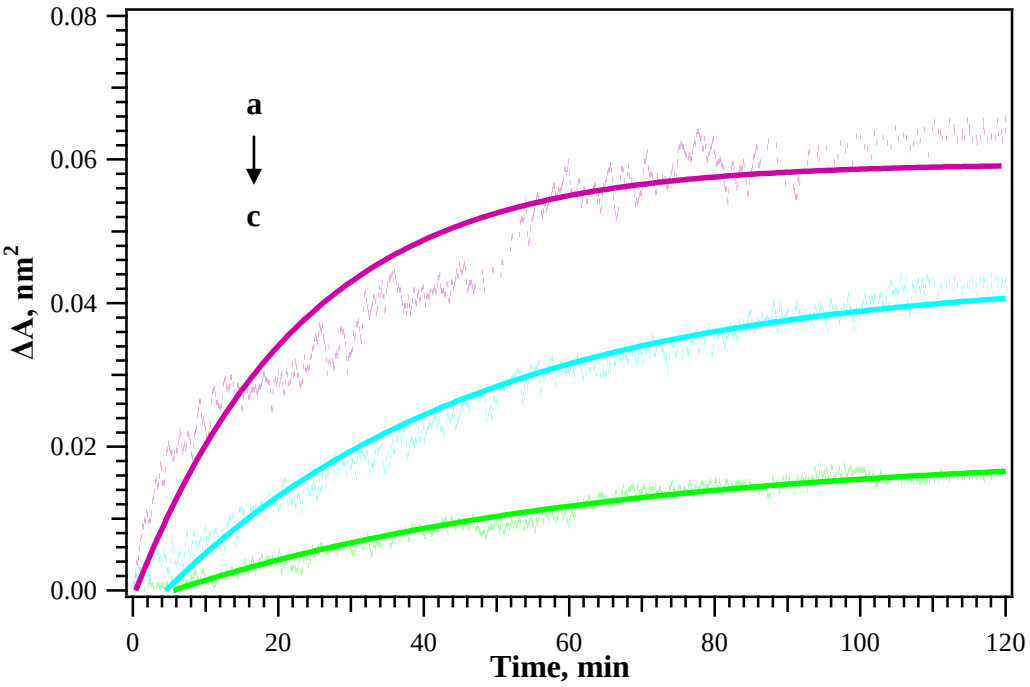

Figure 4.7. Change in mean molecular area, ΔA, of DSPC/DSPE-PEG2000 monolayer containing 3 mol% PEG induced by insulin as a function of time. Dotted curves represent the actual averaged and subtracted ΔA-t curves upon insulin injection at a predefined π of (a) 13, (b) 15, and (c) 17 mN/m whereas solid curves are the exponential fit to the actual measured ΔA-t curves.

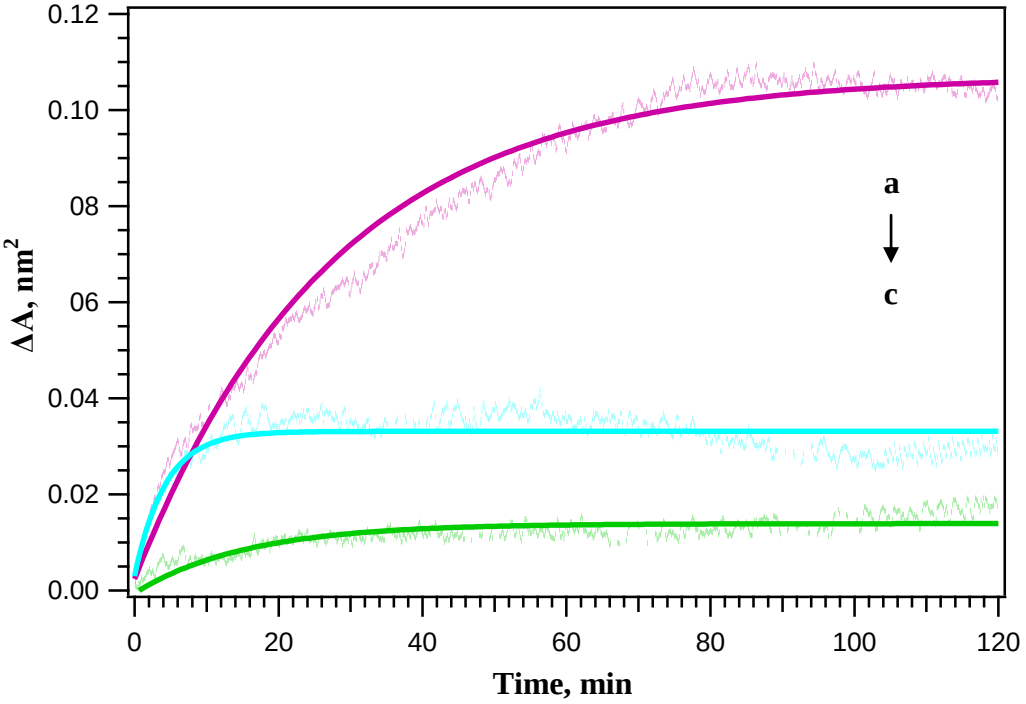

Figure 4.8. Change in mean molecular area, ΔA, of DSPC/DSPE-PEG2000 monolayer containing 6 mol% PEG induced by insulin as a function of time. Dotted curves represent the actual averaged and subtracted ΔA-t curves upon insulin injection at a predefined π of (a) 13, (b) 15, and (c) 17 mN/m whereas solid curves are the exponential fit to the actual measured ΔA-t curves.

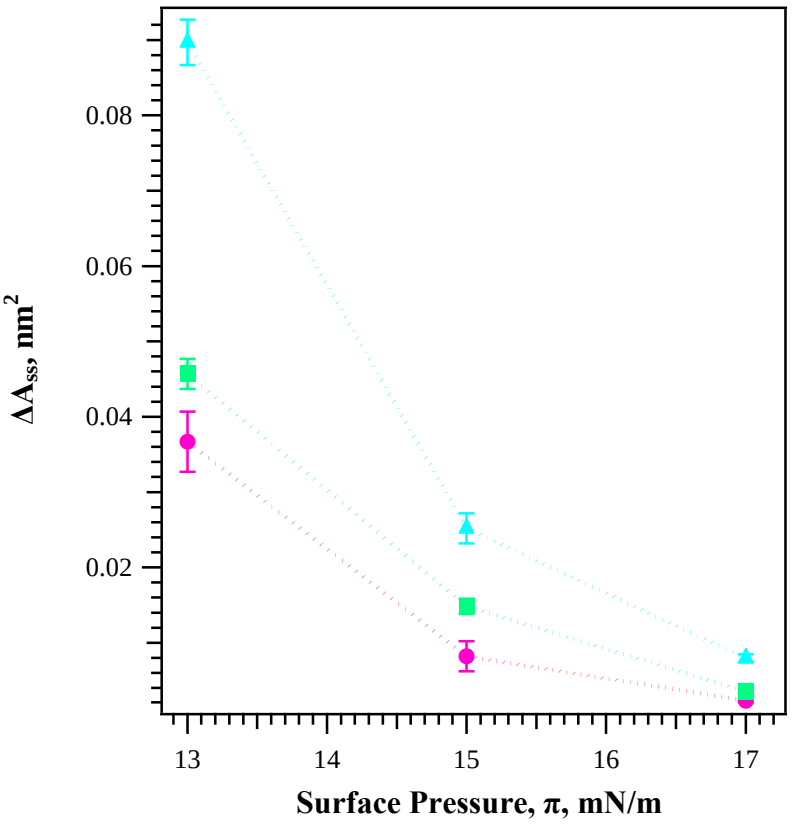

Figure 4.9. ΔA_{ss} values obtained for mixed DSPC/DSPEPEG2000 monolayers plotted against surface pressure, π, containing different mol% PEG: (●) 1, (■) 3, (▲) 6 mol% PEG2000. Error bars indicate ± standard deviation.

4.2. DISCUSSION.

Insulin is a small protein and bears an overall negative charge, –2 per monomer, in the presence of PBS subphase with a pH of ~7.4 [Farias 1989; Henry 2008]. Phosphocholine molecules are zwitterionic but PEG possesses a negative charge [Allen 2002; Baekmark 1995; Tanwir 2008; Vermette 2003]. This overall negative charge distribution should create a repulsive environment between insulin and mixed monolayers. PEG should also play as a steric and entropic repulsive barrier protecting the monolayers upon insulin interactions [Baekmark 1995; Stepniewski 2011; Tanwir 2012; Vermette 2003; Zhao 2002]. However, insulin is known to promote the hydrophobic interactions in order to avoid exposure to the aqueous environment by inserting its hydrophobic residues into the aliphatic region of the phospholipid membrane [Birdi 1976; Farias 1989; Grudzielanek 2007; Kadima 1993; Liang 1994; Nieto-Suarez 2008; Rand 1972; Vermette 2002]. Furthermore, few reports have also purported that ions in the PBS subphase, most importantly cations, can also have a great impact on the protein/membrane, protein/PEG, PEG/membrane interactions [Kadima 1993; Stepniewski 2011; Rand 1972]. Hence, this section will aim at elucidating the effect of varying PEG content in the binary mixtures of phosphocholine and PEG-phospholipid by determining the insulin binding parameters including the insulin penetration area, A_{ins}, and degree of insulin binding, χ_{ins}. The effect PEG content on the phase state of mixed monolayers and its correlation with the χ_{ins} will also be discussed in detail herein.

4.2.1. Determination of Insulin Penetration Area, A_{ins}, for the Binary Mixtures of Phosphocholine and PEG-Phospholipid.

The study of non-specific protein interactions with phospholipid membrane has been found to be very intricate process since every protein possesses unique biophysical properties and thus behaves differently upon interactions with the membrane [Boguslavsky 1994; Hanakem 1996; Seelig 1987]. An estimation of protein penetration area using monolayer area expansion measurements can be an efficient tool to deduce the mechanistic behavior of various types of proteins upon interactions with membranes. For this study, the penetration area of insulin, A_{ins}, in to the binary mixtures of phosphocholine and PEG-phospholipid with varying PEG content of 1, 3, and 6 mol% was calculated using the equation below [Hanakam 1996]

$$\Delta A_{ss}/A \approx K \exp(-\pi A_{ins}/kT) \qquad 4.1$$

where ΔA_{ss} represents the expansion of monolayer mean molecular area due to penetration of protein, A is the area per molecule of phospholipid monolayer without protein, K is constant, π represents the lateral surface pressure, A_{ins} is the area of penetrated insulin on to the monolayer, k is the Boltzmann constant, and T represents the absolute temperature. Rearranging the equation can yield

$$\mathrm{Ln}(\Delta A_{ss}/A) \approx -(A_{ins}/kT)\pi \qquad 4.2$$

A straight line of the ln ($\Delta A_{ss}/A$) curve with respect to surface pressure, π, can thus be used to determine the penetration area of the insulin, A_{ins}, on to the monolayer. To calculate ln ($\Delta A_{ss}/A$), the values of ΔA_{ss} were taken from Figure 4.5 and 4.9 whereas A values were directly obtained from the isotherms of Chapter 3 and 4 in Figure 3.3 and 3.4 for the same surface pressures. Figure 4.10 and 4.11 display the plots of ln ($\Delta A_{ss}/A$) as a function of π from 13 – 17 mN/m for all the binary mixtures of DPPC/DPPE-PEG2000 and DSPC/DSPE-PEG2000. As can be seen in the figures, the plots yield a straight line for all the monolayers which demonstrates that the penetration of insulin is proportional to the Boltzmann factor, $\exp(-\pi A_{ins}/kT)$ and is further used to calculate the penetration area of insulin, A_{ins}, on the mixed monolayers [Boguslavsky 1994; Hanakam 1996]. The calculated values of A_{ins} for all the phosphocholine and PEG-phospholipid monolayers containing 1, 3, and 6 mol% PEG are summarized in Table 4.1 and 4.2. Overall, a decreasing trend of the insulin penetration area is observed with increasing PEG content on both types of binary mixtures from 1 – 6 mol% PEG. For instance, the A_{ins} of insulin on mixed DPPC/DPPE-PEG2000 monolayer containing 1 mol% PEG was determined to be 2.21 ± 0.04 nm^2 which decreased to 1.95 ± 0.06 nm^2 for monolayer containing 6 mol% PEG. Similarly, penetration of insulin, A_{ins}, on mixed DSPC/DSPE-PEG2000 monolayer containing 1 mol% PEG was calculated to be 2.72 ± 0.05 nm^2 which decreased to 2.25 ± 0.07 nm^2 on monolayer containing 6 mol% PEG. Interestingly, the penetration area of insulin determined herein is relatively smaller than the ones in reported data. For instance, the molecular dimension of a wedge shaped insulin monomer has been found to be 2 x 2.5 x 2 nm^3 [Henry 2008; Liu 2002]. The hydrodynamic diameter of insulin monomer has been reported to be 3 nm [Liu 2002; Kadima 1993]. Moreover, Rand et al.

study has estimated the cross-sectional area of insulin molecule to be about 4.35 nm^2 [Rand 1972]. However, a direct comparison of the insulin penetration area determined in this study with the reported data might not correlate well due to different experimental conditions applied. Based on our results, two proposed models might rationalize the relatively small area of insulin, A_{ins}, upon non-specific interactions with the binary mixtures of phosphocholine and PEG-phospholipids. (i) Insulin molecule may change its conformation to a more compact configuration to facilitate the penetration on to the mixed monolayers. In fact, insulin and various other proteins have shown a tendency to change their conformation in order to penetrate depending on the monolayer's physical properties [Jorgensen 2011; Nieto-Suarez 2008; Shahid 2013]. This phenomenon has also been reported by Tah et al. where insulin molecule conforms to a more compact or folded state in order to interact with the vesicle membranes [Tah 2014]. Few reports have also suggested that insulin changes its conformation by partially submerging its hydrophilic residues in to the subphase, when the monolayer mean molecular area changes [Nieto-Suarez 2008]. This conformational change might explain the penetration area of insulin on to the monolayers to decrease in the presence of higher PEG content Table 4.1 and 4.2. On the other hand (ii) Insulin molecule interacts through inserting a small hydrophobic loop/domain instead of entirely inserting itself in to the phospholipid membrane. This is considered as the primary driving force for the non-specific binding of protein on to the membrane [Grudzielanek 2007; Hanakam 1996; Liang 1994]. According to Liang et al. the interaction surface of insulin is comprised of two segments including a hydrophobic binding core and a hydrophilic surface [Liang 1994]. The hydrophobic binding core of insulin has an area of 1.5 nm^2 which is surrounded by polar

and charged amino acids forming a hydrophilic zone. This justifies the relatively small A_{ins} upon interactions with the monolayers in the present study which decreased with an increase of PEG content, as can be seen in Table 4.1 ad 4.2. Further studies would yield more insights to discover the most predictable scheme. Hence, the effect of PEG content on the A_{ins} estimated in this report can be another step towards selecting the optimal mixture composition for developing controlled bio-non-fouling membrane-mimetic surfaces for numerous biomedical applications.

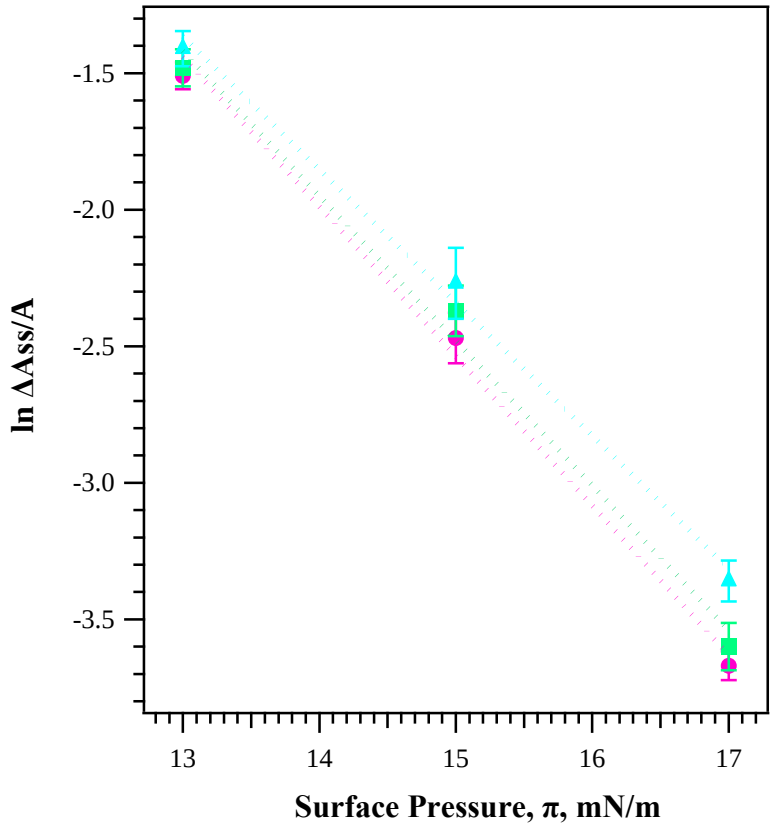

Figure 4.10.: A Semilogarithmic plot of *ΔAss/A* for the binary mixtures of DPPC/DPPE-PEG2000 as a function of surface pressure, π, with different mol % PEG:(●) 1, (■) 3, (▲) 6mol% PEG2000. The dotted lines represent the linear fits to the ln(*ΔAss/A*) – π values. The slopes of the linear fits were used to determine the penetration area of insulin, *Ains* (elaborated in text in more detail). The insulin concentration used in data is ~75 ng/mL in the PBS subphase. Error bars indicate ± standard deviation.

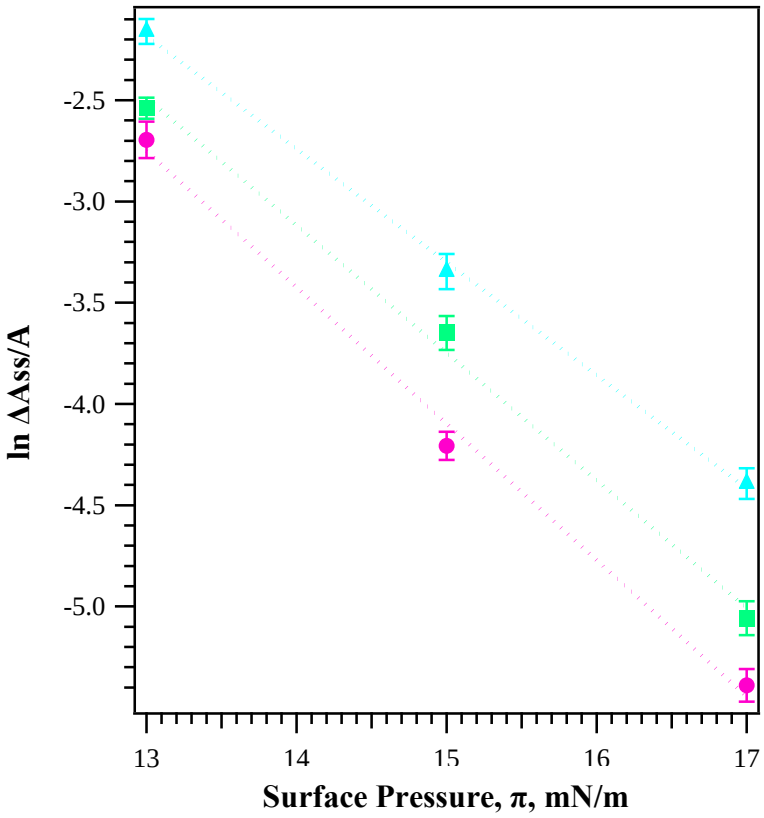

Figure 4.11.: A Semilogarithmic plot of *ΔAss/A* for the binary mixtures of DSPC/DSPE-PEG2000 as a function of surface pressure, π, with different mol % PEG:(●) 1, (■) 3, (▲) 6mol% PEG2000. The dotted lines represent the linear fits to the ln(*ΔAss/A*) – π values. The slopes of the linear fits were used to calculate the penetration area of insulin, *Ains* (elaborated in text in more detail). The insulin concentration used in data is ~75 ng/mL in the PBS subphase. Error bars indicate ± standard deviation.

Table 4.1. Insulin Penetration Area, A_{ins}, for binary mixtures of DPPC and DPPE-PEG2000 containing 1, 3, and 6 mol% PEG2000.

Binary Mixture of DPPC and DPPE-PEG2000	Insulin Penetration Area, A_{ins}, nm^2
1 mol% PEG2000	2.21 ± 0.04
3 mol% PEG2000	2.08 ± 0.05
6 mol% PEG2000	1.97 ± 0.06

Standard deviations calculated for A_{ins} are based on a series of three measurements.

Table 4.2. Insulin Penetration Area, A_{ins}, for binary mixtures of DSPC and DSPE-PEG2000 containing 1, 3, and 6 mol% PEG2000.

Binary Mixture of DSPC and DSPE-PEG2000	Insulin Penetration Area, A_{ins}, nm^2
1 mol% PEG2000	2.72 ± 0.05
3 mol% PEG2000	2.54 ± 0.05
6 mol% PEG2000	2.25 ± 0.07

Standard deviations calculated for A_{ins} are based on a series of three measurements.

4.2.2. Binding Degree of Insulin, χ_{ins}, for Binary Mixtures of Phosphocholine and PEG-Phospholipid.

The calculated A_{ins} values were further used to determine the degree of insulin binding on to mixed DPPC/DPPE-PEG2000 and DSPC/DSPE-PEG2000 monolayers containing 1, 3, and 6 mol% PEG [Boguslavsky 1994; Hanakam 1996; Shahid 2013]. The term χ_{ins} is a ratio between the number of moles of insulin binding on to the monolayer, n_p, and moles of phospholipid molecules constituting the monolayer, n_{pl}. The area expansion measurement can also be used to determine the χ_{ins} based on the equation below [Hanakam 1996]

$$\chi_{ins} = n_{ins}/n_{pl} = (\Delta A/A)(A_{pl}/A_{ins}) \qquad 4.3$$

where $\Delta A/A$ is the relative area increase of monolayer upon insulin binding as mentioned above, A_{ins} represents the penetration area of insulin (obtained from Table 4.1 and 4.2), and A_{pl} is the effective area of phospholipid in a closely packed configuration. A_{pl} can be estimated by extrapolating the low-compressibility region of the monolayer's π – A isotherm to π = 0 mN/m [Shahid 2013]. The effective area of phospholipid, A_{pl}, in the binary mixtures of DPPC/DPPE-PEG2000 containing 1, 3, and 6 mol% PEG2000 is also determined from their monolayer's π – A isotherms from Figure 3.3A. Similarly, A_{pl}, in the mixed DSPC/DSPE-PEG2000 monolayers containing 1, 3, and 6 mol% PEG2000 is also determined from their monolayer's π – A isotherms (Figure 3.5). Table 4.3 and 4.4 summarize the calculated degree of insulin binding, χ_{ins}, for all the binary mixtures based

on the information mentioned above. As seen in Table 4.3, the value for χ_{ins} increases with an increase in PEG content in the mixed DPPC/DPPE-PEG2000 and DSPC/DSPE-PEG2000 monolayers from 1 – 6 mol% PEG. However, the change in the degree of insulin binding for binary mixtures of DPPC/DPPE-PEG2000 is relatively minimal. For instance, at $\pi \sim 13$ mN/m, the χ_{ins} value for mixed DPPC/DPPE-PEG2000 monolayers containing 1 mol% PEG is 0.060 which increases to 0.067 when the PEG content increases to 6 mol% PEG. In contrast, the χ_{ins} value for binary mixtures of DSPC/DSPE-PEG2000 containing 1 mol% PEG is calculated to be 0.013 which increases to 0.032 with PEG increment to 6 mol% PEG at $\pi \sim 13$ mN/m. The number of moles of insulin bound to binary mixtures DSPC and DSPE-PEG2000 is relatively smaller than the binary mixtures of DPPC and DPPE-PEG2000 at all surface pressures presented herein. Interestingly, surface pressure seems to have a greater impact on the χ_{ins} values for all the monolayers than the PEG content. The χ_{ins} values for the DPPC/DPPE-PEG2000 binary mixtures ranged from 0.056 – 0.079 at $\pi \sim 13$ mN/m, depending on the PEG content, which decreased to 0.005 – 0.007 at $\pi \sim 17$ mN/m (Table 4.3). Similarly, the values of χ_{ins} for the binary mixtures of DSPC/DSPE-PEG2000 containing 1, 3 and 6 mol% PEG also decreased from 0.013 – 0.032 at 13 mN/m to 0.0008 – 0.0034 at 17 mN/m, respectively. This reveals that the number of insulin molecules interacting with monolayers for both types of binary mixtures decreases upon increasing the surface pressures. This might justify almost no monolayer area expansion detection at surface pressures above 17 mN/m (data not shown) [Vermette 2003]. Hence, the analysis in this report reveal that increasing the surface pressure has a more pronounced effect in reducing the number of insulin molecules binding to the phosphocholine and PEG-phospholipid binary mixtures.

Table 4.3. Determined degree of insulin binding, $\chi_{ins,}$ for binary mixtures of DPPC and DPPE-PEG2000 containing 1, 3, and 6 mol% PEG2000 using equation 4.3.

π, mN/m	1 mol% PEG2000	3 mol% PEG2000	6 mol% PEG2000
13	0.056 ± 0.004	0.071 ± 0.004	0.079 ± 0.003
15	0.023 ± 0.003	0.028 ± 0.004	0.038 ± 0.006
17	0.005 ± 0.001	0.007 ± 0.001	0.007 ± 0.001

Standard deviations calculated for χ_{ins} are based on a series of three measurements.

Table 4.4. Determined degree of insulin binding, $\chi_{ins,}$ for binary mixtures of DSPC and DSPE-PEG2000 containing 1, 3, and 6 mol% PEG2000 using equation 4.3.

π, mN/m	1 mol% PEG2000	3 mol% PEG2000	6 mol% PEG2000
13	0.013 ± 0.002	0.016 ± 0.003	0.032 ± 0.003
15	0.0031 ± 0.0003	0.0058 ± 0.0006	0.010 ± 0.001
17	0.00080 ± 0.0001	0.0015 ± 0.0003	0.0034 ± 0.0005

Standard deviations calculated for χ_{ins} are based on a series of three measurements.

4.2.3. Grafted PEG Chains Impact on Insulin/Monolayer Interactions.

Based on the results obtained, it can be clearly seen that the incorporation of grafted PEG-phospholipid in to host phosphocholine matrix, DPPC/DPPE-PEG2000 and DSPC/DSPE-PEG2000, indeed aid in reducing the insulin penetration area. Among both binary mixtures, DSPC/DSPE-PEG2000 seems to have a greater impact in reducing the insulin penetration area upon increasing PEG content from 1 – 6 mol% than mixtures of DPPC/DPPE-PEG2000, as can be compared in Table 4.1 and 4.2. Surprisingly, the increment of PEG content in the binary mixtures of DPPC/DPPE-PEG2000 and DSPC/DSPE-PEG2000 seems to reduce the insulin penetration area yet increase the degree of insulin binding, χ_{ins}. Indeed, the degree of insulin binding has increased for both types of binary mixtures at all surface pressures studied herein (Table 4.3 and 4.4). The increase in degree of insulin binding can be attributed to the increase in liquid expanded (LE) phase in the mixed monolayers at higher PEG contents. It has been suggested that increase in PEG content in the binary mixtures of phosphocholine and PEG-phospholipid may contribute towards homogenous distribution of PEG chains but introduce greater separation between the components in order to accommodate the bulky PEG chains and increase the LE phase of the membrane, at any given surface pressure, π [Baekmark 1995; Borden 2006; Kinsinger 2010; Lozano 2009; Tanwir 2008; Tanwir 2012]. To better comprehend the interplay, χ_{ins} and %LE phase of the membrane are plotted as a function of PEG content at $\pi \sim 15$ mN/m, as shown in Figure 4.12 and 4.13. As can be seen in the figures, %LE phase and χ_{ins} increase as the PEG content increase in both binary mixtures of DPPC/DPPE-PEG2000 and DSPC/DSPE-PEG2000. Similar

trends were also observed at π of 13 and 17 mN/m where an increase in PEG content introduces more disorder in the membrane, which eventually causes more insulin to bind to the membrane (data not shown) [Baekmark 1995; Lozano 2009]. Binary mixtures of DPPC/DPPE-PEG2000 exhibit an overall higher χ_{ins} and LE phase than those of DSPC/DSPE-PEG2000 mixtures, at all PEG content studied herein (cf. Figure 4.12 and 4.13). Hence, these findings can aid in selecting the suitable mixture composition as well as tuning and controlling the properties of model membranes for various spectra of biomedical applications.

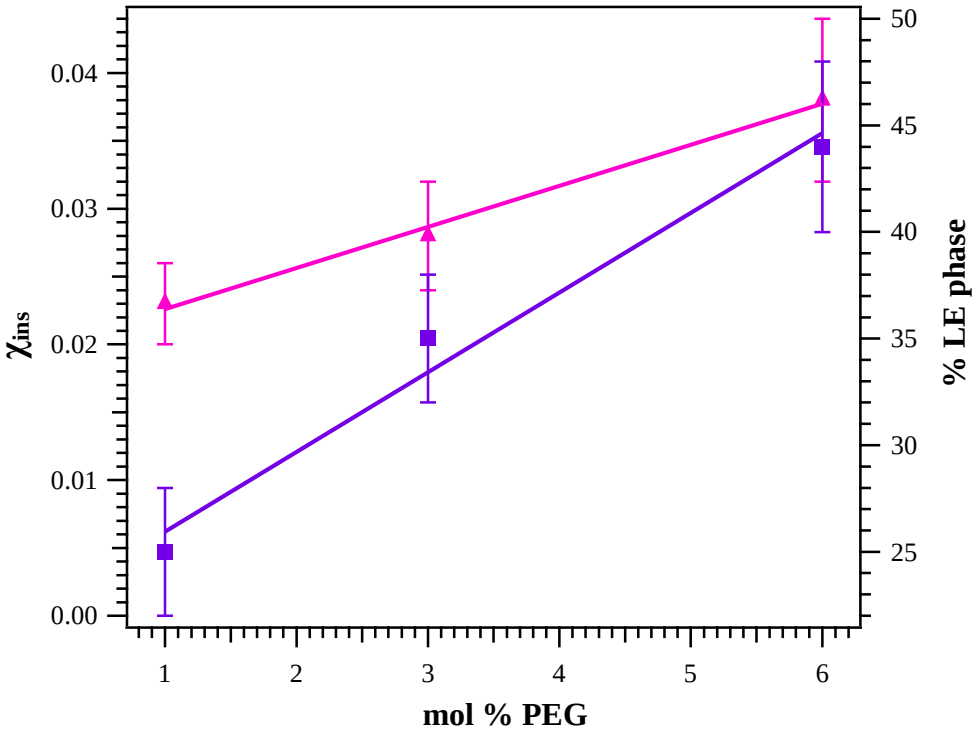

Figure 4.12.: Change in the degree of insulin binding (χ_{ins}) and % liquid expanded (%LE) phase with respect to the PEG content in the binary mixtures of DPPC and DPPE-PEG2000 containing 1, 3, and 6 mol% PEG. Solid lines depict the linear fit to the values. Pink markers and line represent the χ_{ins} whereas purple markers and line represent the %LE phase of the mixtures.

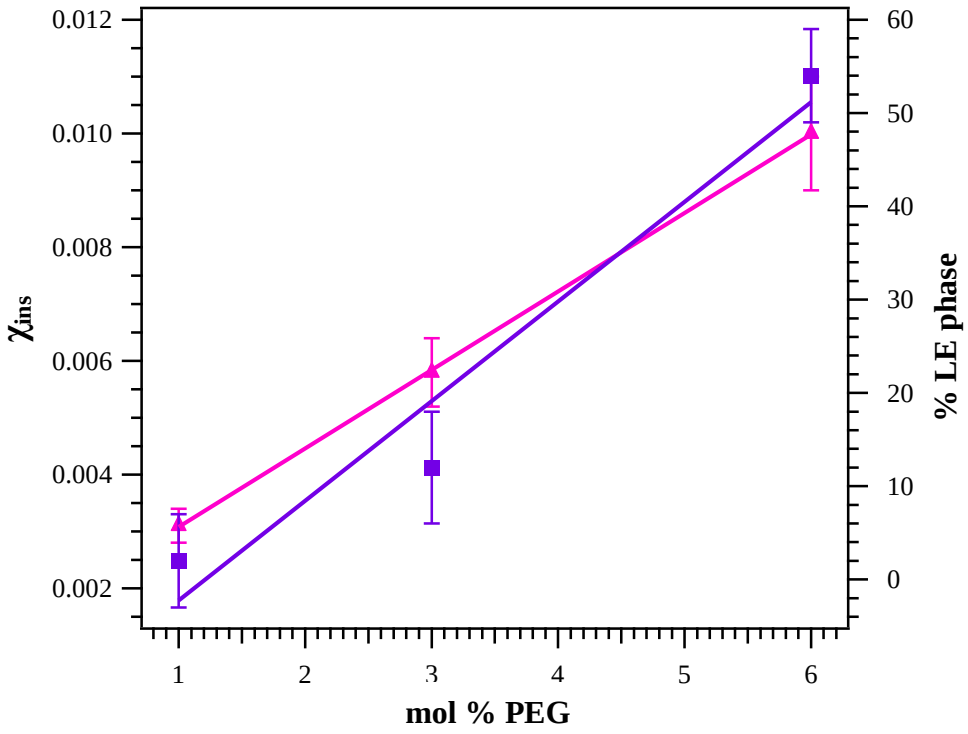

Figure 4.13.: Change in the degree of insulin binding (χ_{ins}) and % liquid expanded (%LE) phase with respect to the PEG content in the binary mixtures of DSPC and DSPE-PEG2000 containing 1, 3, and 6 mol% PEG. Solid lines depict the linear fit to the values. Pink markers and line represent the χ_{ins} whereas purple markers and line represent the %LE phase of the mixtures.

4.3. CONCLUSION.

Analysis of insulin interactions with PEGylated phosphocholine monolayers has indeed revealed an interesting phenomenon through area expansion measurement studies. Insulin penetration area, A_{ins}, decreased from 2.21 nm2 to 1.97 nm2 in the binary mixtures of DPPC/DPPE-PEG2000 and from 2.72 nm2 to 2.25 nm2 in the binary mixtures of DSPC/DSPE-PEG2000 when the PEG content was increased from 1 – 6 mol% PEG, respectively. This shows an overall decrease in A_{ins} with an increase of PEG content in both types of PEGylated phosphocholine mixtures. However, the degree of insulin binding, χ_{ins}, increases upon increasing the PEG content from 1 – 6 mol% PEG in both types of binary mixtures. Interestingly, surface (lateral) pressure significantly reduced the degree of insulin binding, χ_{ins}, as compared to the PEG content in both type of binary mixtures. Among both mixtures, DSPC/DSPE-PEG2000 mixtures had an overall reduced insulin degree of binding upon increasing PEG content as compared to the DPPC/DPPE-PEG2000 mixtures. The increase in χ_{ins} can be directly attributed to an increase in LE phase with an increase of PEG content in both types of PEGylated phosphocholine membranes. Hence, it can be inferred that the optimal PEG content in the PEGylated phosphocholine membrane should be in the range of 1 – 3 mol% PEG for the optimal performance of membrane-mimetic surfaces with reduced non-specific small protein interactions.

4.4. REFERENCES.

Allen, C.; Santos, N. D.; Gallagher, R.; Chiu, G. N. C.; Shu, Y.; Li, W. M.; Johnstone, S. A.; Janoff, A. S.; Mayer, L. D.; Webb, M. S.; Bally, M. B. *Biosci. Rep.* **2002**, *22*, 225 – 250.

Baekmark, T.R.; Elender, G.; Lasic, D.D.; Sackmann, E. *Langmuir* **1995**, *11*, 3975 – 3987.

Birdi, K. S. *J. Coll. and Inter. Sci.* **1976**, *57*, 228 – 232.

Boguslavsky, V.; Rebecchi, M.; Morris, A. J.; Jhon, D-Y.; Rhee, S. G.; Maclaughlin, S. *Biochem.* **1994**, *33*, 3032 – 3037.

Borden, M. A.; Matrinez, G. V.; Ricker, J.; Tsvetkova, N.; Longo, M.; Gillies, R. J.; Dayton, P. A.; Ferrara, K. W. *Langmuir* **2006**, *22*, 4291 - 4297.

Gaines Jr., G.L. Wiley, New York, **1966**.

Grudzielanek, S.; Smirnovas, V.; Winter, R. *Chem and Phys of Lip.* **2007**, *149*, 28 – 39.

Hanakam, F.; Gerisch, G.; Lotz, S.; Alt, T.; Seelig, A. *Biochem.* **1996**, *35*, 11036 – 11044.

Henry, M.; Dupont-Gillain, C.; and Bertrand, P. *Langmuir* **2008,** *24*, 458 – 464.

Jorgensen, L., Bennedsen, P., Hoffmann, S. V., Krogh, R. L., Pinholt, C., Groenning, M., Hostrup, S., Bukrinsky, J. T. *Eur. J. Pharm. Sci.* **2011**, *42*, 509.

Kadima, W.; Ogendal, L.; Bauer, R.; Kaarsholm, N.; Brodersen, K.; Hansen, J. F.; and Porting, P. *Biopolym.* **1993**, *33*, 1643 – 1657.

Kinsinger, M. I.; Lynn, D. M.; Abott, N. L. *Soft Matter* **2010**, *6*, 4095 – 4104.

Liang, D.; Chang, C.; and Wan, Z. *Biophys. Chem.* **1994**, *50*, 63 – 71.

Liu, X.; Kaczmarski,K.; Cavazzini,A.; Szabelski, P.; Zhou, D.; and Guiochon, G. *Biotechnol. Prog.* **2002,** *18*, 796 – 806.

Lozano, M. M. and Longo, M. L. *Soft Matter* **2009**, *5*, 1822 – 1834.

Nieto-Suarez, M.; Vila-Romeu, N.; Dynarowicz-Latka, P. *Coll. and Sur. A* **2008**, *321*, 189 – 195.

Rahmati, K.; Koifman, J.; Tsuokanova, V. *Coll. and Sur. A* **2008**, *321*, 181.

Rand, R. P. and SenGupta, S. *Biochem.* **1972**, *11*, 945 – 949.

Ratner, B. D. and Bryant, S. J. *Annu. Rev. Biomed. Eng.* **2004**, *6*, 41 – 75.

Seelig, A. *Biochim. Biophys. Acta* **1987**, *899*, 196 – 204.

Shahid, M. N. PhD Dissertation, *York University* **2013**.

Shimanouchi, T.; Yoshimoto, N.; Hiroiwa, A.; Nishiyama, K.; Hayashi, K.; Umakoshi, H. *Coll. and Surf. B: Biointerf.* **2014**, *116*, 343 – 350.

Stepniewski, M.; Pasenkiewicz-Gierula, M.; Rog, T.; Danne, R.; Orlowski, A.; Karttunen, M.; Urtti, A.; Yliperttula, M.; Vuorimaa, E.; and Bunker, A. *Langmuir* **2011**, *27*, 7788 – 7798

Tah, B.; Pal, P.; and Talapatra, G. B. *J. of Lumine.* 2014, *145*, 81–87.

Takemoto, N.; Teramura, Y.; and Iwata, H. *Bioconj. Chem.* **2011**, *22*, 673 – 678.

Tanwir, K. and Tsoukanvoa, V. *Langmuir* **2008**, *24*, 14078 – 14087.

Tanwir, K.; Shahid, M. N.; Thomas, A; Tsoukanova, V. *Langmuir* **2012**, *28*, 14000 – 14009.

Vermette, P. and Meagher, L. *Coll. and Surf. B* **2003**, *28*, 153 – 198.

Zhao, H.; Dubielecka, P. M.; Soderlund, T. and Kinnunen, P. K. J. *Biophys. J.* **2002**, *83*, 954 – 967.

Chapter 5: Imaging Co-existing Phases in Poly(Ethylene Glycol) Grafted Phosphocholine Membranes.

This study was performed by analyzing two different types of PEGylated phosphocholine giant unilamellar vesicles (GUVs) as membrane model. DPPC/DPPE-PEG2000 and DSPC/DSPE-PEG2000 with varying PEG content were selected as phosphocholine and PEG-phospholipid mixtures. The morphology, lateral structure, coexisting domains and various other aspects including size, lamellarity, and heterogeneity of the GUVs were visualized and examined by EFM. Moreover, a comparative analysis of the phase state and the lateral surface pressure has been performed to understand the correlation between PEGylated phosphocholine vesicle membrane and monolayer. The effect of different preparation methods and aqueous media on the size, shape, and morphology of vesicle membrane was also investigated. Furthermore, the effect of varying PEG content on the phase behavior of phosphocholine vesicles has also been extensively studied, which can be of great interest for the design of many biomedical applications including carriers for therapeutic and diagnostic agents.

5.1. Preparation Procedures for PEGylated phosphocholine GUVs.

5.1.1. Protocol 1: Gentle Hydration Method.

The DPPC/DPPE-PEG2000 and DSPC/DSPE-PEG2000 GUVs with varying PEG2000 phospholipid content from 1 – 9 mol% were prepared by hydrating the dry phospholipid film technique with slight modifications [Akashi 1996; Bagatolli 2000; Manley 2008; Yamashita 2002; Jesorka 2008]. Stock solutions of phosphocholine with a concentration of 20 mg/mL and PEG-phospholipid, 2 mg/mL, were prepared in chloroform/methanol mixture (60:40 v/v). Pre-calculated volumes of phosphocholine, PEG-phospholipid and 0.05 mol% of DOPE-Rh stock solution with the appropriate molar ratios were mixed in a 1 mL conical glass vial to obtain a 100 μL solution with the final concentration of ~3 mg/mL. The vial was always covered with aluminum foil for light-sensitive components. The solvent mixture was then evaporated in the desiccator attached to a vacuum pump for 3 – 4 hours and was left overnight in the fumehood. Next day, a thin dried film was formed at the bottom of the glass vial. The dried film was pre-hydrated for ~ 30 minutes using warm, moist air. This was done by bubbling the air through deionized water warmed on a hotplate at 50 – 55 ˚C and was directed into a sealed lipid-coated glass conical vial. The vial was filled with the swelling solution of 0.1 M NaCl containing 1 vol% glycerol and was then incubated in an oven overnight at 50 – 60 ˚C to produce GUVs. The temperature of the swelling solution was kept more than the chain-melting transition temperature, T_m, of DPPC (~41.8 ˚C), DSPC (~54.5 ˚C) and when mixed with DPPE-PEG2000 at a concentration ≤10 mol% (~41.8 ˚C). This is

usually done to make the hydrocarbons more flexible and *gauche* conformation [Akashi 1996; Bagatolli 2000; Belsito 2000; Manley 2008; Montesano 2001; Pappalardo 2005; Walde 2001; Zawada 2004]. The phospholipids hydrophobic chains below T_m predominantly exist as a rigid and extended all *trans* conformation, which is not suitable for the vesicle formation [Walde 2001]. The dried film during the incubation was then stripped off from the bottom of the vial surface and formed an opalescence solution containing unilamellar vesicles. The vesicles were then harvested from the center of the vial and gently transferred into an imaging cell. The vesicles in the cell were visualized using an inverted Nikon Eclipse TE2000 microscope (Nikon, Japan) through visible and TRITC channels. In the TRITC channel, the contrast was derived from differences in partitioning of DOPE-Rh into ordered (liquid condensed) and disordered (liquid expanded) phospholipid phases [Manley 2008; Sezgin 2012; Shahid 2011; Tsoukanova 2008]. Headgroup-labeled lipid probe such as DOPE-Rh are typically used for imaging studies since bulky fluorophore attached to the aliphatic chain may interfere with the ordering of the phospholipids in the membrane [Manley 2008]. The red staining in the images thus depicts the LE phase whereas the dark domains correspond to the LC or $L_{\beta'}$ phase in the vesicles. Images were captured using a CCD camera (ORCA ER (AG), Hamamatsu, Japan) through different objectives (10 – 40 X) onto a computer screen by Simple PCI 6 software (Compix Inc. PA). Images most representative of the membrane morphology were chosen for analysis in each series of imaging. Image analysis in terms of the percentage of dark domains, % dark domains, was performed with the Quantify package of Simple PCI 6. In the Quantify package, the value of % dark domains is found by relating the area occupied by domains to the area of the image. Each type of solution

was repeated at least three – five times to obtain highly resolved GUV images. GUVs were also prepared using this protocol but with NaCl and 1 vol% sucrose as the swelling medium. This method, however, did not produce highly resolvable and good quality images. Hence, the images captured from this protocol will not be discussed in detail in this report.

5.1.2. Protocol 2: Solvent Evaporation Method.

The GUVs of the binary mixtures of DPPC and DPPE-PEG2000 in this protocol were prepared using solvent evaporation method as proposed by Moscho and Bagatolli but with slight modifications [Moscho 1996; Bagatolli 2000; Zawada 2004]. DPPC and DPPE-PEG2000 were first dissolved in chloroform/methanol (60:40 v/v) solvent mixture with a concentration of ~20 mg/mL and 2 mg/ml respectively. Pre-calculated volumes of phosphocholine and PEG-phospholipid stock solution with the appropriate molar ratios were mixed in a 1 mL glass vial to obtain a 100 μL solution with the final concentration of ~3 mg/mL. DOPE-Rh was also added in the mixtures at a concentration of ~0.05 mol% for imaging studies. About 3 mL of PBS solution with and without 1 vol% glycerol was added in a 4 mL flat glass vial and heated with constant stirring for ~15 min at 50 – 55 °C, which was above the T_m of phospholipids. The solution containing the phospholipid mixture was then slowly injected (drop wise) into stirred PBS along the wall of the flask. The phospholipid containing PBS solution was stirred for ~30 min at ~60 °C without caps to evaporate the organic solvent [Zawada 2001]. The solution was left to cool down to room temperature (~20 – 21 °C). The vesicles were harvested from

the center of the vial, gently transferred into an imaging cell with a drop of PBS containing 1 vol% of glycerol and observed using an inverted Nikon microscope as described above. Each binary mixture solution was repeated five times to obtain highly resolved GUV images.

5.2. RESULTS.

The main goal of this study was to prepare and study the co-existing phases in the GUVs using EFM. GUVs of DPPC/DPPE-PEG2000 and DSPC/DSPE-PEG2000 with varying PEG content from 1 – 9 mol% were prepared. Two different protocols were used for the preparation of GUVs including gentle hydration and solvent evaporation method. DPPC/DPPE-PEG2000 GUVs were actually prepared using both protocols [Akbarzadeh 2013; Akashi 1996; Manley 2008; Moscho 1996; Thevenot 2007; Walde 2001]. However, GUVs of DSPC/DSPE-PEG2000 were only prepared by the gentle hydration method [Akashi 1996; Manley 2008; Walde 2001]. DOPE-Rh was used as an imaging probe to study the phase state of the GUV as a membrane model. This specifically includes the liquid-disordered (L_d) and gel ($L_{\beta'}$) phases of the membrane model [Bagatolli 2006; Discher 1999; El-Khouri 2011; Manley 2008; Shahid 2011]. L_d phase corresponds to the fluid or liquid expanded phase (LE) whereas $L_{\beta'}$ represents the liquid condensed phase (LC) in a phospholipid monolayer [Bagatolli 2006; Ickenstein 2003; Eeman 2010; Tenchov 2001]. The vesicles were also loaded with 1 vol% glycerol solution, which increased the rigidity of vesicle by osmotic pressure and further enhanced the contrast and resolution of the vesicles' imaging [Akashi 1996; Sun 2005]. Hence, direct imaging

of PEGylated phosphocholine GUVs phase coexistence can be very valuable to correlate phase behavior of GUVs with that of monolayers.

5.2.1. Imaging the Coexisting Domains in DPPC/DPPE-PEG2000 Vesicles Containing 1 mol% PEG Using Protocol 1.

The morphology of DPPC/DPPE-PEG2000 vesicle membranes containing 1 mol% PEG2000 phospholipid was observed through the EFM's visible and TRITC channel. Figure 5.1 shows both visible light images and the corresponding fluorescence images of DPPC/DPPE-PEG2000 giant unilamellar vesicles (GUV) morphology containing 1 mol% PEG2000-phospholipid. The vesicles were primarily spherical in shape. The size of the vesicles observed was ranged from 1 – 85 μm. In visible channel, the edges of most of the vesicles appeared thick and dark (Figure 5.1 A – C). This is described as the result of different refractive indices of internal and external media [Akashi 1996]. Each single band corresponds to a bilayer shell and can be considered as unilamellar vesicle [Akbarzadeh 2013; Akashi 1996; Immordino 2006; Walde 2001]. Aside from GUVs, several multilamellar vesicles, myelin, irregular shaped, and debris were also observed (images not shown). However, these structures did not interfere during the observation and resolution of the desired GUV at a time.

In the TRITC channel, the dark band in the visible channel appeared red, as can be seen in Figure 5.1 D – F. The intensities of unilamellar vesicles with a single dark band were significantly lower (Figure 5.1 D – F) than the vesicles with multiple bands (images not shown) [Akashi 1996; Yamashita 2002]. The former were, hence, used for

further analysis (Figure 5.1 D – F). As can be seen in the figure, two phases can be distinctly seen in the GUVs: (1) liquid-disordered phase stained red with DOPE-Rh fluorescence along with (2) dark DOPE-Rh-excluded liquid-ordered phase domains. The coexistence of these two phases was vividly observed in all sizes of vesicles ranging from 15 to 85 μm in diameter (Figure 5.1). EFM images of GUVs have revealed that the DPPC/DPPE-PEG2000 membranes containing 1 mol% PEG constitute 73% ± 5 of $L_{\beta'}$ phase domains, regardless the vesicle size. However, individual $L_{\beta'}$ domains appeared smaller in small sized vesicles. Vesicles with diameter below 15 μm showed somewhat heterogeneity but the dark $L_{\beta'}$ phase could not be clearly visualized and quantified. Thus, it can be said that the $L_d - L_{\beta'}$ coexistence phase is most probably an inherent property of the DPPC/DPPE-PEG2000 membrane morphology.

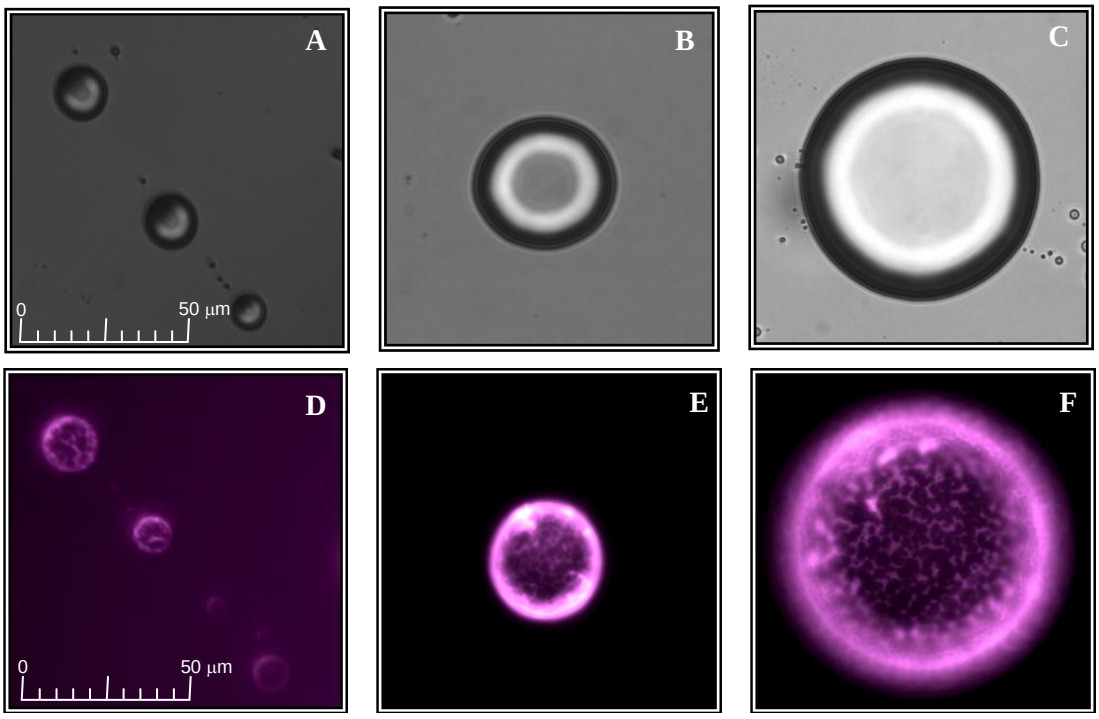

Figure 5.1.: Images of different sizes of DPPC/DPPE-PEG2000 vesicles containing 1 mol% PEG content. [A-C] show images of different sizes of vesicles containing DOPE-Rh probe captured through visible channel. [D-F] Co-existence phase, L_d-$L_{\beta'}$, seen through TRITC channel and distinguished in all sizes of vesicle of ~73%. T = 23 ºC.

5.2.2. Imaging the Coexisting Domains in DPPC/DPPE-PEG2000 Vesicles Containing 3 – 9 mol% PEG Using Protocol 1.

DPPC/DPPE-PEG2000 containing 3, 6, and 9 mol% PEG vesicles were also prepared by the gentle hydration method. The vesicles images in both visible and TRITC channel appeared spherical shaped but rather smaller in size as compared to GUVs containing 1 mol% PEG2000 phospholipid. The diameter of the vesicles observed ranged from 1 – 40 μm. The most typical vesicle structures found in the samples are similar to the ones shown in Figure 5.2. Most of the vesicles seen had a single band around the edges, corresponding to unilamellarity, similar to the ones shown in the visible images (Figure 5.2). Visualizing the coexistence phase in the vesicle membrane morphology containing 3 and 6 mol% PEG2000 content was somewhat difficult as compared to GUVs containing 1 mol% PEG. As quantified, the L_o phase in the vesicle membrane morphology containing 3 and 6 mol% PEG2000-phospholipid content was 62% ± 7 and 53% ± 5, respectively. These values were slightly lower than the vesicles containing 1 mo% PEG with L_o phase of 73%. Furthermore, DPPC/DPPE-PEG2000 membrane vesicles containing 9 mol% PEG appeared blurry and small in size with a diameter of 1 – 5 μm, while the quantity of vesicles produced was also significantly reduced.

Interestingly, the samples containing 3 and 6 mol% PEG content had several vesicles attached to each other making oblique trajectories or tubes as shown in Figure 5.3. This type of structure has also been reported previously for vesicles with and without the incorporation of PEG-phospholipid [Antonietti 2003; Bagatolli 2000; Collier 2001;

Mathivet 1996; Li 2011]. Upon resolving the images, it is observed that most of the tubes were unilamellar containing only single band around the edge of the vesicles, as can be seen in the figure. The coexisting domains were also observed in the tubes but hard to resolve due to the smaller size of the vesicles Figure 5.3.

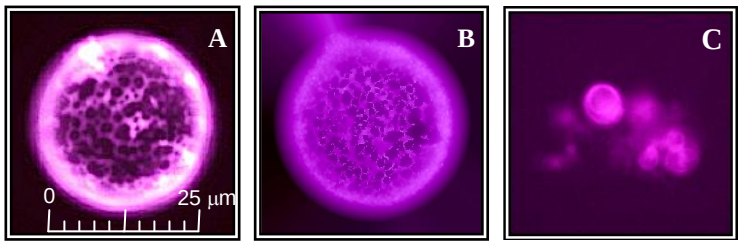

$62_{\pm 7}$% L_o phase $53_{\pm 5}$% L_o phase

Figure 5.2.: Images corresponds to DPPC/DPPE-PEG2000 vesicles containing [A] 3 mol%, [B] 6 mol%, and [C] 9 mol% PEG2000 content. Co-existence phase can be observed in vesicles with 3 and 6 mol% PEG but not in vesicles with 9 mol% PEG. T = 23 ºC.

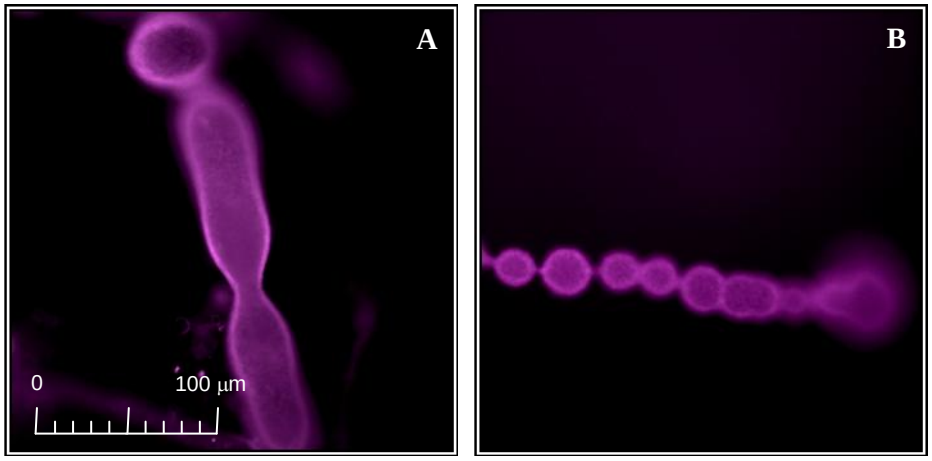

Figure 5.3.: EFM Images of DPPC/DPPE-PEG2000 vesicles containing [A] 3 and [B] 6 mol% PEG000 content forming tubes or oblique trajectories. Co-existence phase exists but not very clear.

5.2.3. Imaging the DSPC/DSPE-PEG2000 Vesicles Prepared by Protocol 1.

GUVs of DSPC/DSPE-PEG2000 were also prepared by protocol 1 as discussed above. The vesicles were predominantly spherical shaped similar to the DPPC/DPPE-PEG2000 GUVs. The size of the vesicles mostly ranged from 1 – 5 μm in diameter. Although several vesicles were unilamellar but the size was quite small (images not shown). The presence of various multilamellar structures and debris in the sample also made it difficult to observe a single unilamellar vesicle at a time. Figure 5.4 shows both visible light image and the corresponding fluorescence image of DSPC/DSPE-PEG2000 vesicle containing 1 mol% PEG2000-phospholipid. The vesicle shown in the figure is unilamellar, due to a single band around the edge, with the diameter of ~12 μm. Further, as can be seen in the figure, the coexisting domains are not clearly visible in the vesicle as compared to the DPPC/DPPE-PEG2000 GUVs (cf Figure 5.4B and Figure 5.1). The size and quantity of the vesicles reduced significantly with increasing PEG content from 1 – 9 mol% (images not shown). In fact, most of the vesicles were very small in size and could not be resolved.

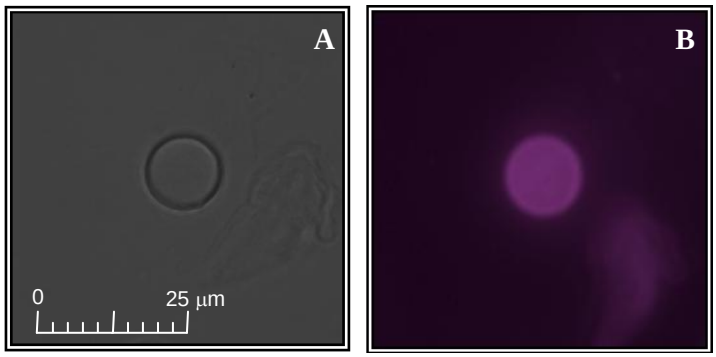

Figure 5.4.: [A] Visible and [B] TRTIC images of DSPC/DSPE-PEG2000 vesicles containing 1 mol% PEG2000-phospholipid. Scale bar is 25 μm.

5.2.4. Imaging the Coexisting Domains in DPPC/DPPE-PEG2000 Vesicles Using Protocol 2.

Protocol 2, solvent evaporation method, was also used to prepare the vesicles of DPPC/DPPE-PEG2000 with varying PEG content. The vesicles mostly appeared circular in shape and smaller in size in the range of 1 – 10 μm in diameter. However, a very few vesicles with the diameter slightly more than 10 μm were also observed using this protocol. For the clarity of presentation, Figure 5.5 displays the visible and TRITC images of such DPPC/DPPE-PEG2000 vesicle containing 1 mol% PEG with a diameter of ~30 μm. The visible image of the vesicle shows a clear single band depicting the unilamellarity of the vesicle Figure 5.5A. The TRITC image in Figure 5.5B shows a bright fluorescent spherical shaped vesicle but the coexistence domains were not clearly seen. The size of the vesicles did not change significantly with the increment of PEG content from 1 – 6 mol% (images not shown). The tubular structures, similar to the ones seen in protocol 1, were also not observed in samples prepared by protocol 2. Interestingly, the DPPC/DPPE-PEG2000 vesicles containing 9 mol% PEG2000 could not be formed using this preparation method.

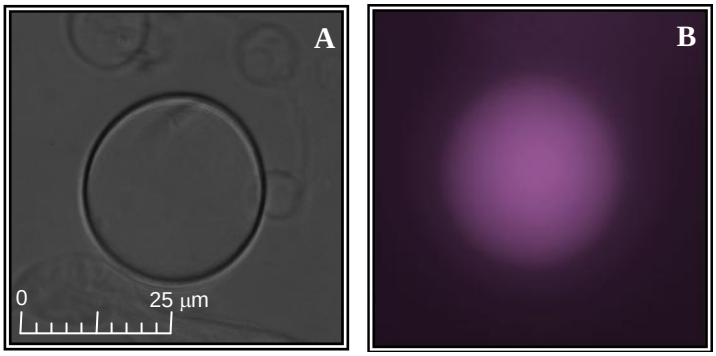

Figure 5.5.: [A] Visible and [B] TRTIC images of DPPC/DPPE-PEG2000 vesicles containing 1 mol% PEG2000-phospholipid. Scale bar is 25 μm.

5.3. DISCUSSION.

A comprehensive analysis of results presented above illustrates that many factors affect the properties of vesicles including size, shape, lamellarity as well as morphology. Among these factors, mixture composition, PEG2000 content as well as the preparation procedure utilized, play a key role and hence will be the focus of this discussion [Immordino 2001; Popovska 2013]. Most importantly, various challenges are also involved in producing and imaging giant unilamellar vesicles, in particular upon inclusion of PEG content. A careful overview of the results herein provides crucial information about the effectiveness of each method as well as the mechanism of vesicle formation. Based on the results, it can also be seen that DPPC/DPPE-PEG2000 GUVs prepared by gentle hydration method were giant and highly resolvable as compared to the solvent evaporation technique. Moreover, the mixture composition also has a significant impact on the vesicle formation as well as morphological properties and will be discussed below. Hence, this report will highlight some of the key factors involved in the vesicle formation as well as the change in morphology with respect to different experimental conditions including variation in PEG content.

5.3.1. Imaging the Phase Coexistence in DPPC/DPPE-PEG2000 GUVs with Varying PEG2000 Content.

Imaging the phase coexistence in GUVs by fluorescence microscopy has gained great interest in recent years to better comprehend the lateral organization and physical properties of membrane models for numerous biomedical applications [Akashi 1996;

Bagatolli 2006; Bagatolli 2000; Veatch 2003; Walde 2001]. However, the complexities involved including preparation procedures, mixture composition selection, addition of cholesterol as well as experimental conditions such as temperature and aqueous media has made it a very difficult task to achieve [Akashi 1996; Bagatolli 2006; Bagatolli 2000; Edwards 1997; Immordino 2001; Korlach 1999; Sun 2005; Veatch 2003; Walde 2001; Wesolowska 2009]. Most importantly, formation of vesicles and imaging the phase coexistence in PEGylated vesicles without the addition of cholesterol or negatively charged phospholipids has also been very challenging [Akashi 1996; Edwards 1997; Sezgin 2012; Veatch 2003]. Edwards et al. study has reported that most lipid mixtures incorporate about 30 – 50 mol% of cholesterol to produce liposomes [Edwards 1997]. In this project, we have not only successfully prepared phosphocholine GUVs with varying PEG2000 content but also visualized the phase coexistence without any other additives stated above. Upon detailed analysis, it was observed that various factors can have a substantial impact on the quantity, size, shape as well as the morphology of GUVs. Among these factors, PEG has shown to play a significant role in the formation of GUVs. For instance, an increase in PEG content significantly reduced the number of GUVs formed in each binary mixture. Increase in PEG content from 1 to 9 mol% has also affected the size of GUVs from 100 to 10 μm, respectively. Further, a change in PEG content from 1 to 9 mol% also affected the phase coexistence as well as the resolution capability of GUVs. GUVs containing 1 mol% PEG were easily resolved whereas vesicles containing 9 mol% PEG2000 were very small and hard to resolve. High amount of small vesicles and phospholipid aggregates were also observed in these GUVs. This could be due to the formation of micelles or other plausible types of phospholipid

aggregates with an increase of PEG content, which made it difficult to resolve by EFM technique. This is also consistent with a previous study which reports on the formation of phosphocholine micelles and open bilayer discs when PEG content was present at a concentration of ~10 mol% [Edwards 1997]. This could be attributed to bulky headgroup of DPPE-PEG2000, which upon increasing PEG content causes disruption in the vesicle formation [Kastantin 2009]. These results are also consistent with the literature data on PEGylated phosphocholine membrane models [Bedu-Addo 1996; Belsito 2000; Edwards 1997; Ickenstein 2003; Montesano 2001; Lasic 1991; Szleifer 1998]. In particular, Belsito et al. have reported a strong influence of PEG content on the size of the phosphocholine aggregates [Belsito 2000]. A study by Lasic et al. has shown a reduction in the radius of egg yolk phosphatidylcholine dispersions with inclusion of DPPE-PEG2000 content [Lasic 1991]. Bedu-Addo et al. also reported that the size of the phosphocholine liposomes significantly reduced upon increasing PEG-phospholipid content [Bedu-Addo 1996]. Moreover, a report by Szleifer showed a decrease in the aggregates size with the incorporation of PEG-phospholipid content from 0.2 to 10 mol% [Szleifer 1998]. Another study by Edwards et al. reports a formation of open bilayer discs with high PEG2000 concentration (~10 mol%) in phosphocholine mixtures which would not be useful for drug delivery options [Edwards 1997]. Hence, it can be inferred that as the amount of PEG content increases in the DPPC/DPPE-PEG2000 vesicles, the L_d phase also consequently increases. This in turns prevents the formation of vesicles and induces the formation of micelle and other plausible phospholipid aggregates.

5.3.2. Effect of PEG Content on the Phase State of PEGylated Phosphocholine Vesicle Membrane Models.

An increase in PEG content increased the phase separation in the phosphocholine membranes vesicles. This suggests that high PEG content introduces more disorder in the phosphocholine membranes, which may result in a significant change in the phase behavior of the vesicle membrane models and might not be optimal for engineering efficient bio-non-fouling membrane-mimetic surfaces. For instance, DSPC/DSPE-PEG2000 mixtures containing 1 mol% PEG contain ~73% of LC ($L_{\beta'}$) state, which reduces to ~ 53% in vesicles with 6 mol% PEG content. This indicates that DPPC/DPPE-PEG2000 vesicle membrane model containing 1 mol% PEG mainly exist as the LC ($L_{\beta'}$) whereas mixtures containing more than 3 mol% PEG have appreciable amount of LE (L_d) phase. These results correlate well with literature suggesting that an increase in PEG content reduces the $L_{\beta'}$ phase and induces phase separation in the membrane models [Bedu-Addo 1996; Belsito 2000; Edwards 1997; Montesano 2001; Lasic 1991; Szleifer 1998]. Hence, it can be proposed that incorporating 1 – 6 mol% PEG content in the PEGylated phosphocholine binary mixtures can be useful for liposomal formulations with efficient bio-non-fouling properties.

5.3.3. Relevance Between DPPC/DPPE-PEG2000 Monolayers and Vesicles Phase Behavior.

GUVs are considered as an intermediate step between a typical biological membrane and simple model systems including monolayers and bilayers [Bagatolli 2006; Nag 2002]. However, it has been found to be a fairly challenging task to image the

morphology and coexisting phases in GUVs without the addition of cholesterol or negatively charge phospholipid molecules [Akashi 1996; Bagatolli 2000; Bagatolli 2006]. Furthermore, data demonstrating a direct comparison of the vesicle morphology with simple model systems such as monolayers are also very scarce [Lozano 2009b]. Figure 5.6 illustrates a direct comparison between DPPC/DPPE-PEG2000 membrane model systems including monolayers and GUVs with varying PEG2000 content from 1 to 6 mol%. As seen in the figure, all GUVs show morphological resemblance with mixed monolayers of the same composition at $\pi \approx 15$ mN/m. This is in good agreement with the literature which states that the lateral surface pressure of a typical biological membrane lies between the range of 15 – 35 mN/m [Lozano 2009a; Kontilla1988]. Both membrane models including vesicles and monolayer of DPPC/DPPE-PEG2000 containing 1 mol% PEG2000 constitutes up to 75% $L_{\beta'}$ phase. Similarly, the membrane morphology of DPPC/DPPE-PEG2000 containing 3 and 6 mol% PEG2000 also display significant resemblance with respect to the $L_{\beta'}$ phase, as illustrated in Figure 5.6. Furthermore, an increase in PEG content from 1 to 6 mol% shows a substantial reduction in the $L_{\beta'}$ phase from 75% to 58% in monolayers as well as from 73% to 53% in GUVs. This correlates well with the literature data which states that an increase in PEG content reduces the $L_{\beta'}$ phase in the membrane models [Bedu-Addo 1996; Belsito 2000; Edwards 1997; Montesano 2001; Lasic 1991; Szleifer 1998]. In fact, further increase in PEG2000 content to 9 mol% hindered the formation of large sized GUVS as well as made it difficult to image the coexistence of vesicles. Therefore, a direct comparison of DPPC/DPPE-PEG2000 membrane models containing 9 mol% will not be discussed in this report. Based on the comparative analysis, it can be concluded that the membrane

morphology of GUVs indeed display similar features as for the monolayer membrane model systems. Thus, monolayers can certainly serve as a simple yet efficient platform of a typical biological membrane to assess the properties of membrane-mimetic surfaces including phase behavior, mixture compositions, as well as lateral organization for numerous biomedical applications including nanosensor templates, biomedical implants, diagnostic devices and nanocarriers.

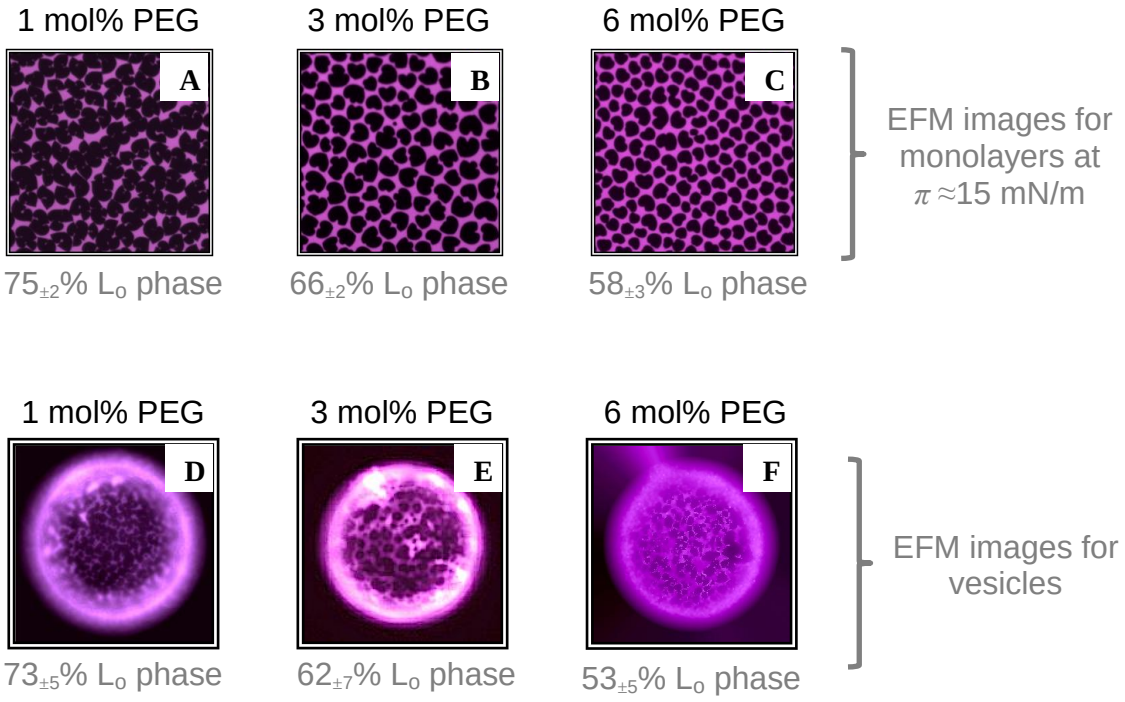

Figure 5.6.: EFM images of DPPC/DPPE-PEG2000 membrane with varying PEG content from 1 to 6 mol % PEG2000. Image A, B, C display the monolayer morphology of DPPC/DPPE-PEG2000 mixtures containing 1, 3, 6 mol% PEG at π = 15 mN/m. Image D, E and F depicts GUVs membrane morphology of the same mixture compositions as the monolayer.

5.3.4. Effect of Aqueous Medium on the DPPC/DPPE-PEG2000 GUVs.

Aqueous medium has shown to play a pivotal role towards the phase behavior of phosphocholine and PEG-phospholipid membrane, as discussed thoroughly in Chapter 3. Interestingly, the vesicles of DPPC/DPPE-PEG2000 also appeared quite differently when incubated in different aqueous medium. For instance, DPPC/DPPE-PEG2000 GUVs containing 1 mol% PEG were highly resolvable with good quality images when incubated in 0.1 M NaCl containing 1 vol% glycerol swelling solution (Figure 5.1). In contrast, vesicles of the same binary mixture were not highly resolvable when prepared in 0.1 M NaCl containing 1 vol% sucrose swelling solution (images not shown). Although, high concentration of salt solutions containing little amount of sucrose and glucose, as a swelling medium, has been suggested to produce high contrast images of GUVs [Akashi 1996; Bagatolli 2000]. Furthermore, DPPC/DPPE-PEG2000 GUVs did not grow very large in size when incubated in PBS containing 1 vol% glycerol with those incubated in 0.1 M NaCl solution containing 1 vol% glycerol [cf. Figure 5.1 and 5.5]. The images were also not highly resolvable to visualize the coexistence domains, when PBS was used as a swelling solution. This difference was quite remarkable since both solution, PBS and 0.1 M NaCl, contained 1 vol% glycerol. In addition, PBS solution has been used in several studies to produce vesicle and liposomes [Montesano 2001; Moscho 1996; Zawada 2004]. Hence, it can be said that DPPC/DPPE-PEG2000 GUVs images were highly resolvable when incubated in 0.1 M NaCl swelling solution containing 1 vol% glycerol.

5.3.5. Trends in DPPC/DPPE-PEG2000 and DSPC/DSPE-PEG2000 Vesicles.

A change in the aliphatic chain length from C_{16} to C_{18} for both phosphocholine and PEG-phospholipid has shown a remarkable effect on the phase behavior of GUVs prepared by the gentle hydration method (protocol 1) (cf. Figure 5.1 and 5.4). The DPPC/DPPE-PEG2000 GUVs obtained by protocol 1 grew large in size with up to 85 μm in diameter whereas the DSPC/DSPE-PEG2000 GUVs remained considerably small with the maximum size of ~12 μm. Interestingly, both types of GUVs were spherical in shape which is rather difficult to obtain without the addition of cholesterol [Edwards 1997, Veatch 2003]. The amount of debris, myelin and multilamellar structures was also considerably high in the DSPC/DSPE-PEG2000 samples as compared to the DPPC/DPPE-PEG2000 samples (cf. Figure 5.1 and 5.4). Hence, locating and imaging the unilamellar vesicles in DSPC/DSPE-PEG2000 samples was a challenging task. The formation of debris and multilamellar structures using this type of protocol has also been reported by some earlier studies [Akashi 1996; Bagatolli 2000]. These types of structures are usually attributed to modifications on the lipid film imposed by tangential forces during hydration that dominate the vesicle formation and causes high heterogeneity in the internal structure of the vesicles [Bagatolli 2000].

Furthermore, coexistence domains were only observed in DPPC/DPPC-PEG2000 GUVs but not in DSPC/DSPE-PEG2000. This is in fact consistent with the reported data where microbubbles comprised of DPPC and PEG2000 formed domains as compared to the DSPC and PEG2000 membrane model [Lozano 2009b]. This is also in good accord

the literature data where monolayer composed of DSPC as host matrix completely forms a condensed type membrane above 15 mN/m [Chou 2002; Chou 2003; Tanwir 2012].

5.3.6. Formation of Vesicles Tubes or Trajectories.

One of the most interesting observations in vesicles containing more than 1 mol% PEG2000 content is the existence of tubes/tethers or trajectories connecting several vesicles together like pearls of a necklace (Figure 5.3) [Antonietti 2003; Bagatolli 2000; Mathivet 1996]. It has been suggested by Antonietti et al. and other reports that many factors are usually involved in the formation of these structures including temperature fluctuation, inclusion of high polymer content as well as their interactions within the matrix [Antonietti 2003; Schara 2009; Stuklej 2013]. This might explain the reason that these tubes were not observed in the vesicles containing only 1 mol% of PEG2000 content. Most of the vesicles in the trajectories had similar features and morphology as individual vesicles of the same mixture. This behavior has also been reported by Bagatolli et al., which points towards similar phospholipid packing between the tubes and vesicles [Bagatolli 2000]. Furthermore, these kinds of tubes or tethers are also considered as one of the main component of the cloud, which is observed in the sample after preparation using both gentle hydration and solvent evaporation method [Angelova 1992; Bagatolli 2000]. In the case of our study, the formation of tubes was not observed for GUVs prepared by solvent evaporation method. The main cause of these structures formation is still unknown. However, a model proposed by Mathivet et al. suggests that unilamellar structures form tubular shapes to make a network by connecting vesicles for

possible biological relevance including protein and solutes transportation as well as cell – cell communication system [Angelova 1992; Bobrovska 2013; Collier 2001; Mathivet 1996; Schara 2009; Stukelj 2013]. These types of structures containing PEG-phospholipids can also have great implications in tissue engineering as well as in application for controlled release of drugs [Collier 2001; Shi 2010; Taguchi 2011; Takeuchi 2013]. Hence, it can be deduced that DPPC/DPPE-PEG2000 GUVs containing PEG2000 somewhere in the range of 3 – 6 mol% promotes the formation of tubes since these tubular structures were not observed in vesicles containing 1 and 9 mol% PEG2000 content. Hence, these findings can expand new horizons for possible implications in the field of biomedical applications.

5.4. CONCLUSIONS.

The morphology of DPPC/DPPE-PEG2000 and DSPC/DPPE-PEG2000 GUVs was visualized by EFM. A comparative analysis has revealed that the coexisting phases were present in GUVs bearing 1 – 6 mol% of PEG content. Increasing PEG2000 content increased phase separation and resulted in an overall increase in L_d phase in the vesicles. Furthermore, a reduction in the amount and size of GUVs was also observed with increase in PEG-phospholipid content. In particular, GUVs with 9 mol% PEG2000-phospholipid were unable to form giant vesicles that might be associated to high concentration of PEG-phospholipid. Formation of vesicle tubes has also been observed in DPPC/DPPE-PEG2000 GUVs containing 3 and 6 mol% PEG2000. Most importantly, the membrane morphology of DPPC/DPPE-PEG2000 GUVs containing 1, 3 and 6 mol% PEG2000 has shown a great resemblance with the monolayers of the same binary mixtures at ~15 mN/m. These findings are remarkable in terms of using a simple membrane model such as a monolayer to study various aspects of membrane mimetic surface at a fundamental level, which might be challenging with other membrane models. In conclusion, it can be proposed that PEG content somewhere between 1 – 6 mol% might be useful in order to develop efficient drug delivery system with controlled bio-non-fouling properties without comprising their structural stability.

5.5. REFERENCES.

Akashi, K.; Miyata, H.; Itoh, H.; and Kinosita, K. *Biophys. J.* **1996**, *71*, 3242 – 3250.

Akbarzadeh, A.; Rezaei-Sadabady, R.; Davaran, S.; Joo, S. W.; Zarghami, N.; Hanifehpour, Y.; Samiei, M.; Kouhi, M.; and Nejati-Koshki, K. *Nano. Res. Let.* **2013**, *8*, 1 – 9.

Angelova, M. I.; Soleau, S. Me1eard, P.; Faucon, J. F. and Bothorel, P. *Progr. Coll. Polym. Sci.* **1992**, *89*, 127 – 131.

Antonietti, M. and Forster, S. *Adv. Mate.* **2003,** *15*, 1323 – 1333.

Bagatolli, L.A.; Parasassi, T.; and Gratton, E. *Chem. and Phys. of Lip*. **2000**, *105*, 135 – 147.

Bagatolli, L.A. *Biochim. et Biophys. Acta*, **2006**, *1758*, 1541–1556.

Bedu-Addo, F. K., Tang, P.; Xu, Y.; and Huang, L. *Pharm. Res.* **1996**, 13, 710 – 717.

Belsito, S.; Bartucci, R.; Montesano, G.; Marsh, D.; and Sportelli, L. *Biophys. J.* **2000**, *78*, 1420 – 1430.

Bobrovska, N.; Gozdz, W.; Kralj-Iglic, V.; Iglic, A. PLoS ONE, **2013**, *8*, 1 – 6.

Collier, J. H. and Messersmith, P. B. *Annu. Rev. Mater. Res.* **2001**, *31*, 237 – 63.

Discher, B. M.; Schief, W. R.; Vogel, V.; Hall, S. B. *Biophys. J.* **1999**, *77*, 2051.

Edwards, K.; Jonsson, M.; Karlsson, G.; and Silvander, M. *Biophys. J.* **1997**, *73*, 258 – 266.

Eeman, M. and Deleu, M. *Biotechnol., Agron., Soc. Environ.***2010**, *14*, 719.

El-Khouri, R. J.; Frey, S. L.; Szmodis, A. W.; Hall, E.; Kauffman, K. J.; Patten, T. E.; Lee, K. Y. C.; and Parikh, A. N. *Langmuir* **2011**, *27*, 1900.

Ickenstein, L. M.; Arfvidsson, M. C.; Needham, D.; Mayer, L. D.; and Edwards, K. *Biochim. Biophys. Acta* **2003**, *1614*, 135.

Immordino, M. L. Dosio, F.; and Cattel, L. *Intl. J. of Nanomed.* **2006**, *1 (3)*, 297 – 315.

Jinjun, S.; Votruba, A. R.; Farokhzad, O. C.; and Lange, R. *Nano Lett.* **2010**, *10*, 3223 – 3230.

Jesorka, A.; Orwar, O. *Annu. Rev. Anal. Chem.* **2008**, *1*, 801 – 832.

Kastantin, M.; Ananthanarayanan, B.; Karmali, P.; Ruoslahti, E.; and Tirrell, M. *Langmuir* **2009**, *25*, 7279–7286.

Korlach, J.; Schwille, P.; Webb, W.W.; and Feigenson, G.W. *Proc. Natl. Acad. Sci. U. S. A.*, **1999**, *96*, 8461–8466.

Konttila, R.; Salonen, I.; Virtanen, J. A.; and Kinnunen, P. K. J. *Biochem.* **1988**, *27*, 7443.

Lasic, D. D.; Woodle, M. C.; Martin, F. J. and Valentincic, T. *Period. Biol.* **1991**, *93*, 287 – 290.

Li, Y.; Lipowsky, R. and Dimova, R. *PNAS* **2011**, *108*, 4731 – 4736.

Lozano, M. M. and Longo, M. L. *Soft Matter* **2009a**, *5*, 1822.

Lozano, M. M. and Longo, M. L. *Langmuir* **2009b**, *25*, 3705 – 3712.

Manley, S. and Gordon, V. D. *Current Protocols in Cell Biology*, John Wiley & Sons Inc., USA, **2008.**

Mathivet, L., Cribier, S., Devaux, P.F., *Biophys. J.* **1996**, *70*, 1112 – 1121.

Montesano, G.; Bartucci, R.; Belsito, S.; Marsh, D. and Sportelli, L. *Biophys. J.* **2001,** *80*, 1372 – 1383.

Moscho, A.; Orwar, O.; Chiu, D. T.; Modi, B. P.; and Zare, R. N. *PNAS* **1996**, *93*, 11443 – 11447.

Nag, K.; Pao, J.S.; Harbottle, R.R.; Possmayer, F.; Petersen, N.O.; Bagatolli, L.A. *Biophys. J.* **2002**, *82*, 2041 – 2051.

Pappalardo, M.; Milardi, D.; Grasso, D. and La Rosa, C. *J. of Therm. Anal. and Calor.*, **2005**, *80*, 413 – 418.

Popovska, O.; Simonovska, J.; Kavrakovski, Z.; and Rafajlovska, V. *Intl. J. of Pharm. and Phyto. Res.* **2013**, *3 (3)*, 182 – 189.

Schara, K.; Jansai, V.; Sustari, V.; Dolinari, D.; Pavlic, J. I.; Lokar, M.; Kralj-Iglic, V.; Veranic, P.; Iglic, A. *Cell. and Molec. Biol. Lett.*, **2009**, *14* 636 – 656.

Shahid, M. N.; Tsoukanova, V. *The J. of Phys. Chem. B* **2011**, *115*, 3303.

Sezgin, E. and Schwille, P. *Molec. Memb. Biol.* **2012,** *29*, 144 – 154.

Stukelj, R; Sustar, V; Mrvar-Brecko, A; Veranic, P; Hagerstrand, H; Kralj-Iglic, V; Sevsek, F. *Gener. Physio. and Biophys.* **2013**, *32*, 33 – 45.

Sun, B. and Chiu, D. T. *Anal. Chem.* **2005,** *77*, 2770 – 2776.

Szleifer, I.; Gerasimov, O. V. and Thompson, D. H. *PNAS* **1998**, *95*, 1032 – 1037.

Taguchi, T. *Sci. Technol. Adv. Mater.* **2011**, *12*, 1 – 8.

Takeuchi, S. 17th International Conference on Miniaturized Systems for Chemistry and Life Sciences, Germany 1300 – 1301.

Tenchov, B.; Koynova, R.; Rapp, G. *Biophys. J.* **2001**, *80*, 1873.

Thevenot, J.; Troutier, A. L.; David, L.; Delair, T. and Ladaviere, C. *Biomacromole.* **2007**, *8*, 3651 – 3660.

Tsoukanova, V. and Christian, S. *Langmuir* **2008,** *24*, 13019 – 13029.

Veatch, S. L. and Keller, S. L. *Biophys. J.* **2003,** *85*, 3074 – 3083.

Walde, P. and Ichikawa, S. *Biomole. Eng.* **2001**, *18*, 143 – 177.

Wesołowska, O; Michalak, K.; Maniewska, J. and Hendrich, A. B. *Acta Biochim. Polon.* 2009, *56*, 33 – 39.

Yamashita, Y.; Oka, M.; Tanaka, T. and Yamazaki, M. *Biochim. et Biophys. Acta* **2002**, *1561*, 129 – 134.

Zawada, Z. H. *Cellular & Mole. Biol. Lett.* **2004**, *9*, 603 – 615.

Chapter 6: Examining the Non-Specific Interactions of Insulin with DPPC/DPPE-PEG2000 Model Membranes.

This chapter will highlight some of the key aspects associated with the possible changes in the phase behavior of DPPC/DPPE-PEG2000 membrane model upon interactions with insulin. The changes in the insulin conformation, in particular, prior and after interacting with the DPPC/DPPE-PEG2000 model membrane have also been examined comprehensively. Giant (GUVs) and small unilamellar vesicles (SUVs) have been used as typical membrane models for the insulin-membrane interactions study. The preparation protocol for SUVs will only be discussed herein since preparation procedures for GUVs have already been discussed in detail in Chapter 5. Two-channel epifluorescence microscopy (EFM) has been utilized to examine the changes in the phase behavior of GUVs upon insulin binding. Furthermore, circular dichroism spectroscopy (CD) has been employed to attain complementary information about insulin conformation and its secondary structure upon binding onto the DPPC/DPPE-PEG2000 SUVs. Importantly, the conformational changes of insulin upon interactions with the SUVs have been analyzed in terms of α-helical content. The effect of varying PEG content in SUVs on the insulin conformation will also be analyzed in detail. CD data analysis has been summarized in terms of CD phase diagram to determine different states of insulin species present upon interactions with SUVs with varying PEG content.

6.1. Molecular Dimension and Conformational Behavior of Insulin Molecule.

Insulin is a small protein with 51 amino acids with considerable α–helical structure and bears an overall negative charge, –2 per monomer, in the presence of PBS subphase with a pH of about 7.4 [Farias 1989; Henry 2008]. Insulin primarily exists as three structural states in blood stream known as a monomer, dimer (possess 2 monomers), and hexamers (possess 6 insulin molecules) [Henry 2008; Liu 2002]. The hydrodynamic diameter of zinc-free human insulin monomer has been approximated to be 3 nm and exhibits a wedge shape with molecular dimensions of 2 x 2.5 x 2 nm^3 [Liu 2002; Henry 2008]. An insulin monomer is considered to be the biologically active form [Liu 2002; Perez-Lopez 2011] Insulin dimer exhibits an oblong shape with molecular dimensions of 2 x 2.5 x 4 nm^3 [Henry 2008]. Insulin hexamer, on the other hand, has molecular dimensions of 4.9 x 3.4 nm^2 and considered to be the inactive form of insulin [Henry 2008; Perez-Lopez 2011]. The existence of insulin structural state is primarily dependent on the concentration of the solution. The concentration range for the monomeric state of insulin lies between 0.1 – 1 μM [Pocker 1980] and hence a concentration of 0.7 μM of insulin has been used in our study.

Studies have shown that Insulin changes its conformational behavior as well as fibrillation and aggregation states at different experimental conditions, in particular in the presence of hydrophobic environment [Grudzielanek 2007; Liu 2002; Perez-Lopez 2011; Sefton 1984]. Electrostatic and hydrophobic interactions are considered to be the primary interactions for the non-specific insulin/membrane interactions. Additionally, phase

behavior of phospholipid membranes can also affect the conformational behavior, aggregation and fibrillation state of insulin upon interactions [Birdi 1976; Nosrati 2009; Perez-Lopez 2011]. Few studies have also documented a partial unfolding of several proteins upon non specific interactions with the membranes. These proteins include insulin, cytochrome c, phospholipase A2, and pheromone-binding protein [Gobrenko 2006; Grudzielanek 2007; Wojtasek 1999]. Hence, the affect of non-specific interactions of insulin with PEGylated phosphocholine membrane on the insulin folding/unfolding as well as conformational changes, in terms of α-helcial content, is essential. In this study, CD spectroscopy has been utilized to analyze the changes in the conformational behavior of insulin upon non-specific interactions with PEGylated phosphocholine vesicle membrane models.

6.2. RESULTS.

6.2.1. In-Situ Imaging of Insulin/GUV Interactions.

The first part of this chapter will focus on the effect of insulin interactions on the phase behavior of the DPPC/DPPE-PEG2000 GUV membrane containing 1 mol% PEG content. A procedure to label insulin with the FITC fluorophore to study the insulin/membrane interactions will be described. Furthermore, the insulin binding on the GUV as a membrane model has been visualized using two channel EFM and discussed in detail.

6.2.1.1. Methodology for In-Situ Insulin/GUV Imaging.

The effect of insulin binding on the morphology of DPPC/DPPE-PEG2000 GUVs was performed by two-channel EFM (TRITC and FITC channels). DPPC/DPPE-PEG2000 GUVs were prepared using the protocol described in Chapter 5. In this study, DOPE-Rh was used to image the GUV morphology whereas FITC-insulin was used to monitor the insulin binding on to the GUV membrane upon interactions. For this purpose, FITC labeled insulin was injected in the GUV imaging chamber slightly away from the vesicle of interest. The imaging was done by switching between TRITC and FITC channel. In the TRITC channel, the contrast was derived from differences in partitioning of DOPE-Rh into ordered (liquid condensed) and disordered (liquid expanded) phospholipid phases [Tsoukanova 2008; Tanwir 2012]. The areas appeared red in the TRITC channel due to the fluorescence from the DOPE-Rh fluorophore. Conversely, in the FITC channel, areas were stained green due the fluorescence of FITC fluorophore of FITC-insulin. The green stain thus corresponds to the binding of insulin on to the vesicle. Both channels were equipped with Nikon CFI infinity optics combining a medium width excitation filter attaching to a bandpass barrier filter. This filter has the ability to detect the detection of fluorescence from one of the fluorophores and cutting off that from the other fluorophore. To visualize the DOPE-Rh molecule, a green excitation filter set (the Nikon TRITC HYQ filter combination, 545CWL excitation filter, 570LP dichroic mirror and 620CWL barrier filter) was used. On the other hand, to observe the fluorescence from the fluorescein fluorophore of FITC-insulin, a blue excitation filter set (the Nikon B-1E filter combination, 480CWL excitation filter, 505LP dichroic mirror, and 540CWL

barrier filter) was used. The images were captured by a Hamamatsu CCD camera, ORCA ER(AG) (Hamamatsu, Japan) directly onto a computer screen using Simple PCI 6 software (Compix Inc., PA). Image analysis in terms of the percentage of dark domains, % dark domains, was performed with the Quantify package of Simple PCI 6. In the Quantify package, the value of % dark domains is found by relating the area occupied by domains to the area of the image.

6.2.1.2. Protocol to Label Insulin with FITC Fluorophore.

To better comprehend the insulin interactions with the vesicle membrane, insulin was labeled with the FITC fluorophore by covalent binding of fluorophore to the amino group of protein using Molecular Probes protocol with slight modifications [Haugland 2005]. About 6 mg/mL of insulin was treated with FITC (molar ratio dye : insulin as 3:1) at room temperature with stirring in the dark for about an hour in 20 μL of 1M $NaHCO_3$ buffer (adjusted to pH 9). FITC of concentration ~10 mg/mL was prepared by dissolving FITC dye in 24 μL of DMSO and immediately added to the insulin solution. The insulin-FITC solution was then purified using dialysis against PBS for ~ 48 hours, at 4 ^{o}C, to remove the free FITC molecules. The fluorescence intensity of the labeled insulin was measured using UV-Visible spectrophotometer (Nano Drop ND1000, Thermo). The absorbance of labeled insulin was measured at 280 nm whereas absorbance of FITC was measured at 494 nm to determine the molar ratio of FITC to insulin. The molar ratio of FITC to insulin was estimated to be 1.46:1. The solution was always covered with aluminum foil for light-sensitive components and stored at 4 ^{o}C.

6.2.1.3. In-Situ EFM Imaging of Insulin Interactions with DPPC/DPPE-PEG2000 GUVs.

The imaging of insulin interactions with DPPC/DPPE-PEG2000 GUVs were performed using visible light microscopy as well as by switching between FITC and TRITC channels in EFM. Visible light microscopy was used to examine the size, shape and lamellarity of vesicles. FITC channel allowed monitoring the insulin binding on the vesicle membrane whereas TRITC channel provided information about the changes occurred in the membrane morphology due to insulin binding. Figure 6.1 exhibits the images of DPPC/DPPE-PEG2000 GUV containing 1 mol% PEG captured before and after insulin injection. Before insulin interactions, the vesicle seen in the visible light image appeared unilamellar with the diameter of ~83 μm (Figure 6.1D). The vesicle also comprised of 73% of the L_o phase, as can be seen from the TRITC image (Figure 6.1A). Interestingly, insulin injection caused a fast movement and rearrangement of the $L_{\beta'}$ phase domains during the first 5 min of interaction time. Vesicle size also increased from 83 to 90 μm in diameter after insulin injection, as can be seen from visible light image (cf. Figure 6.1D and E). Moreover, the $L_{\beta'}$ phase of the vesicle increased from 73% to 90% after the insulin penetration as observed by TRITC channel (Figure 6.1B). Identical patterns in FITC and TRITC images clearly indicate that insulin binds to the expanded/disordered phase of the vesicle (cf. Figure 6.1B & C). After ~1 h interaction time, monitoring the insulin/vesicle interactions became almost impossible due to image blurriness and contrast over time.

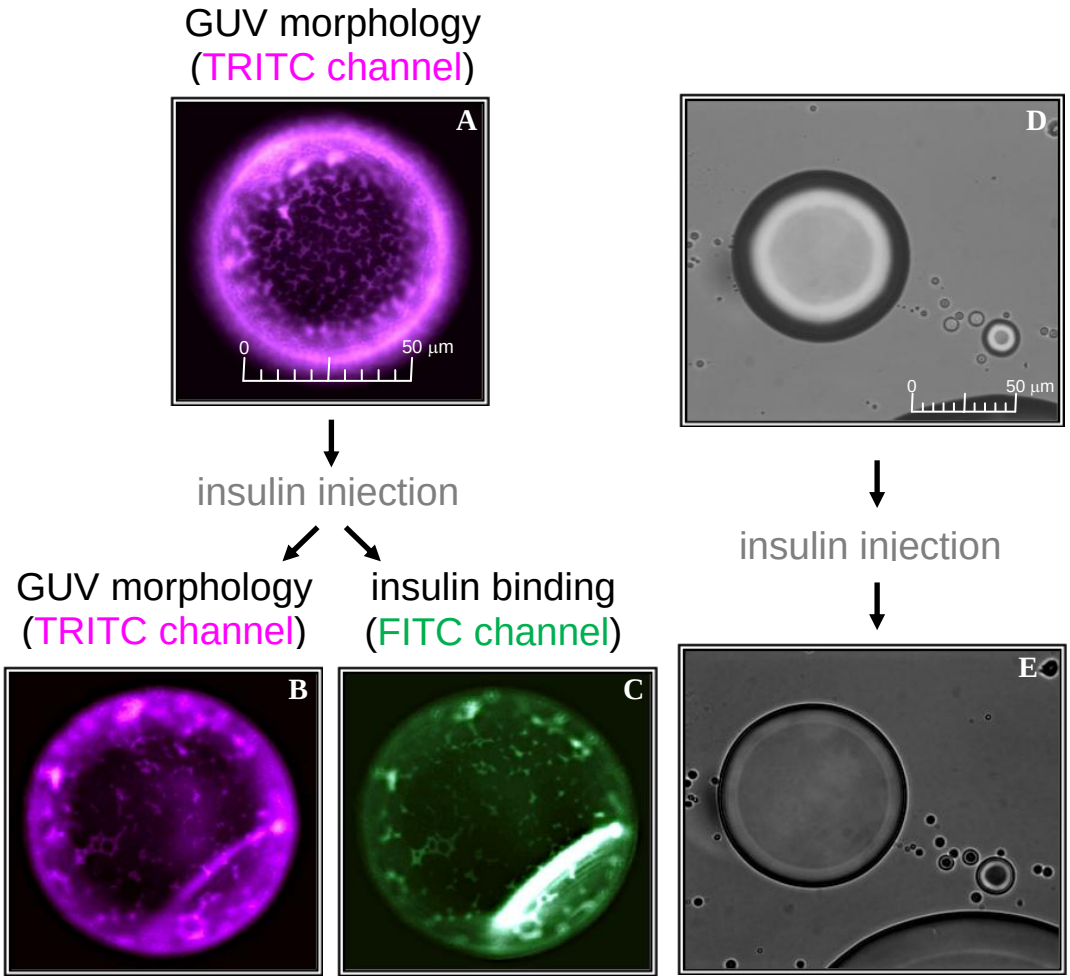

Figure 6.1.: Insulin interaction with the DPPC/DPPE-PEG2000 vesicle containing 1 mol% PEG content by EFM. [A] TRITC channel and [D] visible light show images of GUV before insulin injection. [B] TRITC channel, [C] FITC channel, [E] visible light depict images of vesicle after insulin injection.

6.2.2. Examining Insulin/Membrane Interactions by Circular Dichroism (CD) Spectroscopy.

This section of the report will elaborate on the use of CD spectroscopy to study the effect of insulin/membrane interactions on the secondary structure of insulin. Procedure to prepare and image SUVs as well as methodology for CD measurements will be explained in detail. Most importantly, the effect of insulin/membrane interactions on the insulin secondary structure and its folded/unfolded conformations will also be determined using CD data analysis.

6.2.2.1. CD Spectroscopy to Study Insulin/Membrane Interactions.

Circular Dichroism (CD) spectroscopy is being extensively used to gain complimentary structural and conformational information of proteins in solution [Greenfield 1996; Greenfield 2006; Kelly 2005; Sreerama 2004; Sreerama 2004a; Woody 1995]. CD refers to the differential absorption of left- and right-handed circularly polarized light by an optically active chiral molecule (protein) at a selective wavelength [Kelly 2005; Shahid 2013; Sreerama 2004]. The unequal absorption of left- and right-handed light of a sample gives rise to a CD spectrum which provides specific structural information of the molecule. CD spectrum may exhibit positive and negative peaks depending on the structure of the molecule. The CD measurements of proteins are usually carried out in the visible and ultraviolet (UV) region based on the electronic excitations [Sreerama 2004; Woody 1995]. However, measurement in the infrared spectral region has also been progressively gaining interest to obtain information about the vibrational

excitations of the molecules [Autschbach 2011; Sreerama 2004; Woody 1995; Yang 2011]. This type of CD is known as vibrational circular dichroism (VCD). This report will only cover the UV-vis region of the CD spectrum to gain the structural information about proteins. The CD spectrum of a protein, in the UV region, is generally divided in to three distinctive wavelength ranges [Shahid 2013; Sreerama 2004; Woody 1995]. This includes (i) the far UV, which ranges between 190 – 250 nm, where peptide contributes, (ii) the near UV, which lies between 250 – 300 nm, where contribution from aromatic side chains is observed, and (iii) the near UV-visible, which ranges from 300 – 700 nm, where contributions from extrinsic chromophores dominate [Kelly 2005; Shahid 2013; Sreerama 2004; Woody 1995; Greenfield 2006]. The absorption peak in the far UV region is primarily due to the weak but broad n $\rightarrow$ π * and π $\rightarrow$ π * transitions in the peptide bond, which occur around 220, 208 and 190 nm, respectively [Kelly 2005; Sreerama 2004]. Hence, different types of proteins secondary structures give rise to distinctive CD spectra in this range, which can be used to obtain the structural information of proteins. For instance, proteins containing β-sheets will exhibit a CD spectrum with a positive band around 198 nm and a negative band around 215 nm [Greenfield 1996; Greenfield 2006; Kelly 2005; Sreerama 2004]. The CD spectrum of proteins with α-helical content can be characterized by one positive band at 192 nm and two negative bands of 208 and 222 nm. The two CD signals at 208 and 222 nm can also be further used in estimating the α-helical content of the protein [Greefield 1969; Kelly 2005; Seelig 2000]. In fact, CD spectroscopy has been used in several studies to monitor the changes in the protein secondary structure, by estimating the α-helical content, upon interactions with membranes and various other molecules [Mollmann 2006; Nosrati

2009; Pal 2011; Seelig 2000; Shahid 2011; Tah 2014]. Hence, the goal of this study is to assess the folding/unfolding states as well as conformational changes in the insulin's secondary structure, in terms of α-helical content, upon interactions with small unilamellar vesicles as membrane models using far-UV CD spectroscopy.

6.2.2.2. Preparation of Small Unilamellar Vesicles (SUV) for CD Measurements.

CD experiments were performed with DPPC/DPPE-PEG2000 small unilamellar vesicles (SUVs) with varying PEG content from 1 – 6 mol%. A procedure to prepare SUVs was relatively similar to that described for GUVs in Chapter 5 with few variations. First, the phospholipid stock solutions of DPPC and DPPE-PEG2000 were prepared in chloroform/methanol (60:40 v/v) solvent at a concentration of 20 mg/mL and 2 mg/mL, respectively. The binary mixtures of DPPC and DPPE-PEG2000 containing 1, 3, 6, and 9 mol% PEG were obtained by calculating and mixing appropriate molar ratios. Each appropriate mixture was then transferred to a 6 ml glass vial with the flat bottom surface. The organic solvent was evaporated on a hotplate at 60 – 70 ˚C for ~30 min and then left in a desiccator overnight. Next day, the dried film was hydrated with PBS solution, pH ~7.4, to achieve a final concentration of 0.4 mM. The solution was stirred for 30 min at 70 ˚C followed by sonication process for 30 min at 50 ˚C in a water bath-type sonicator to produce a dispersion of SUVs ≤ 10 μm in diameter. The size was confirmed by visualizing SUVs before and after sonication by EFM. The CD measurements were performed within 5 hours of the SUVs preparation.

6.2.2.3. Methodology for CD Measurements.

Far-UV CD spectra of the SUVs and insulin at a concentration of ~0.7 μM in PBS were obtained by using a Jasco J-810 spectropolarimeter equipped with a temperature controlled sample holder. A rectangular cell with a path length of 1 cm was used for all the measurements. Each spectrum was recorded from 260 to 200 nm with a scan rate of 10 nm/min and a bandwidth of 1 nm at 20 ˚C. The spectra were obtained every hour after the insulin injection into SUVs dispersions over 3 h interaction time. All spectra were collected by averaging the signal at every 0.5 nm for 2 s. Each plot shows the average of three spectra. The PBS baseline was also measured to be used to subtract from all the average CD scans. Moreover, the spectra of insulin interacting with SUVs were corrected by subtracting the spectra of vesicles alone in PBS. Every measurement was performed three times.

6.2.2.4. Far-UV-CD Spectrum of Native Insulin.

Figure 6.2 exhibits the far-UV CD spectrum of native insulin in PBS at 20 °C. The CD spectrum is shown from 200 – 250 nm for the simplicity of the results as well as for comparative analysis discussed later in the chapter. Figure 6.2 displays the CD spectrum of insulin in the range of 200 – 250 nm exhibiting two negative bands at ~209 and ~222 nm. This is considered as a typical characteristic of a native insulin monomer with α-helix conformation [Ahmad 2004; Ahmad 2005; Ettinger 1971; Shahid 2013; Tah 2014]. The two minima in the CD spectrum stated above correspond to two different transitions in the peptide. The negative band at ~222 nm is attributed to the n → π*

transition due to the large magnetic dipole moment alongside the carbonyl bond whereas the $\pi \rightarrow \pi^*$ transition adjacent to the peptide bond gives rise to a negative band in the CD spectrum at ~208 nm [Beychok 1964; Ettinger 1971; Kelly 2005; Shahid 2013; Sreerama 2004]. Moreover, both negative bands around 208 and 222 nm in the CD spectrum have also been associated to the strong contributions originating from cysteine and tyrosine amino acid residues in the protein, respectively [Ettinger 1971; Shahid 2013; Nosrati 2009; Beychok 1964]. Hence, any conformational change in the insulin secondary structure upon interactions with the membrane model (SUV) will be detected as the intensity change in the CD spectra between the wavelength range of 200 – 250 nm. Furthermore, changes in the CD spectra can also aid in determining the folded/unfolded state of insulin upon interactions with SUV membrane models.

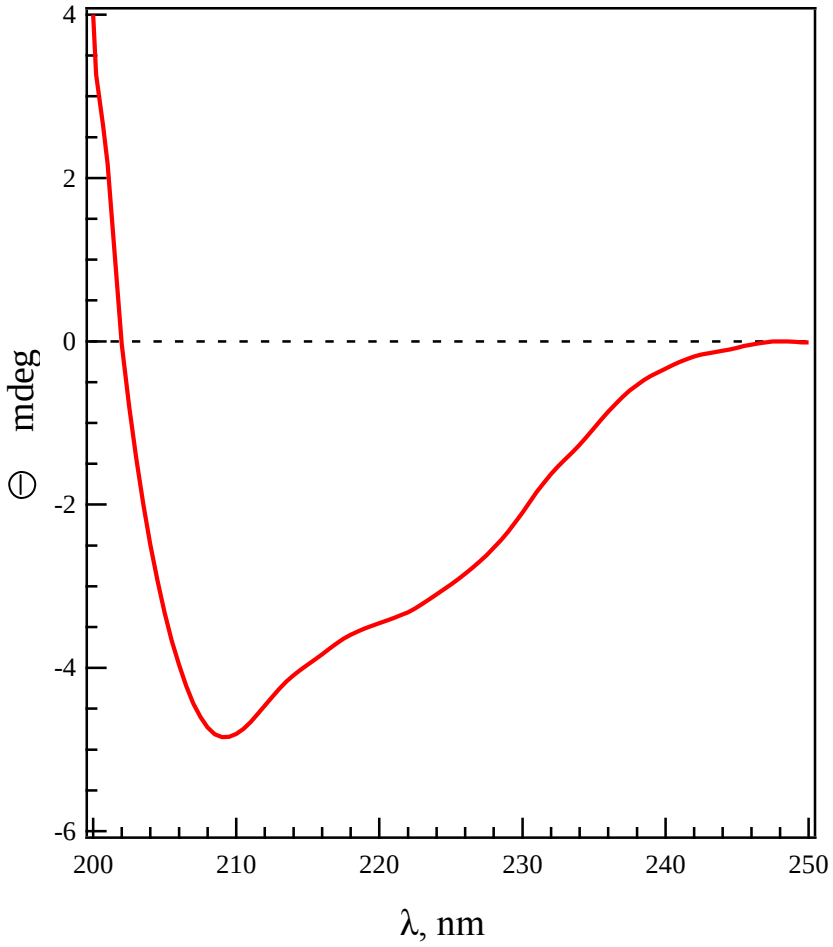

Figure 6.2.: Far-UV CD spectrum of native insulin in PBS, pH~7.4 at 20 ˚C. The negative bands at ~209 nm and ~222 nm depict an α- helical configuration in the insulin monomer.

6.2.2.5. Conformational and Structural Changes of Insulin upon Interactions with DPPC/DPPE-PEG2000 SUV Membranes.

Small unilamellar vesicles (SUVs) were prepared to examine the changes in the secondary structure of insulin upon interaction with DPPC/DPPE-PEG2000 membrane by circular dichroism spectroscopy (CD). The primary reason for selecting SUVs instead of GUVs was due to the increased light scattering, which could interfere with the insulin spectra and yield poor results. Figure 6.3 shows the images of well-dispersed DPPC/DPPE-PEG2000 SUVs membrane morphology in PBS with various PEG content from 1 to 6 mol%. The size of SUVs decreased with increasing PEG2000 content (Figure 6.3 A – C). As can be seen in the figure, the size of the SUVs containing 1 mol% PEG lies in the range of 2 – 8 μm, which decreased to 1 – 2 μm in diameter with increasing PEG content to 6 mol%. This trend is in well agreement with the DPPC/DPPE-PEG2000 membrane GUVs upon varying PEG content (cf. Figure 5.1, 5.2 with Figure 6.3). After performing the EFM imaging, all the remaining SUV solutions were further used to study the insulin/membrane interactions by CD spectroscopy as discussed below.

The far-UV CD spectra of insulin upon interactions with DPPC/DPPE-EPG2000 SUVs with varying PEG content were collected in PBS at 20 °C (Figure 6.4). The red dashed line in Figure 6.4 represents the native insulin CD spectrum as a reference while all the other ones represent the CD spectra of insulin upon interactions with SUVs containing 1 to 6 mol% PEG. Interactions of insulin with DPPC/DPPE-PEG2000 SUVs, in two hours of interaction time, caused significant changes in the CD spectra. All the features of insulin's CD spectra remain the same with respect to the native insulin

spectrum. However, the mean residue ellipticity, [θ], at both negative bands (209 and 222 nm), changed with increasing PEG2000 content from 1 – 6 mol% PEG2000 in the SUVs. The intensity of the insulin CD spectrum showed a great effect at 209 nm where it decreased significantly in the presence of vesicles containing 6 mol% PEG-phospholipid. This effect is not much seen at 222 nm since all the bands are close to that of the native insulin. The CD spectrum of insulin in the presence of all kind of vesicles shows a considerable secondary structure (Figure 6.4). This emphasizes that the protein has not unfolded but endured a slight change in the conformation during the interactions. This correlates well with several reported data where insulin changes its conformation but does not unfold [Ahmad 2004; Ahmad 2005; Tah 2014]. This might points towards the insulin molecule to conform to a more compact conformation in order to interact with the SUVs with increasing PEG content. Hence, further analysis of insulin CD spectra in terms of α-helical content can be really helpful in understanding the changes in insulin secondary structure in the presence of DPPC/DPPE-PEG2000 SUVs with varying PEG content [Kelly 2005; Seelig 2000; Tah 2014].

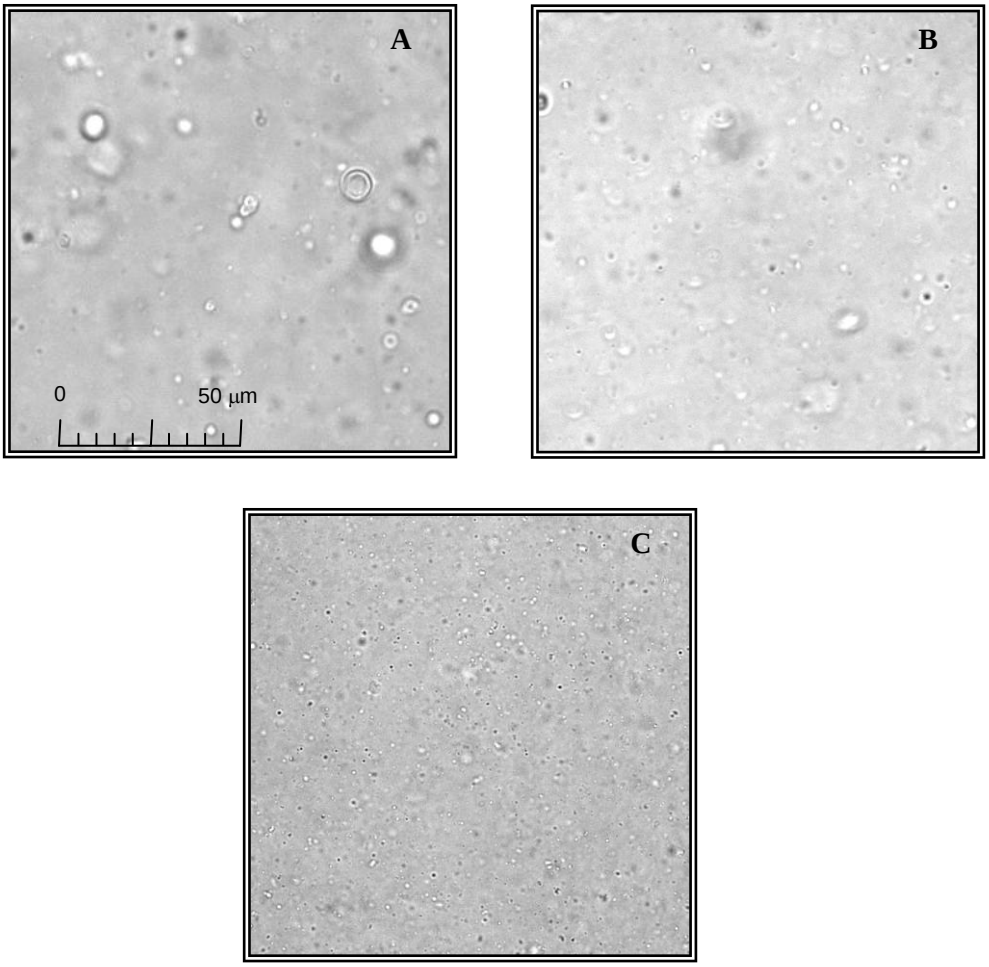

Figure 6.3.: EFM images of DPPC/DPPE-PEG2000 small unilamellar vesicles (SUV) bearing (A) 1, (B) 3, and (C) 6 mol% of PEG content. These images were captured before CD measurements were performed in order to verify the dispersion of SUVs in PBS. T = 23 ºC.

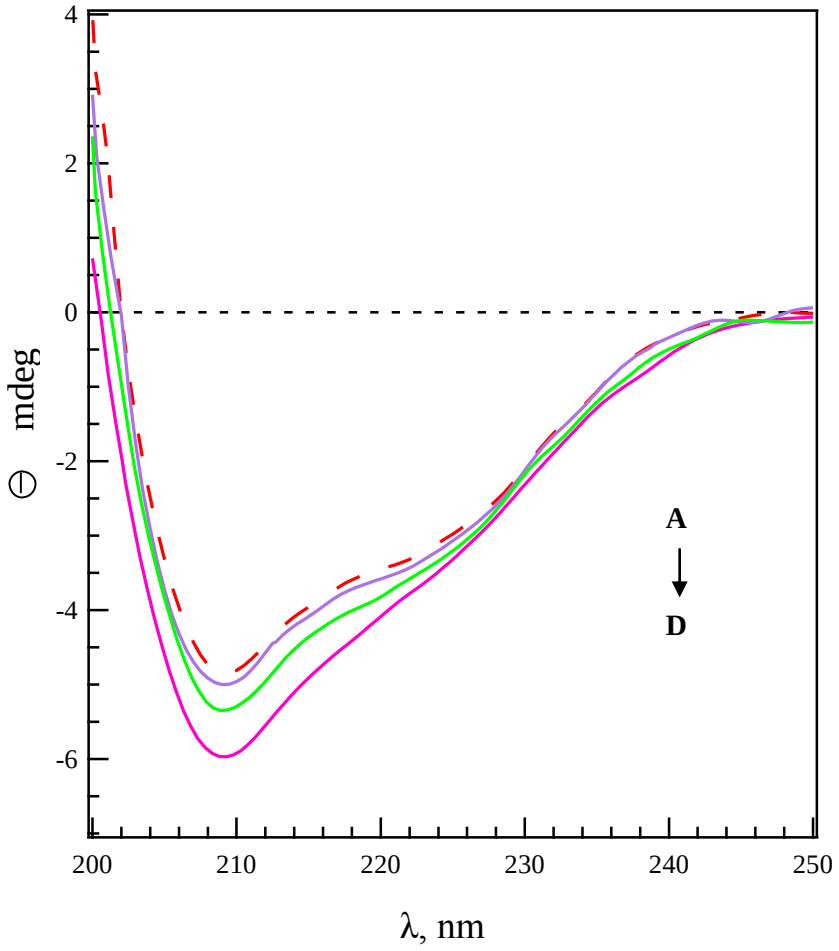

Figure 6.4.: Far-UV CD spectra beginning from (A) the native insulin to insulin interacting with DPPC/DPPE-PEG2000 vesicles containing (B) 1 mol%, (C) 3 mol%, and (D) 6 mol% PEG content, in PBS. Negative bands at 222 nm and 209 nm show typical feature of α-helical structure. T = 20 ˚C.

6.3. DISCUSSION.

Phospholipid membrane models have become efficient tools to investigate various aspects of cellular membranes [Bagatolli 2006; Bagatolli 2000; Korlach 1999; Sun 2005; Sezgin 2012; Veatch 2003; Walde 2001]. Unilamellar vesicles and liposomes have also been widely used as platforms to study the protein/membrane interactions for various biological processes including cell division, cell-cell communication, transportation, as well as protein L_o/L_d preferential studies in membrane [Bagatolli 2006; Gobrenko 2006; Jalmar 2010; Kalvodova 2005; Kim 1998; Krishnan 2009; Mathivet 1996; Netz 1996; Sezgin 2012; Vermette 2003; Vogel 2013]. Several studies have also aimed to understand the encapsulation efficiency of PEGylated membrane models to deliver small proteins, peptides, DNA, and other biomolecules both *in vitro* and *in vivo* [Chan 2012; Kim 1999; Iwanga 1999; Swaminathan 2012]. However, the effect of protein binding, in particular small protein, on the morphology and phase behavior of PEGylated membrane models still needs to be explored extensively [Kozarac 1987; Rahmati 2008; Nosrati 2009; Shahid 2013]. Therefore, Chapter 4 of this dissertation was entirely devoted to comprehend the changes induced by insulin binding on the PEG-grafted phosphocholine monolayers. Importantly, this chapter has encompassed the effect of insulin binding on the size, morphology, and phase state of DPPC/DPPE-PEG2000 GUVs using visible light and two channel EFM. Moreover, this chapter has also aimed at elucidating the effect of protein/membrane interactions on the conformational behavior of small protein e.g. insulin, which still requires great attention [Ahmad 2004; Gobrenko 2006; Grudzielanek 2007].

6.3.1. Imaging the Non-Specific Interactions of Insulin with Model Membrane.

The effect of non-specific insulin interactions on the size of the DPPC-DPPE-PEG2000 GUVs containing 1 mol% PEG was investigated using EFM. Interestingly, the vesicles appeared considerably larger in diameter upon insulin binding, as seen in the visible image in Figure 6.1 D and E. Based on the reported data, expansion of vesicles can certainly be attributed to the insulin insertion in to the hydrophobic moiety of phosphocholine membrane, which eventually made the vesicles appear larger in diameter [Hanakem 1996; Li 2013; Shahid 2013; Wiessner 1982]. In fact, several studies on protein/membrane interactions have reported on the area expansion of PEGylated and non-PEGylated membrane models upon binding of protein [Hanakem 1996; Nosrati 2010; Shahid 2013; Seelig 2000]. This appears to be in good correlation with our insulin/monolayer studies as well where insulin binding induced the area expansion of both DPPC/DPPE-PEG2000 and DSPC/DSPE-PEG2000 monolayers [Chapter 4]. For instance, the mean molecular area of DPPC/DPPE-PEG2000 monolayer containing 1 mol% PEG increased up to ~4.5 nm^2 upon interactions with insulin at $\pi \sim 15$ mN/m (a π value that is considered to lie in the range relevant to typical membrane pressure [Konttila 1988]). Hence, this indicates that membrane area expansion is indeed the result of insulin insertion in to the membrane.

The effect of insulin binding on the phase behavior of GUVs containing varying PEG content of 1, 3 and 6 mol% was also visualized using two channel EFM. However, direct imaging of changes in GUVs phase coexistence with higher PEG content was very

challenging due to the existence of high L_d phase even prior to insulin injection (images not shown). Hence, for the clarity of presentation, this discussion will only be limited to the DPPC/DPPE-PEG2000 GUVs containing 1 mol% PEG. The binding of insulin seemed to partition in to the L_d phase of the DPPC/DPPE-PEG2000 GUV membrane containing 1 mol% PEG content, which can be verified by identical patterns in the TRTIC and FITC images of GUV in Figure 6.1 B and C. Furthermore, an increased $L_{\beta'}$ phase from 73% to 90% upon insulin binding to the L_d phase of the membrane has also found to be a very distinct observation (Figure 6.1 A and B). This suggests that insulin preferably partitions into the L_d phase of the membrane while forcing phospholipids to stay in a more closely packed configuration. The orderliness of the vesicles can also be somewhat associated to the steric repulsion and redistribution of the PEG chains upon the compression exerted by insulin [Halperin 2007; Vermette 2003]. This might result in an increased $L_{\beta'}$ phase in the membrane, as can be seen in Figure 6.1B. Similar types of results have also been reported by several studies [Farias 1986; Sanchez 2002; Theumer 2012]. Farias et al. has indicated that insulin decreases the fluidity (L_o phase) of a phospholipid vesicle membrane [Farias 1986]. A study performed by Theumer et al. reported that the LC ($L_{\beta'}$) phase of the DPPC monolayer increased when the FB1 molecule, a mycotoxin, partitioned in to the LE (L_d) phase of the membrane [Theumer 2012]. The effect of PLA_2s protein binding in to the LE phase on the packing behavior of GUV's LC ($L_{\beta'}$) phase has also been demonstrated in detail by Sanchez et al. [Sanchez 2002]. In contrast, several studies have also associated the (i) protein insertion, (ii) competitive interactions of PEG-grafted phospholipid and protein molecules as well as (iii) entrapment of insulin in the polymer chains with the disruption of phospholipid

packing in the membrane [Allen 2002; Shahid 2013; Wang 2002]. Nevertheless, an increased $L_{\beta'}$ phase in the vesicle due to insulin insertion is indeed an unique phenomenon seen in this study. These findings, hence, can have significant implications to understand the mechanisms governing the morphological changes of membrane mimetic surfaces in the presence of different types of dissolved biomolecules.

6.3.2. Changes in Insulin α-Helical Content upon Interactions with DPPC/DPPE-PEG2000 SUVs.

The percentage of α-helix can be calculated using various methods which can provide valuable information about the structural changes of protein upon exposure to different experimental conditions [Greenfield 1969; Kelly 2005; Mollmann 2006; Seelig 2000; Tah 2014]. In this report, we have used the equation described by Seelig et al. to calculate the α-helical content in insulin as follows [Seelig 2000],

$$f_h = \frac{[\theta]_{222}}{\theta_h^n} \times 100\,\% \qquad 6.1$$

where [θ] depicts the molar mean residue ellipticity at 222 nm, in deg cm^2 $dmol^{-1}$, which can be calculated by the equation specified by Sreerama et al. as shown below [Sreerama 2004],

$$[\theta] = {}^{100\theta}\!/_{Cl} \qquad 6.2$$

Where θ is the residue ellipticity (mdeg) obtained from the CD spectrum at a given wavelength, *C* represents the molar concentration, and *l* represents the pathlength in (cm) of the sample [Sreerama 2004]. Molar ellipticity can either be defined as deg.M^{-1}.m^{-1} or as deg.cm^2.$dmole^{-1}$ since these units are equivalent. θ_h^n in equation 6.1 is expressed as the maximum absorption of an α-helix in the protein with number of (n) amino acid residues and can be calculated as described by Seelig et al. shown below,

$$\theta_h^n = (1 - k/n)\theta_h^\infty \qquad 6.3$$

In equation 6.3, *k* represents the wavelength-dependent constant, which is found to be 2.57 at a wavelength of 222 nm [Seelig 2000]. θ_h^∞ is considered to be the maximum ellipticity of an α-helix in the molecule with infinite length of -39,000 deg cm^2 $dmol^{-1}$ whereas *n* represents the number of amino acid residues constitutes the α-helical portion of the protein [Seelig 2000]. There are three α-helices in the insulin secondary structure from (i) A2 – A8 residues, (ii) A13 – A20 residues, and (iii) B9 – B19 residues [Periard 1984; Yan 2003]. The number of amino acid making up the entire α-helical portion of the insulin molecule is 23. Table 6.1 summarizes the percentage of α-helix of insulin after 2 h of interactions with the DPPC/DPPE-PEG2000 SUVs. The percentage of α-helical content in insulin monomer is about 25.4% in PBS. This value is in well correlation with the previous literature values [Ettinger 1971; Rawitch 1980; Sadhale 1999]. Increasing the PEG content from 1 to 6 mol% in the SUVs increases the α-helical content from 26.2% to 29.2% in insulin, respectively. The change in the insulin helical content is not very significant but it indicates that the insulin is slightly changing its conformation for

non-specific interactions with the PEGylated phosphocholine. These findings further imply that insulin does not unfold upon interactions with the PEG-grafted vesicle membrane [Ahmad 2004; Ahmad 2005; Tah 2014].

Table 6.1.

Changes in the α-helical structure content of insulin due to PEG increment in DPPC/DPPE-PEG2000 SUVs

Mixtures	Helix insulin (%)
Native Insulin	25 ± 1
Insulin/SUV with 1 mol% PEG	26 ± 1
Insulin/SUV with 3 mol% PEG	27 ± 2
Insulin/SUV with 6 mol% PEG	29 ± 1

6.3.3. CD Phase Diagram.

CD data analysis has been used as a conventional method to obtain complementary information about the folded/unfolded conformation of proteins. In fact, CD phase diagrams derived from the CD data can also be very useful in resolving complex structural transition of proteins [Ahmad 2004; Ahmad 2005; Kuznetsova 2002]. To determine different types of conformational species of insulin present in the solution, the CD phase diagram of the insulin was obtained by plotting the mean residue ellipticity at 222 nm as a function of mean residue ellipticity at 209 nm, calculated using equation 7.2, and is shown in Figure 6.5 [Ahmad 2004; Ahmad 2005; Kuznetsova 2002; Sreerama 2004]. The linearity of the plot will reflect the all-or-none transition in the insulin whereas non-linearity of the diagram will point towards the structural transformations of the insulin molecule. As can be seen from the CD Phase diagram in Figure 6.5, there is only one linear segment for insulin in the presence of vesicles with increasing PEG content, which implies the existence of two species of insulin with a little change in the secondary structure. These monomeric conformations are known as the native monomer (M) and a compact monomer with increased α-helical structure (M_C) [Ahmad 2004]. Thus, it is observed that the α-helical content of insulin increases as the PEG concentration increases in the DPPC/DPPE-PEG2000 vesicles, which may suggest that insulin molecule slightly conforms into a compact state in order to get through the PEG chains and penetrate the membrane. It can further be speculated that the primary domain penetrating the membrane can be insulin's α-helical structure since insulin sequence contains ~17 hydrophobic amino acid residues out of which 10 are found in the α-helix

portion of insulin, as estimated using Yan et al. and Stretton et al. studies [Stretton 2002; Yan 2003]. Hence, it can be concluded that insulin changes its conformation, to some extent, upon interactions with the DPPC/DPPE-PEG2000 membrane vesicles with increasing PEG content but does not unfold.

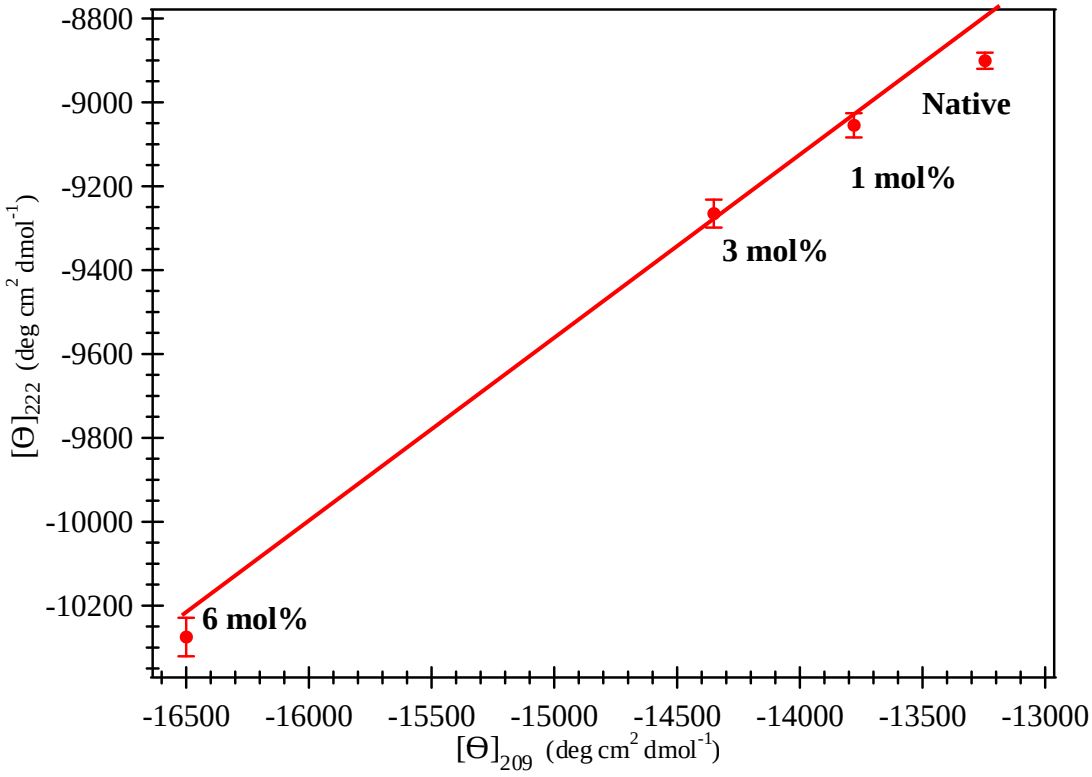

Figure 6.5.: CD phase diagram obtained by plotting 222 nm mean residue ellipticity, [θ], as a function of 209 nm mean residue ellipticity, [θ], for far-UV CD to show changes in insulin conformation state due to interactions with DPPC/DPPE-PEG2000 vesicles with various PEG content from 1, 3, and 6 mol% PEG. The values beside each point in the plot correspond to the PEG concentration incorporated in the vesicles for insulin/membrane interactions.

6.4.CONCLUSIONS.

Examining the insulin/membrane interactions has revealed a quite intricate effect on the phase behavior of DPPC/DPPE-PEG2000 GUVs. In-situ analysis of insulin interactions with DPPC/DPPE-PEG2000 membrane containing 1 mol% PEG vesicle has shown that membrane expanded as well as became more ordered. The expansion and orderliness of the vesicles is considered to be due to the steric repulsion and redistribution of the PEG chains upon the compression exerted by insulin. Furthermore, the effect of insulin/membrane interactions with varying PEG content shows a modest change in the insulin conformation. Circular dichroism data analysis illustrated that the α–helical content of insulin increased upon increasing the PEG content in the DPPC/DPPE-PEG2000 vesicles. This implies that insulin turns into slightly more compact conformation in order to avoid PEG chains and binds the phospholipid membranes. However, the change in the helical content is minimal which further reveals that insulin does not unfold or denature upon interactions with DPPC/DPPE-PEG2000 SUVs. Hence, these findings may aid gaining more insight to further comprehend the mechanisms involved in membrane interactions with small biomolecules.

6.5. REFERENCES.

Ahmad, A.; Millett, I. S.; Doniach, S.; Uversky, V. N.; Fink, A. L. *The J. of Biol. Chem.*, **2004**, *279*, 14999 – 15013.

Ahmad, A.; Uversky, V. N.; Hong, D.; Fink, A. L. *J. of Biol. Chem.* **2005**, *280*, 42669 – 42675.

Autschbach, J.; Nitsch-Velasquez, L.; Rudolph, M. *Top. Curr. Chem.* **2011**, *298*, 1 – 98.

Bagatolli, L. A.; Parasassi, T.; and Gratton, E. *Chem. and Phys. of Lip.* **2000**, *105*, 135 – 147.

Bagatolli, L.A. *Biochim. et Biophys. Acta*, **2006**, *1758*, 1541 – 1556.

Beychok S. and Fasman, G. D. *Biochem.* **1964**, *3*, 1675 – 1678.

Chan C-L.; Majzoub, R. N.; Shirazi, R. S.; Ewert, K. K.; Chen Y-J.; Liang, K. S.; Safinya, C. R. *Biomat.* **2012**, *33*, 4928 – 4935.

Ettinger, M. J. and Timasheff, S. N. *Biochem.* **1971**, *10*, 824 – 831.

Farias, R. N.; Vinals, A. E. L.; Posse, E.; and Morero, R. D. *Biochem. J.* **1989**, *264*, 285 – 287.

Gobrenko, G. P. and Kinnunen, P. K. J. *Chem. and Phys. of Lip.* **2006**, *141*, 72 – 82.

Grudzielanek, S.; Smirnovas, V.; and Winter R. *Chem. and Phys. of Lip.* **2007,** *149*, 28 – 39.

Greenfield, N. and Fasman, G. D. *Biochem.* **1969**, *8*, 4108 – 4116.

Greenfield, N. J. *Anal. Biochem.* **1996**, *235*, 1 – 10.

Greenfield, N. J. *Nat. Protoc*. **2006**, *1*, 2876 – 2890.

Hanakam, F.; Gerisch, G.; Lotz, S.; Alt, T.; and Seelig, A. *Biochem.* **1996,** *35*, 11036 – 11044.

Haugland, R. P. *The Handbook: A Guide to Fluor. Prob. and Label. Technol*. 10th ed. Oregon: Molecular Probes, **2005.**

Iwanga, K.; Ono, S.; Narioka, K.; Kakemi, M.; Morimoto, K.; Yamashita, S.; Namba, Y.; and Oku, N. *J. of Pharma. Sci.s* **1999**, *88*, 248 – 252.

Jalmar, O.; Garcia-Saez, A. J.; Berland, L.; Gonzalvez, F.; and Petit, P. X. *Cell Death and Dis.* **2010**, *1*, 1 – 9.

Halperin, A.; Fragneto, G.; Schollier, A.; and Sferrazza, M. *Langmuir* **2007,** *23,* 10603 – 10617.

Henry, M.; Dupont-Gillain, C.; and Bertrand, P. *Langmuir* **2008,** *24,* 458 – 464.

Kalvodova, L.; Kahya, N.; Schwille, P.; Ehehalt, R.; Verkade, P.; Drechsel, D.; and Simons, K. *The J. of Biol.Chem.* **2005**, *280*, 36815 – 36823.

Kelly, S. M.; Jess, T. J.; and Price, N. C. *Biochim. et Biophys. Acta* **2005**, *1751*, 119 – 139.

Kim, A.; Yun, M-O.;Oh, Y-K.; Ahn, W-S. Kim, C-K. *Intl. J. of Pharma.* **1999**, *180*, 75 – 81.

Korlach, J.; Schwille, P.; Webb, W.W.; and Feigenson, G.W. *PNAS* **1999**, *96,* 8461– 8466.

Krishnan, K.; Holub, O.; Gratton, E.; Clayton, A. H. A.; Cody, S.; and Moens P. D. J. *Biophys. J.* **2009**, *96*, 5112–5121.

Kuznetsova, I. M.; Stepanenko, O. V.; Turoverov, K. K.; Zhu, L.; Zhou, J. M.; Fink, A. L.; Uversky, V. N. *Biochim. et Biophys. Acta* **2002**, *1596*, 138 – 155.

Li, S. and Leblanc, R.M. *J. Phys. Chem. B* **2014**, *118*, 1181 − 1188.

Liu, X.; Kaczmarski, K.; Cavazzini, A.; Szabelski, P.; Zhou, D.; and Guiochon, G. *Biotechnol. Prog.* **2002,** *18,* 796 – 806.

Mathivet, L., Cribier, S., Devaux, P.F., *Biophys. J.* **1996**, 70, 1112 – 1121.

Mollmann, S. H.; Jorgensen, L.; Bukrinsky, J. T.; Elofsson, U.; Norde, W.; and Frokjaer, S. *Eur. J. of Pharm. Sci.* **2006**, *27*, 194 – 204.

Netz, R. R.; Andelman, D. and Orland, H. J. *Phys. II France* **1996**, *6*, 1023 – 1047.

Nosrati, N. MSc Dissertation, *York University* **2009**.

Pal, P.; Mahato, M.; Kamilya, T.; and Talapatra, G. B. *Phys. Chem. Chem. Phys*. **2011**, *13,* 9385 – 9396.

Perez-Lopez, S; Blanco-Vila, N. M.; and Vila-Romeu, N. *J. Phys. Chem. B* **2011**, *115*, 9387 – 9394.

Periard, P. and Raffray, Y. *Spectrochim. Acta* **1984**, *40A*, 719 – 721.

Pocker, Y. and Biswas, S. B. *Biochem.* **1980**, *19*, 5043 – 5049.

Rahmati, K.; Koifman, J.; and Tsoukanova, V. *Coll. and Surf. A. Phys. Eng. Asp.* **2008**, *321*, 181 – 188.

Sanchez, S.; Bagatolli, L. A.; Gratton, E.; and Hazlett T. L. *Biophys. J.* **2002**, *82*, 2232 – 2243.

Seelig, A; Blatter, X. L.; Frentzel, A.; Isenberg, G. *The J. of Biol. Chem.* **2000**, *275*, 17954 – 17961.

Sefton, M. V. and Antonacci, G. M. *Diabetes* **1984**, *33*, 674 – 680.

Sezgin, E. and Schwille, P. *Molecular Membrane Biology* **2012,** *29*, 144 – 154.

Shahid, M. N.; Tsoukanova, V. *The J. of Phys. Chem. B* **2011**, *115*, 3303 – 3314.

Shahid, M. N. PhD Dissertation, *York University* **2013**.

Sreerama, N. and Woody, R. W. *Meth. in Enzym.* **2004**, *383*, 318 – 351.

Sreerama, N. and Woody, R. W. *Prot. Sci.* **2004a**, *13*, 100 – 112.

Stretton, A. O. W. *Genetics* **2002**, *162*, 527 – 532.

Sun, B. and Chiu, D. T. *Anal. Chem.* **2005,** *77*, 2770 – 2776.

Swaminathan, J. and Ehrhardt, C. *Expert Opin. Drug Deliv.* **2012**, *9*, 1489 – 1503

Tah, B.; Pal, P.; and Talapatra, G. B. *J. of Luminsci.* 2014, *145*, 81–87.

Tanwir, K.; Shahid, M. N.; Thomas, A; Tsoukanova, V. *Langmuir* **2012**, *28*, 14000 – 14009.

Theumer M. G.; Clop, P. D.; Rubinstein, H. R.; and Perillo, M. A. *J. Phys. Chem.B* **2012**, *116*, 14216 − 14227.

Tsoukanova, V.; Christian, S. *Langmuir* **2008,** *24*, 13019 – 13029.

Veatch, S. L. and Keller, S. L. *Biophys. J.* **2003,** *85*, 3074 – 3083.

Vogel, S. K.; Heinemann, F.; Chwastek, G.; and Schwille, P. *Cytoskeleton* **2013**, *70*, 706 – 717.

Walde, P. and Ichikawa, S. *Biomole. Eng.* **2001**, *18*, 143 – 177.

Wang, X., Zhang, Y., Wu, J., Wang, M., Cui, G., Li, J., and Brezesinski, G. *Coll. and Sur. B* **2002**, *23*, 339.

Wiessner, J. H. and Hwang, K. J. *Biochim. et Biophys. Acta*, **1982**, *689*, 490 – 498.

Woody, R. W. *Meth. in Enzym.* **1995**, *246*, 34 – 71.

Wojtasek, H. and Leal, W. S. *The J. of Biol. Chem.* **1999**, *274*, 30950 – 30956.

Yan, H.; Guo, Z-U.; Gong, X-W.; Xi, D.; and Feng Y-M. *Pro. Sci.* **2003**, *12*, 768 – 775.

Yang, G. and Xu, Y. *Top. Curr. Chem.* **2011**, *298*, 189 – 236.

Chapter 7: Conclusions.

PEGylated phosphocholine membrane models were examined in terms of phase behavior, morphology, composition, aliphatic chain length, as well as PEG content in aqueous medium of physiological relevance (PBS) at 20 ^{o}C. Two types of membrane models including monolayer and unilamellar vesicles were used to accomplish the aim of this study.

7.1. KEY FINDINGS.

In the first study, monolayers were used to assess the phase behavior of binary mixtures, DPPC/DPPE-PEG2000 and DSPC/DSPE-PEG20000, in terms of phase state, miscibility, compressibility, as well as PEG lateral distribution. Two-channel EFM imaging was used to monitor the phase state and PEG distribution in the monolayers simultaneously. This has enabled us to gain detailed information about the effect of varying PEG content and its distribution on the phase behavior of monolayers. These findings were summarized in phase diagrams to demonstrate distinct phase states on PBS. A comprehensive analysis of phosphocholine and PEG-phospholipids binary mixtures has given a new insight on the mixing behavior of PEGylated phosphocholine membranes on PBS in a range of 1 – 9 mol% PEG. Depending on the composition, both homogeneous mixing and completely immiscible phases have been observed in the mixtures. For instance, remarkable changes in the phase behavior of DSPC/DSPE-PEG2000 mixtures have been observed upon increasing PEG content from 1 – 9 mol%. DSPC/DSPE-PEG2000 mixture containing 1 mol% PEG predominantly forms immiscible LC phase which turns to the coexistence of mixed LE and LC phases in mixture containing 9 mol%. In fact, there is a unique mixture composition seen at 3 mol% PEG, which features a single

homogenously mixed phase in the LC state. This unique mixture exists in a very small range of PEG content and hence was not identified in previous studies. These findings thus imply that the phase behavior of PEGylated phosphocholine membranes may significantly change in response to slight changes in composition which can be used for rational design of PEGylated membranes in the stealth technology to maintain a balance between the retention and release of therapeutic as well as diagnostic agents. These results have been successfully published in the Langmuir Journal in 2008 and 2012 [Tanwir 2008; Tanwir 2012]. The key findings from the study above have been successfully presented in the CSC conference in 2011. Some of the results from this investigation have also been exhibited at the Canadian Society for Chemistry (CSC) and Surface Canada conferences in 2009.

In the second study, a comprehensive analysis of insulin interactions with PEGylated phosphocholine monolayers has indeed demonstrated an intricate phenomenon through area expansion measurement studies. Insulin penetration area, A_{ins}, decreases with an increase of PEG content in both DPPC/DPPE-PEG2000 and DSPC/DSPE-PEG2000 mixtures. However, the degree of insulin binding, χ_{ins}, increases upon increasing the PEG content in both types of binary mixtures. Interestingly, surface (lateral) pressure significantly reduced the degree of insulin binding, χ_{ins}, as compared to the PEG content in both type of binary mixtures. Among both mixtures, DSPC/DSPE-PEG2000 mixtures had an overall reduced binding degree of insulin upon increasing PEG content from that of DPPC/DPPE-PEG2000 mixtures. Further analysis of mixtures revealed that the fluidity of monolayers (LE phase) increases with increasing PEG content, which may consequently increase the χ_{ins} in the PEGylated phosphocholine membrane models. Hence, the knowledge gained herein can provide fundamental knowledge about the

mechanisms involved in the non-specific interactions of small proteins with the PEGylated phosphocholine membrane in order to improve the performance of various biomedical devices as well as therapeutic/diagnostic agents carriers with reduced protein adsorption. These findings have also been successfully presented in the CSC conference in 2010.

The third study entailed visualizing the morphology of PEGylated phosphocholine GUVs using EFM. A comparative analysis has revealed that coexisting phases were present in GUVs bearing 1 – 6 mol% of PEG content. Increasing the PEG2000 content resulted in an overall increase in L_d phase in the vesicles. Furthermore, a reduction in the amount and size of GUVs was also observed with an increase in PEG-phospholipid content. In particular, GUVs with 9 mol% PEG2000-phospholipid were unable to form giant vesicles that might be associated to high concentration of PEG-phospholipid. Formation of vesicle tubes has also been observed in DPPC/DPPE-PEG2000 GUVs containing 3 and 6 mol% PEG2000, which can have great implications for applications with controlled release. Most importantly, the membrane morphology of DPPC/DPPE-PEG2000 GUVs containing 1, 3 and 6 mol% PEG2000 has shown a great resemblance with the monolayer membrane models of the same binary mixtures at a surface (lateral) pressure of ~15 mN/m. This indeed is one of the key findings in this work illustrating a direct comparison between vesicle membrane and a monolayer as membrane models. Hence, it can be proposed that PEG content somewhere between 1 – 6 mol% can be useful in order to develop efficient drug delivery system with controlled bio-non-fouling properties. Results from this investigation have been successfully presented at the CSC and Pacifichem conferences in 2010.

In this study, the insulin/membrane interactions were carried out using vesicle as a membrane model. This study revealed quite an intricate effect on the phase behavior of DPPC/DPPE-PEG2000 GUVs. In-situ analysis of insulin interactions with DPPC/DPPE-PEG2000 membrane containing 1 mol% PEG vesicle has shown that membrane expanded as well as became more ordered. The expansion and orderliness of the vesicles is considered to be due to the steric repulsion and redistribution of the PEG chains upon the compression exerted by insulin. Furthermore, the effect of insulin/membrane interactions with varying PEG content showed a modest change in the insulin conformation. Findings from this study have been successfully presented at the CSC conference in 2010.

In the final investigation, the structural changes of insulin, in terms of α–helical content, were determined upon interactions with DPPC/DPPE-PEG2000 vesicles using circular dichroism spectroscopy. The data analysis illustrated that the α–helical content of insulin increased upon increasing the PEG content in the DPPC/DPPE-PEG2000 vesicles. This implies that insulin turns into slightly more compact conformation in order to avoid PEG chains and binds the phospholipid membranes. This further reveals that insulin does not unfold or denature upon interactions with DPPC/DPPE-PEG2000 SUVs as the CD spectra of insulin did not change upon interactions of PEGylated phosphocholine vesicles. This study further demonstrated the existence of two species of insulin molecule with a little change in the secondary structure known as a native monomer (M) and a compact monomer with increased α-helical structure (M_C). Results of this study have been successfully exhibited at the CSC conference in 2010.

7.2. REFERENCES.

Tanwir, K. and Tsoukanvoa, V. *Langmuir* 2008, *24*, 14078 – 14087.

Tanwir, K.; Shahid, M. N.; Thomas, A; Tsoukanova, V. *Langmuir* 2012, *28*, 14000 – 14009.